CHAPTER V

RESULTS AND DISCUSSION

5.1 X-Ray Diffraction Patterns (XRD)

The X-ray diffraction patterns and the degree of crystallization (see calculation in Appendix A-1) of all catalysts prepared are shown in Figures 5.1-5.13. The XRD patterns of commercially available NaY - type zeolite "JRC-Z-Y" supplied by Tosoh Corporation were also demonstrated for comparison. The XRD patterns of the catalysts prepared were determined on D-5000 X-ray diffractometer with Ni-filtered CuKα radiation at the angle 2θ ranging from 4 to 50 degree. The comparison of the individual patterns with the pattern of commercial JRC-Z-Y zeolite due to the effect of the amount of H_2O/SiO_2 mole ratio, pH value, crystallization temperature and time of crystallization are discussed below.

5.1.1 Effect of H_2O/SiO_2 ratio on NaY - type zeolite synthesis

The degree of crystallization and the XRD patterns of NaY-type zeolite catalysts prepared by using different amount of H_2O/SiO_2 mole ratio are shown in Figures 5.1 and 5.2, respectively. Each sample was prepared with gel mixture pH of 13.5, crystallization temperature of 95 °C for 72 h.

The H_2O/SiO_2 ratios were varied during the range of 32.5 to 54.5 as shown in Figure. 5.1. The catalyst samples with H_2O/SiO_2 ratios ranging from 43.5 to 49 exhibited high degree of crystallization with the maximum at

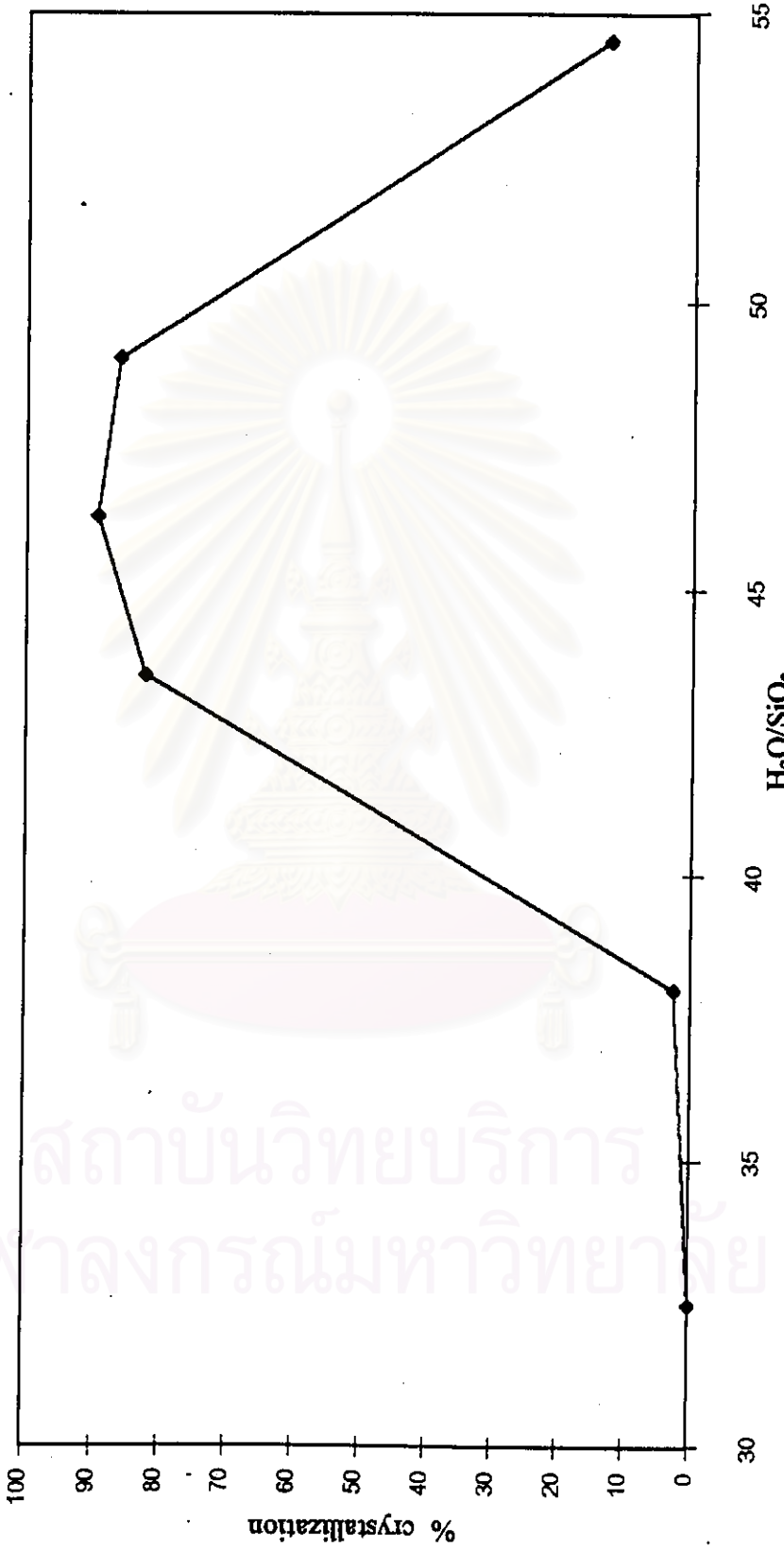

Figure 5.1 The degree of crystallization of prepareed catalysts with different H_2O/SiO_2 ratios by mole

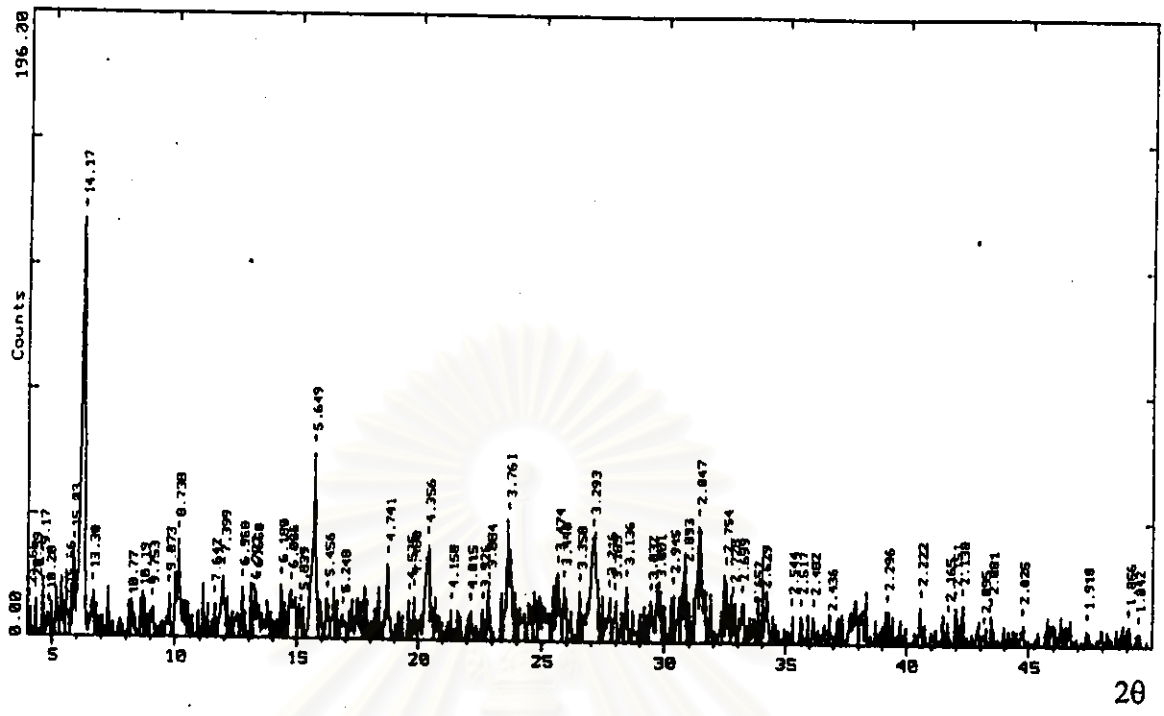

a) H_2O/SiO_2 ratio of 54.5 by mole

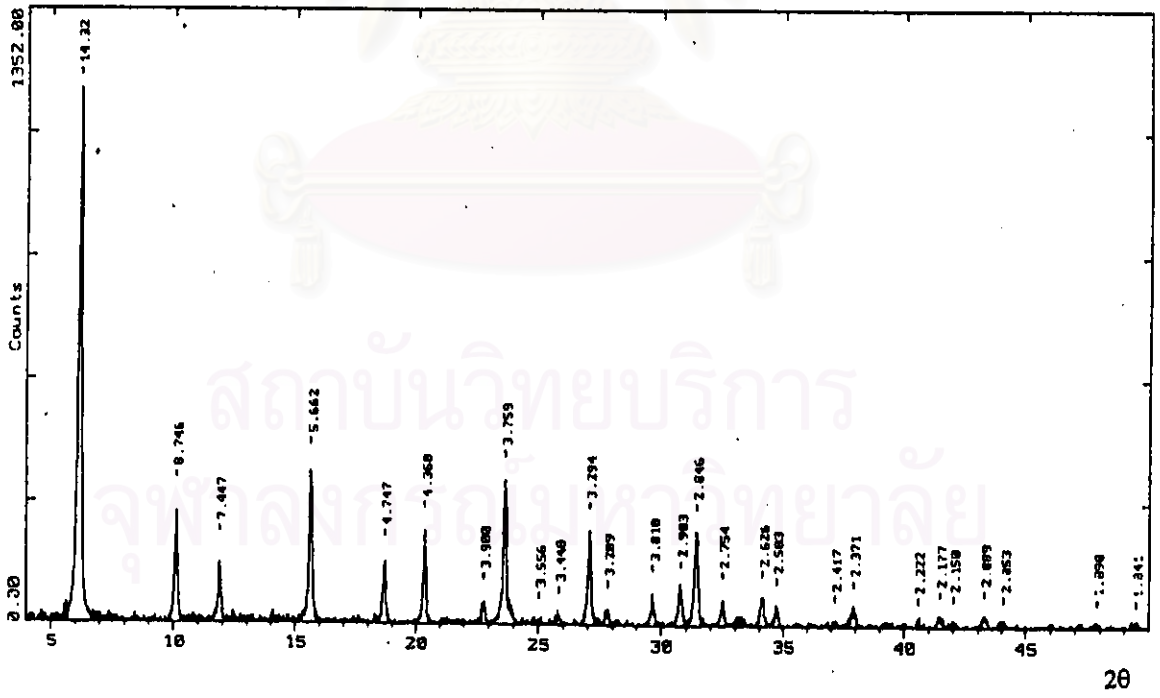

b) H_2O/SiO_2 ratio of 49 by mole

Figure 5.2 The XRD patterns of prepared zeolite catalysts with different H_2O/SiO_2 ratios by mole

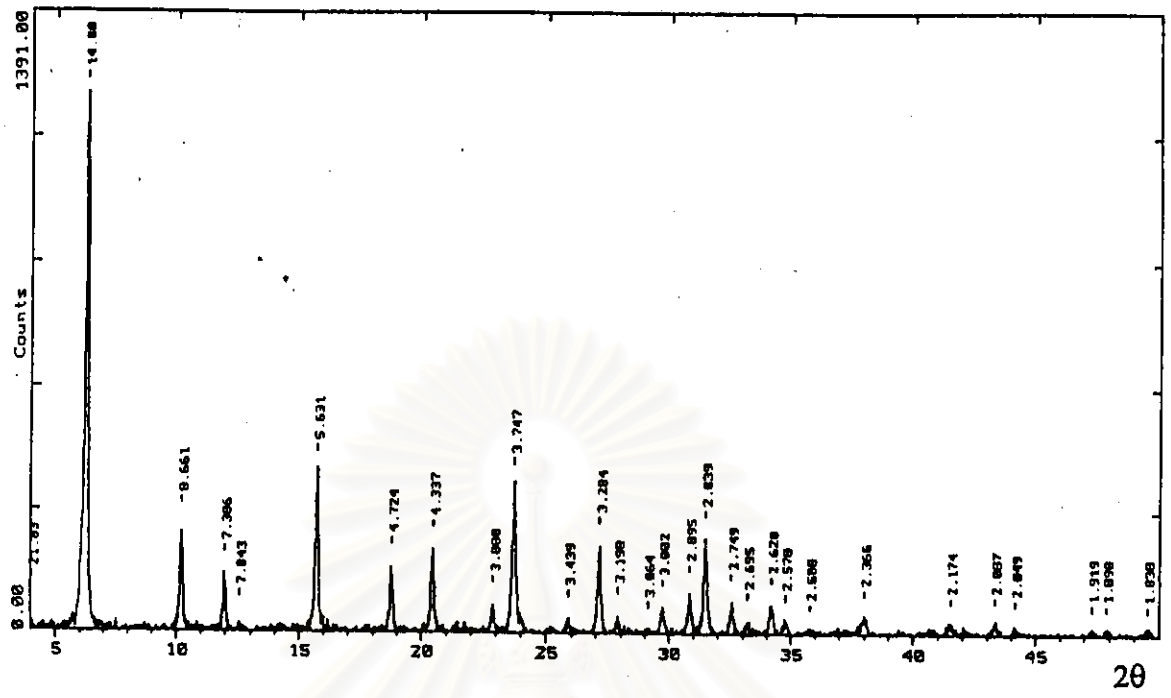

c) H_2O/SiO_2 ratio of 46.25 by mole

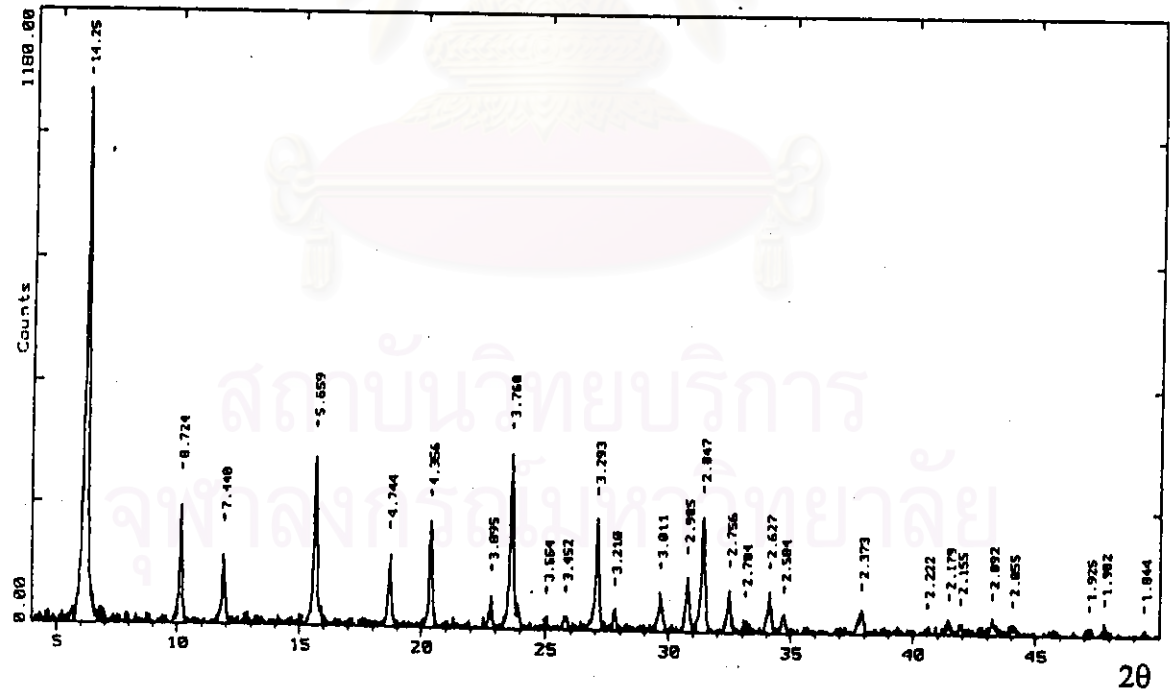

d) H_2O/SiO_2 ratio of 43.5 by mole

Figure 5.2 The XRD patterns of prepared zeolite catalysts with different H_2O/SiO_2 ratios by mole (continued)

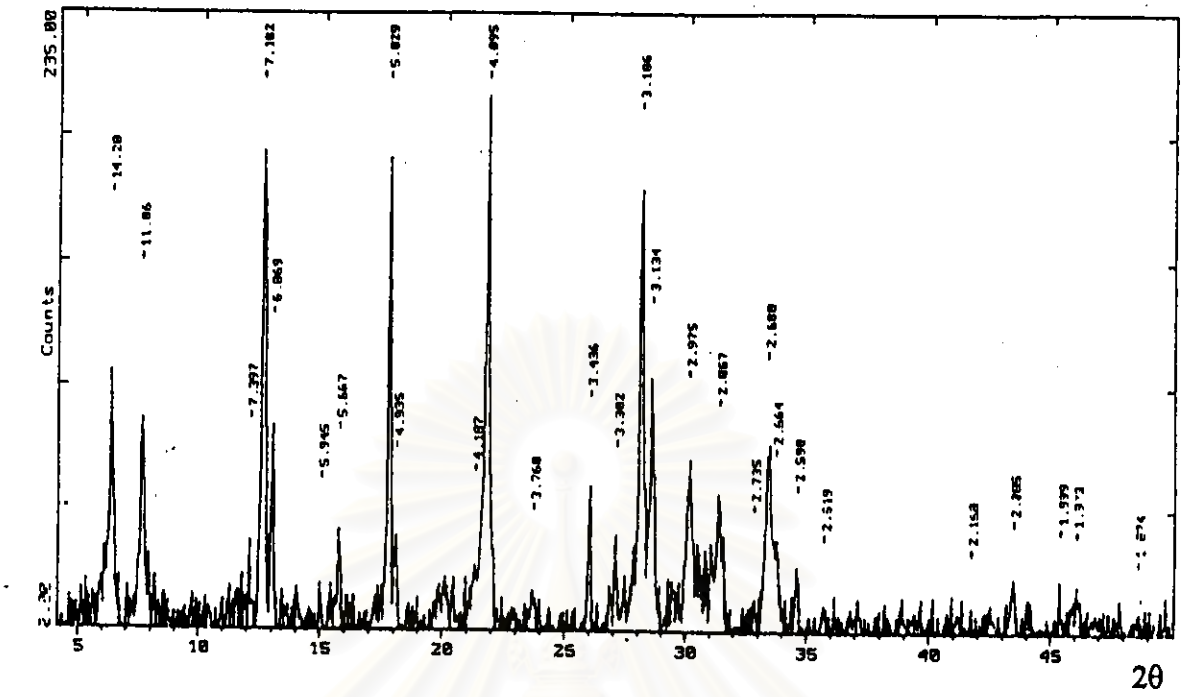

e) H_2O/SiO_2 ratio of 38 by mole

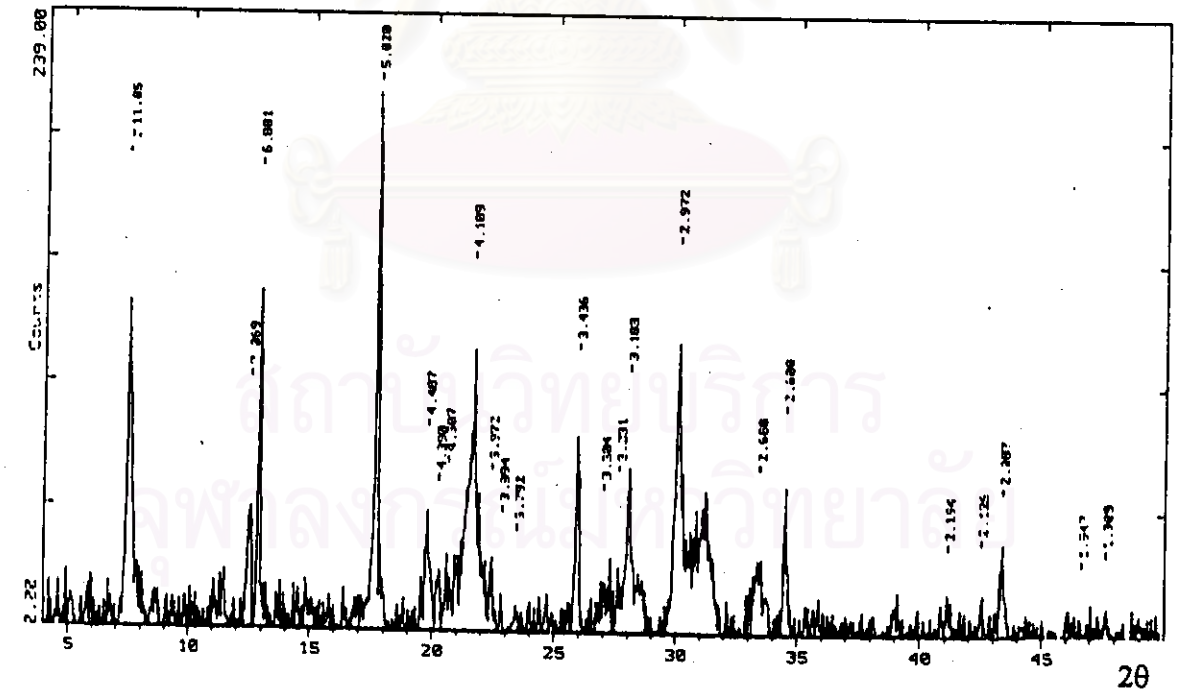

f) H_2O/SiO_2 ratio of 32.5 by mole

Figure 5.2 The XRD patterns of prepared zeolite catalysts with different H_2O/SiO_2 ratios by mole (continued)

H_2O/SiO_2 ratios of 46.25. It has been found that the optimum H_2O/SiO_2 ratios strongly influenced the formation of pure phase of NaY with high degree of crystallization.

5.1.2 Effect of pH value on NaY-type zeolite synthesis

The degree of crystallization and the XRD patterns of catalysts with H_2O/SiO_2 ratios of 46.25 are shown in Figure 5.3 and Figures 5.4 to 5.9. Each sample was prepared with various gel pH between 11-14 while the other conditions were unchanged

When the pH 14 was used, the XRD patterns of NaY-type zeolite crystal was obtained in the first 24 hr of crystallization time thereafter the crystallization degree was reduced with the increasing of characteristic peak of impurity phase. Until the crystallization time was raised to 96 hr, the XRD pattern showed no NaY-type zeolite crystal but impurity phase was formed. At pH 13.7, the optimum monophasic and highest crystallization degree of desired NaY-type zeolite was observed, at 48 hr crystallization time. Then the crystallization degree was slightly decreased and little characteristic peak of impurity phase was simultaneously found. At the pH 13.5 and 13, the XRD patterns were initially appeared at 48 hr of crystallization time, the monophasic and high crystallization degree were observed at 72 hr of crystallization time and then the crystallization degrees were slightly decreased. However, at pH 12 the XRD pattern of monophasic NaY-type zeolite crystal was observed at longer crystallization time of 96 hr. Furthermore, the XRD pattern of NaY-type zeolite prepared at pH 11 revealed that substantially no NaY zeolite was formed throughout the crystallization time of 96 h.

Since the pH and the solubility of reactant in gel mixture are governed by the presence of OH^- (1,34). Consequently, the higher pH value may cause more concentration of dissolved reactants thus enhancing the rate of crystal

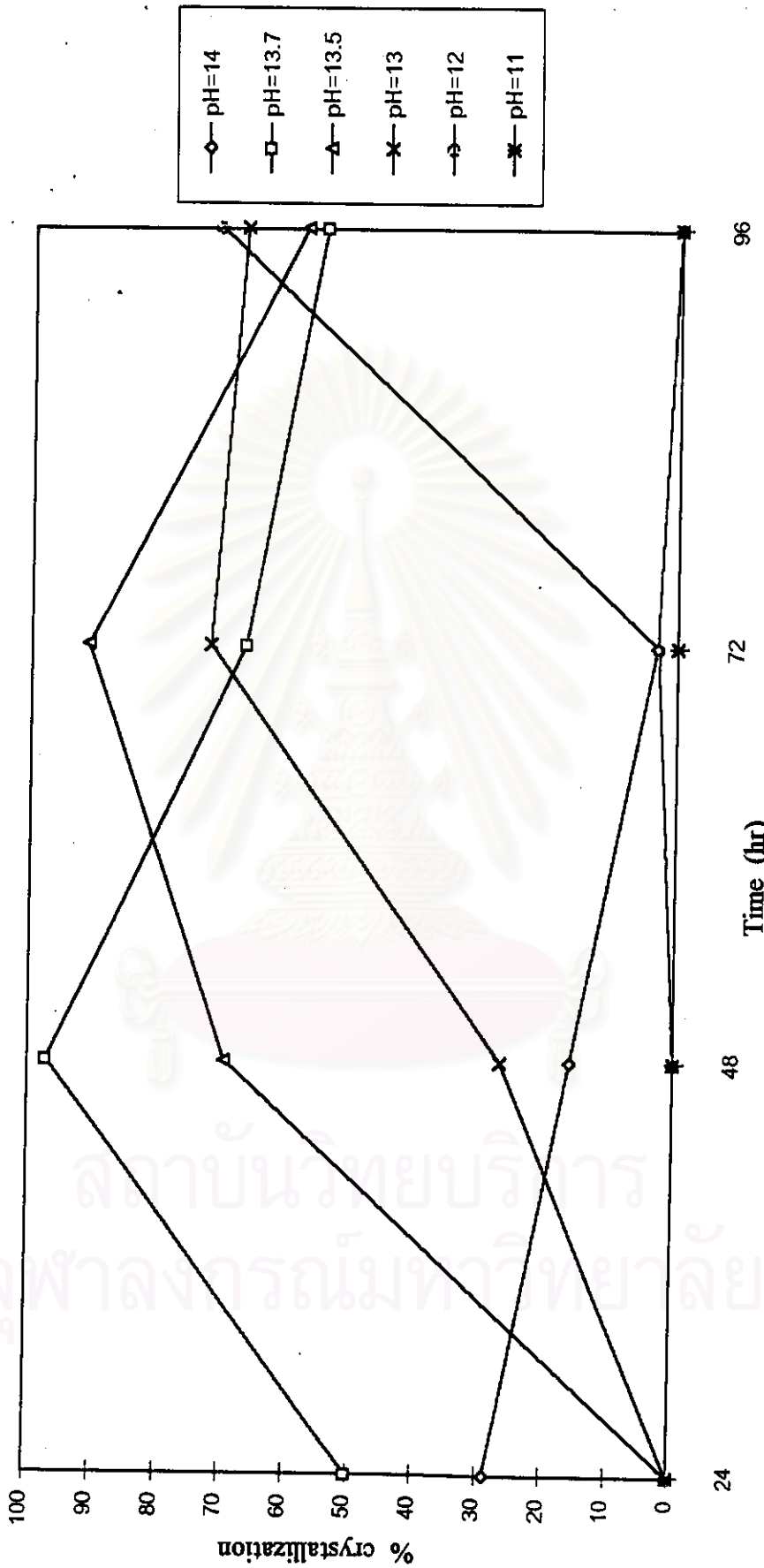

Figure 5.3 The degree of crystallization of prepared catalysts at different pH values for various crystallization times

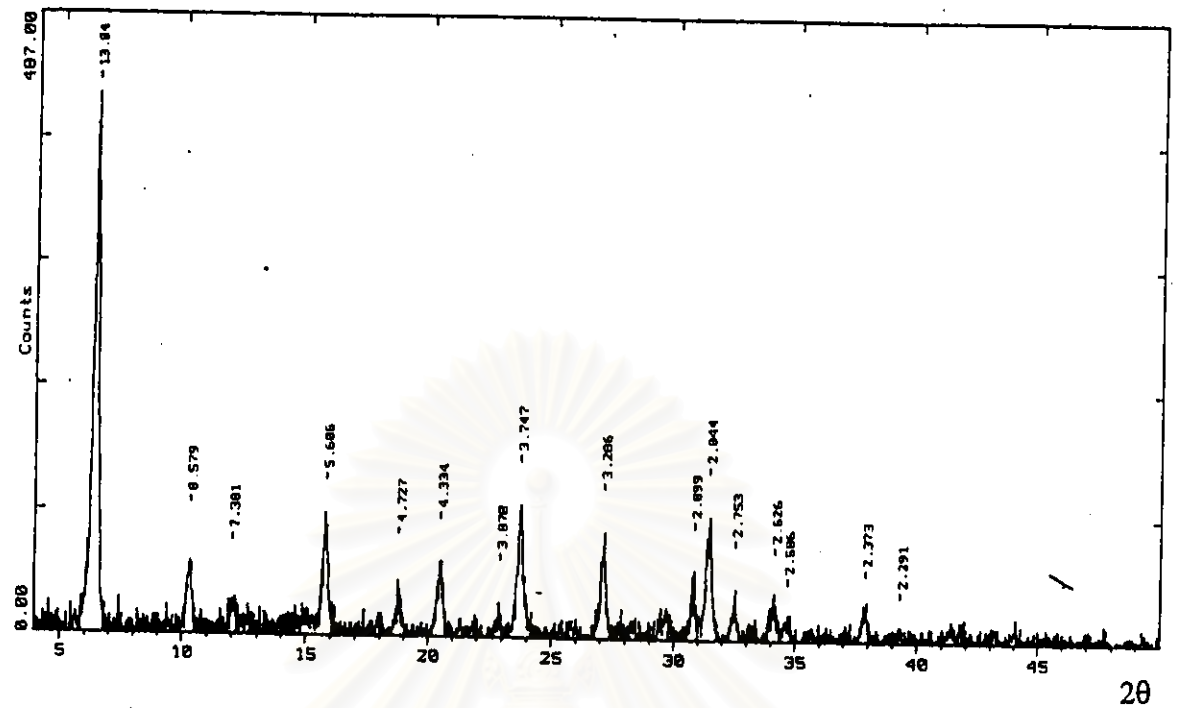

a) 24 hr of crystallization time

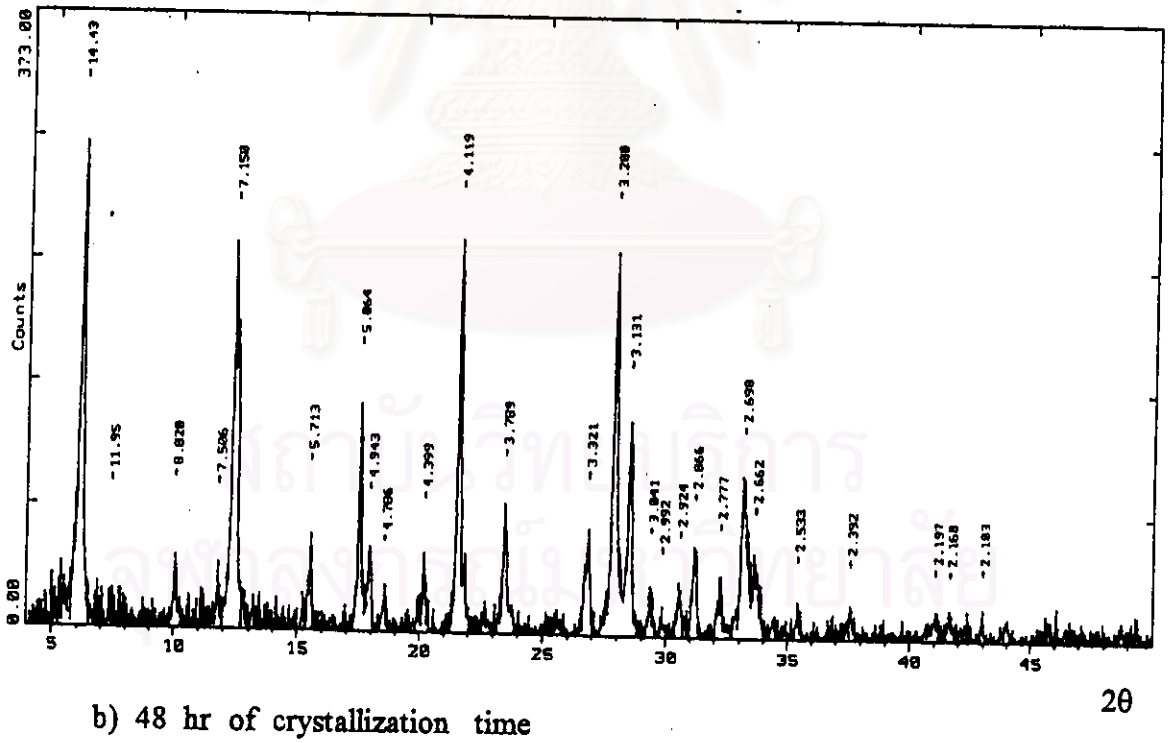

b) 48 hr of crystallization time

Figure 5.4 The XRD patterns of prepared catalysts at pH 14 for various crystallization times

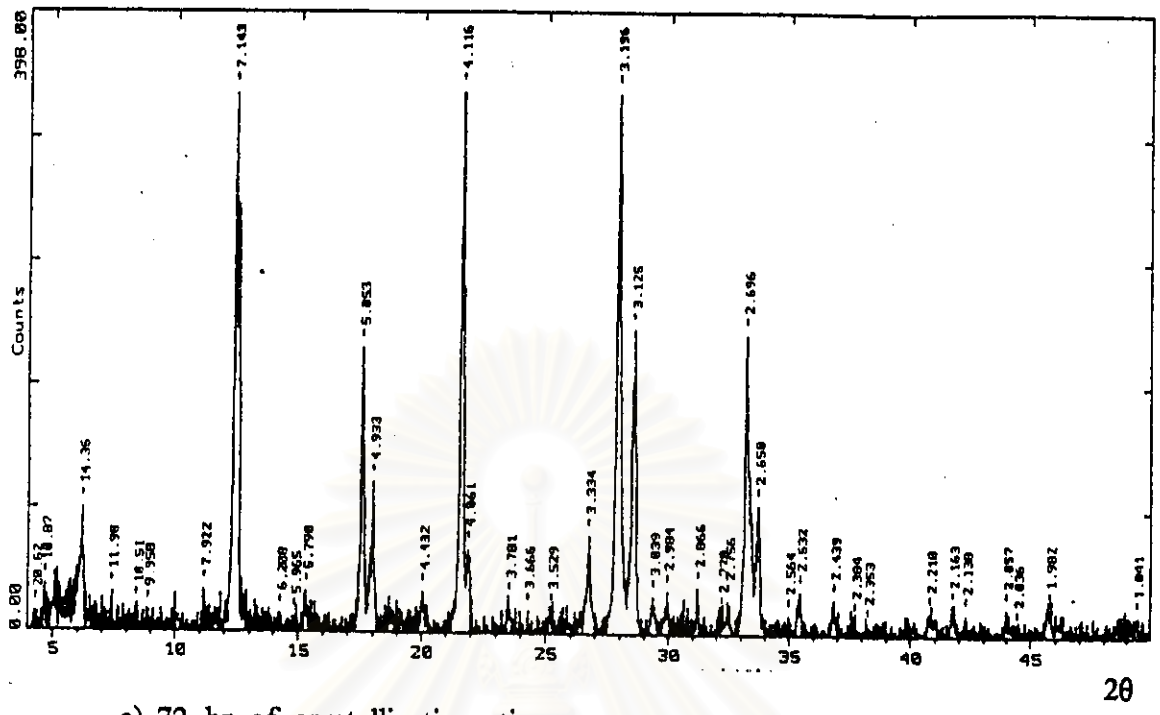

c) 72 hr of crystallization time

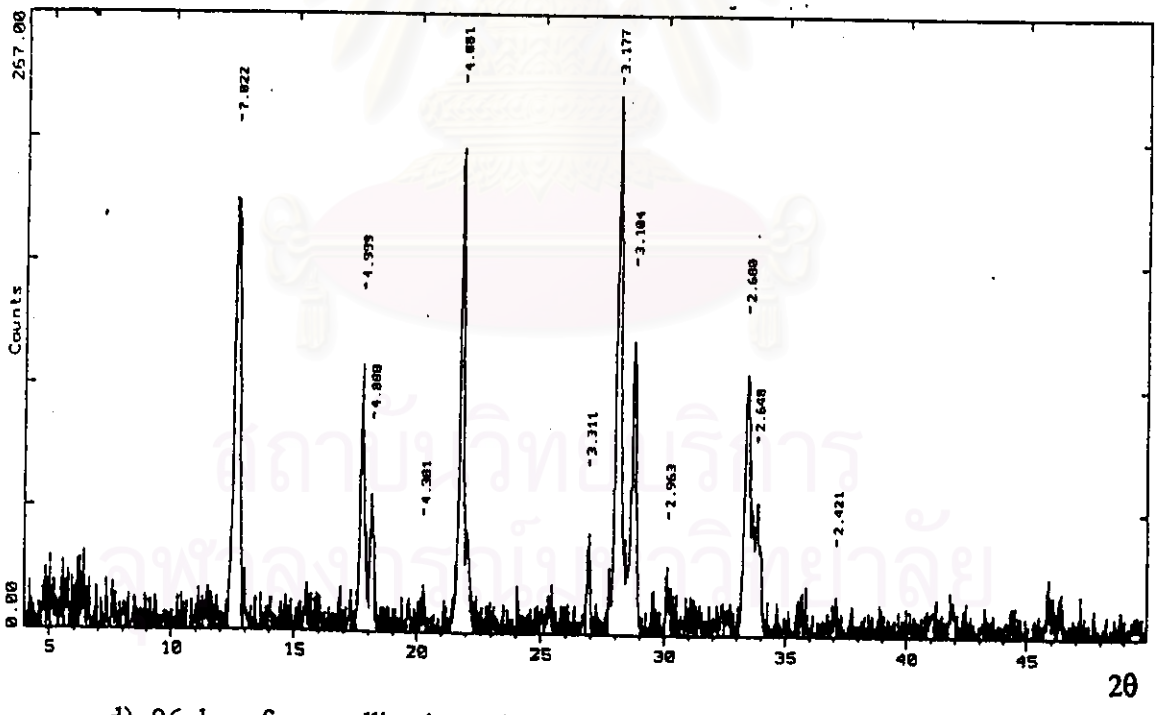

d) 96 hr of crystallization time

Figure 5.4 The XRD patterns of prepared catalysts at pH 14 for various crystallization times (continued)

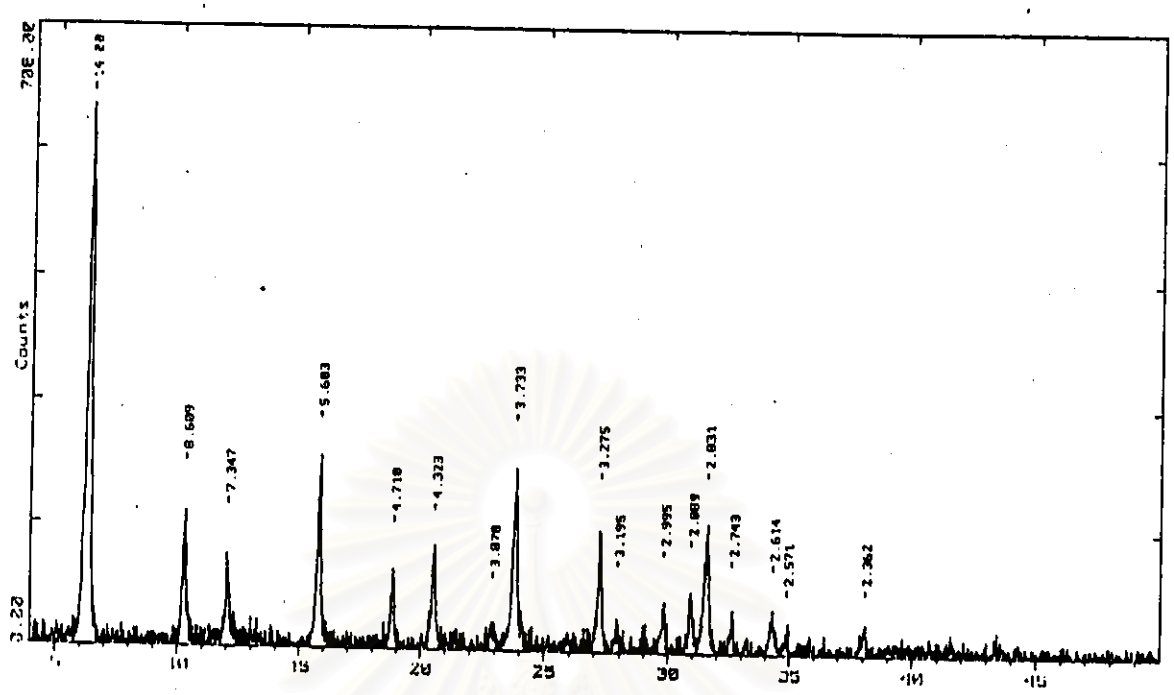

a) 24 hr of crystallization time

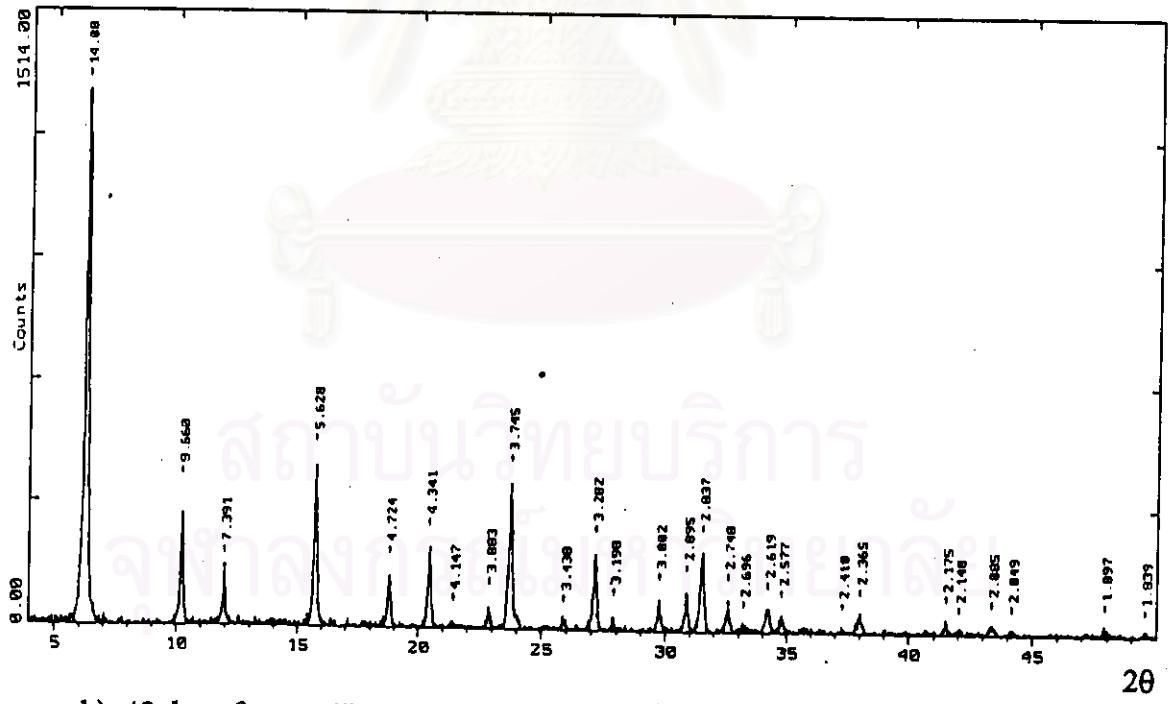

b) 48 hr of crystallization time

Figure 5.5 The XRD patterns of prepared catalysts at pH 13.7 for various crystallization times

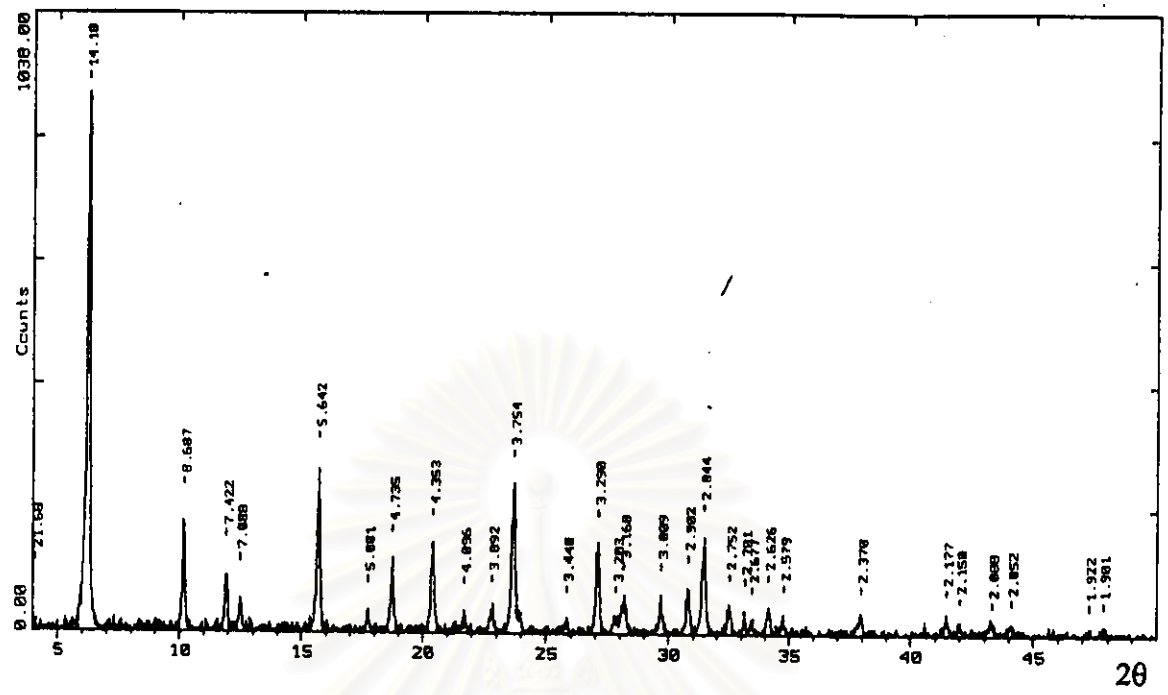

c) 72 hr of crystallization time

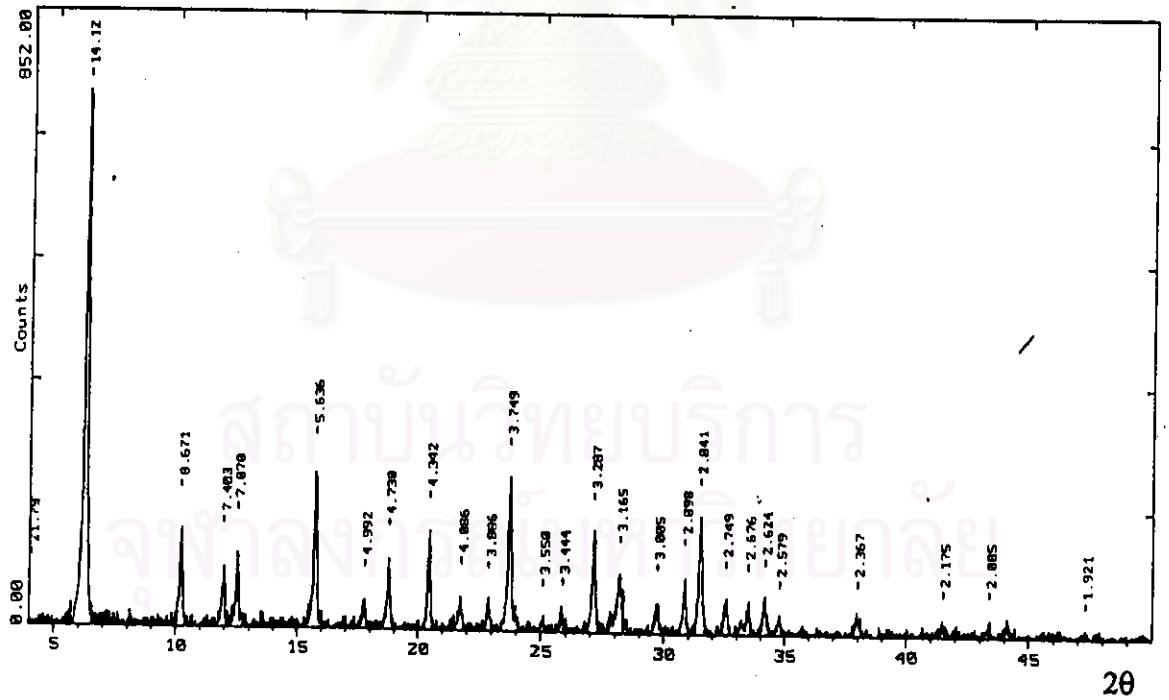

d) 96 hr of crystallization time

Figure 5.5 The XRD patterns of prepared catalysts at pH 13.7 for various crystallization times (continued)

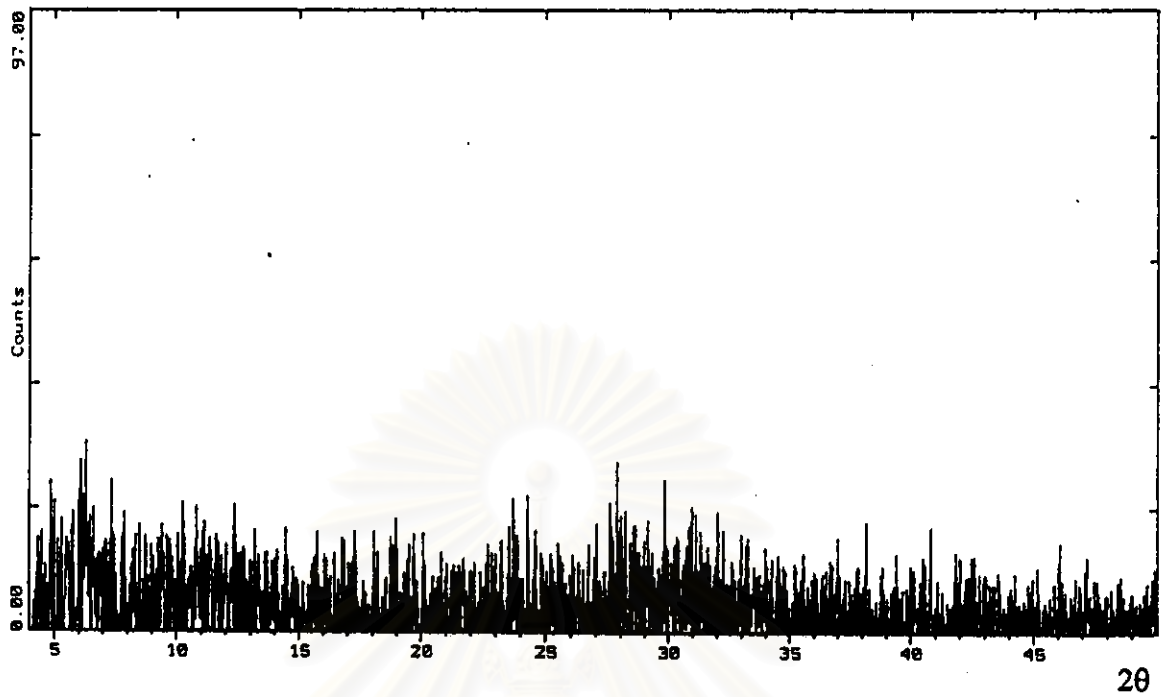

a) 24 hr of crystallization time

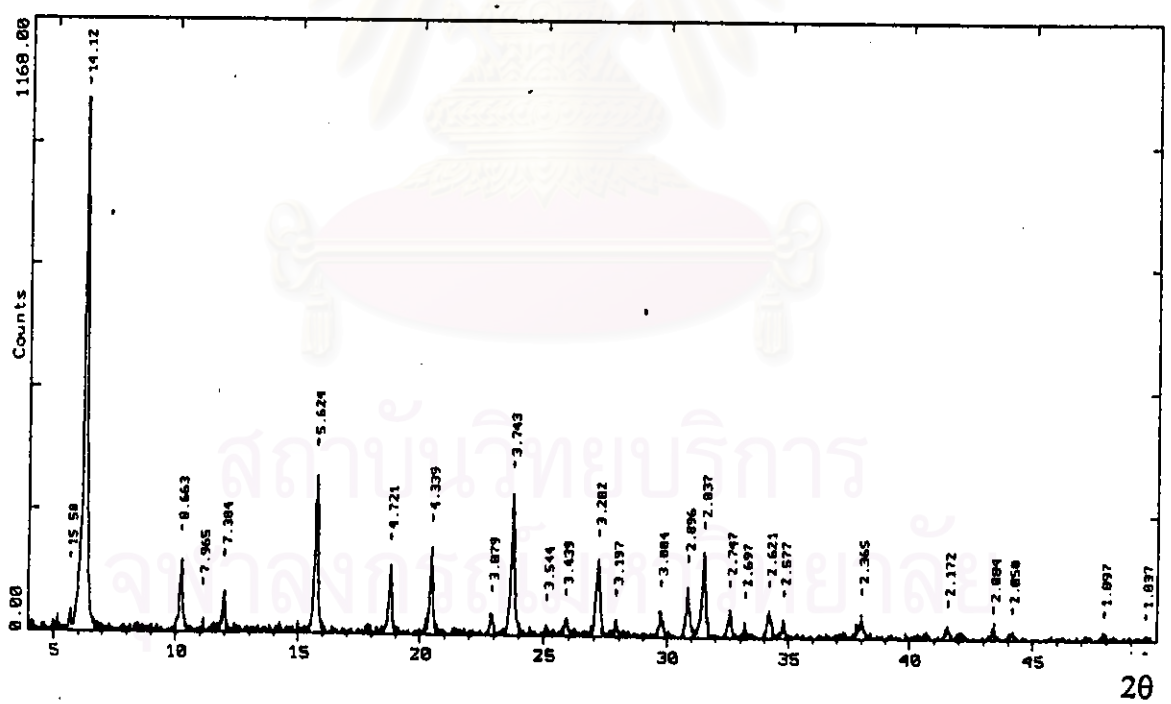

b) 48 hr of crystallization time

Figure 5.6 The XRD patterns of prepared catalysts at pH 13.5 for various crystallization times

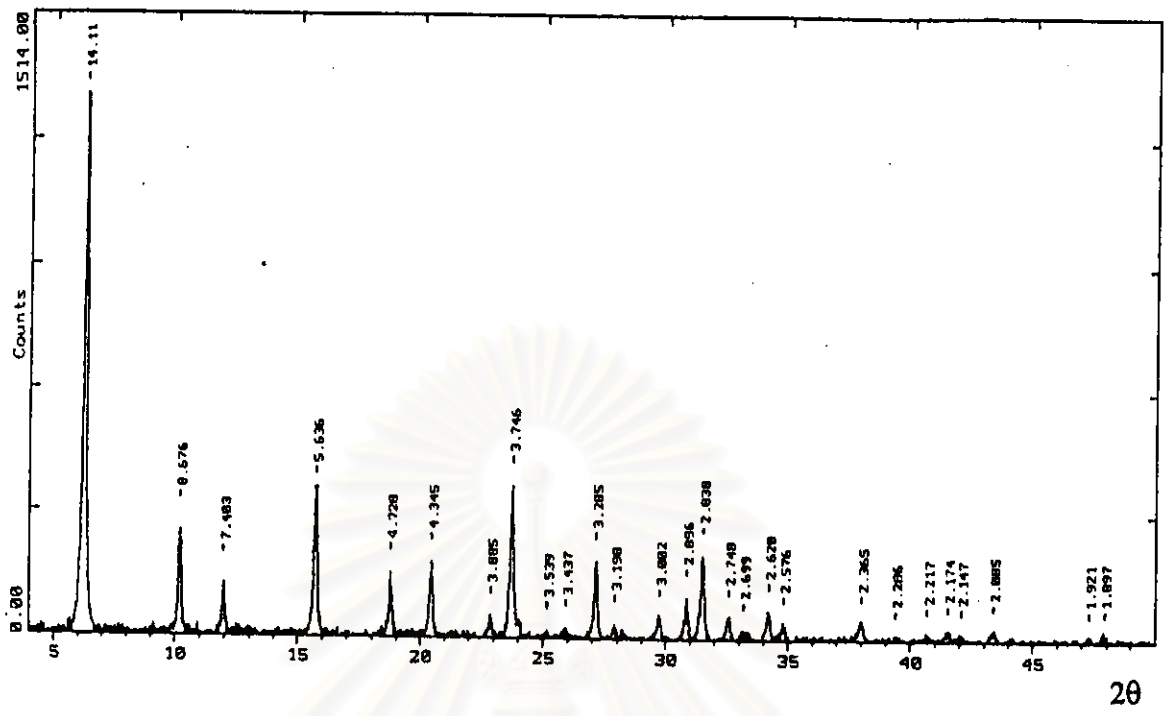

c) 72 hr of crystallization time

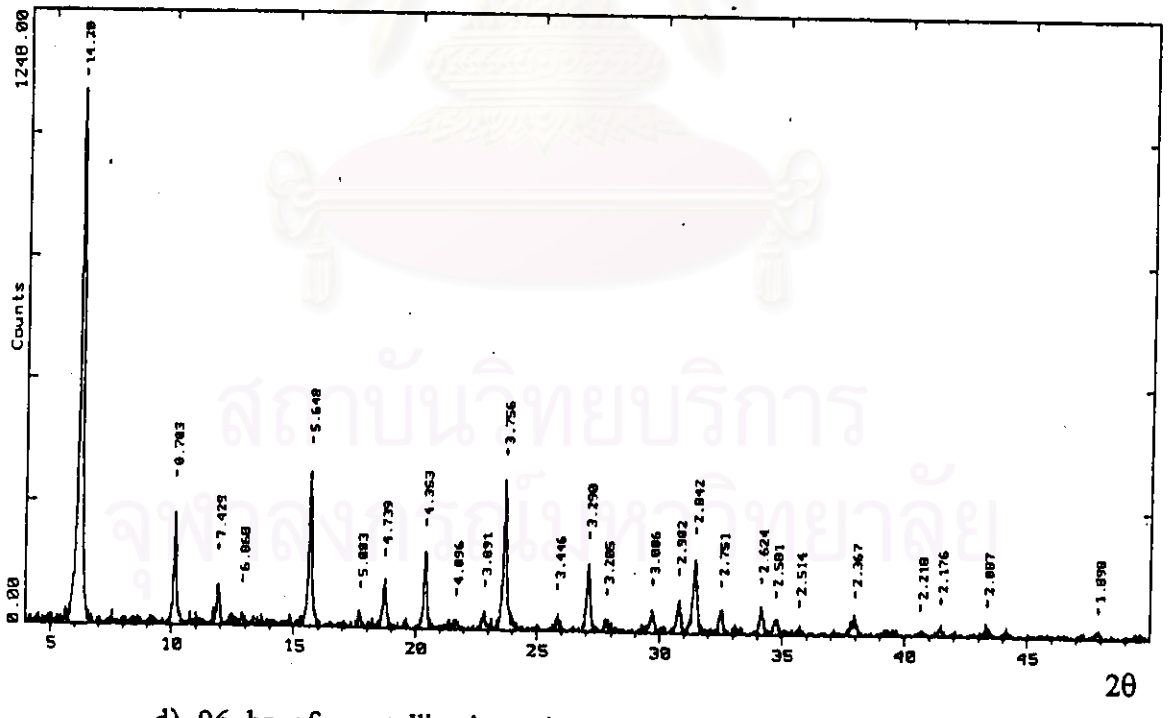

d) 96 hr of crystallization time

Figure 5.6 The XRD patterns of prepared catalysts at pH 13.5 for various crystallization times (continued)

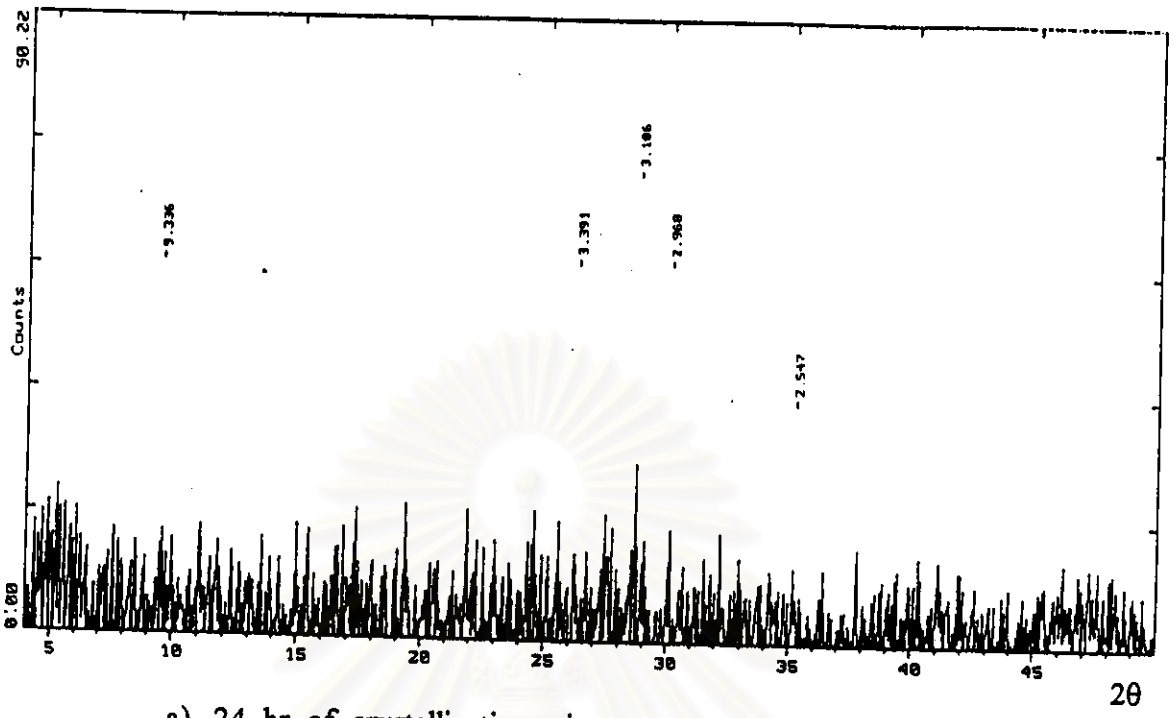

a) 24 hr of crystallization time

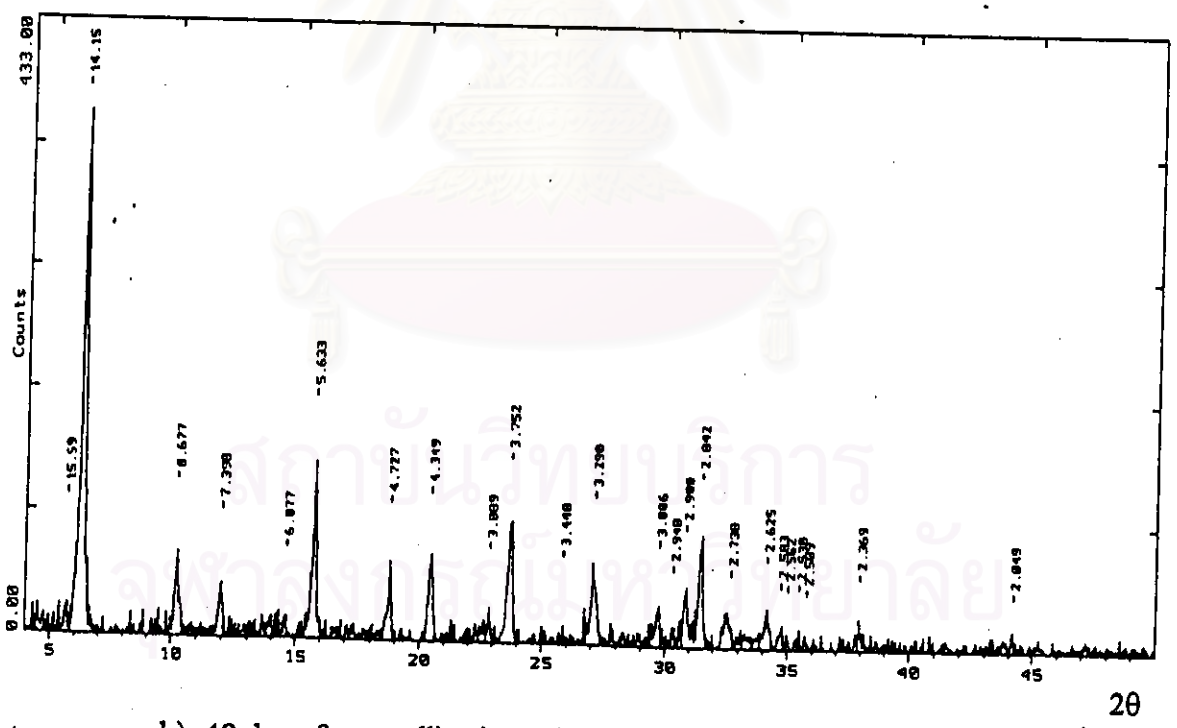

b) 48 hr of crystallization time

Figure 5.7 The XRD patterns of prepared catalysts at pH 13 for various crystallization times

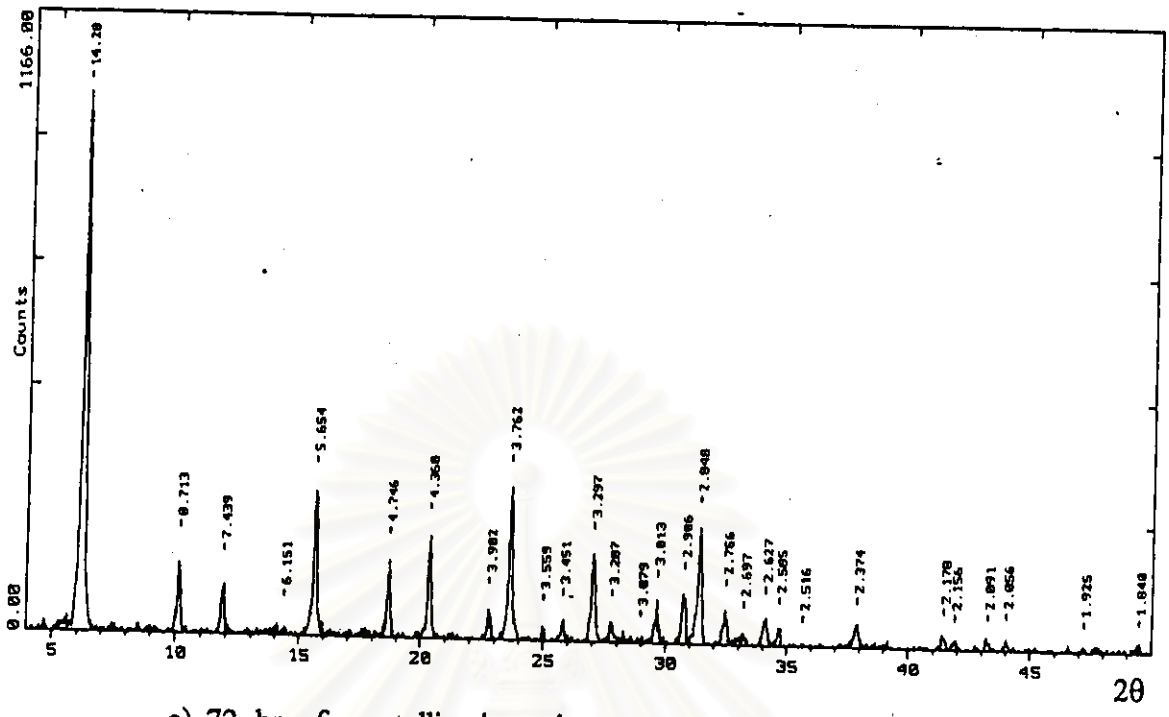

c) 72 hr of crystallization time

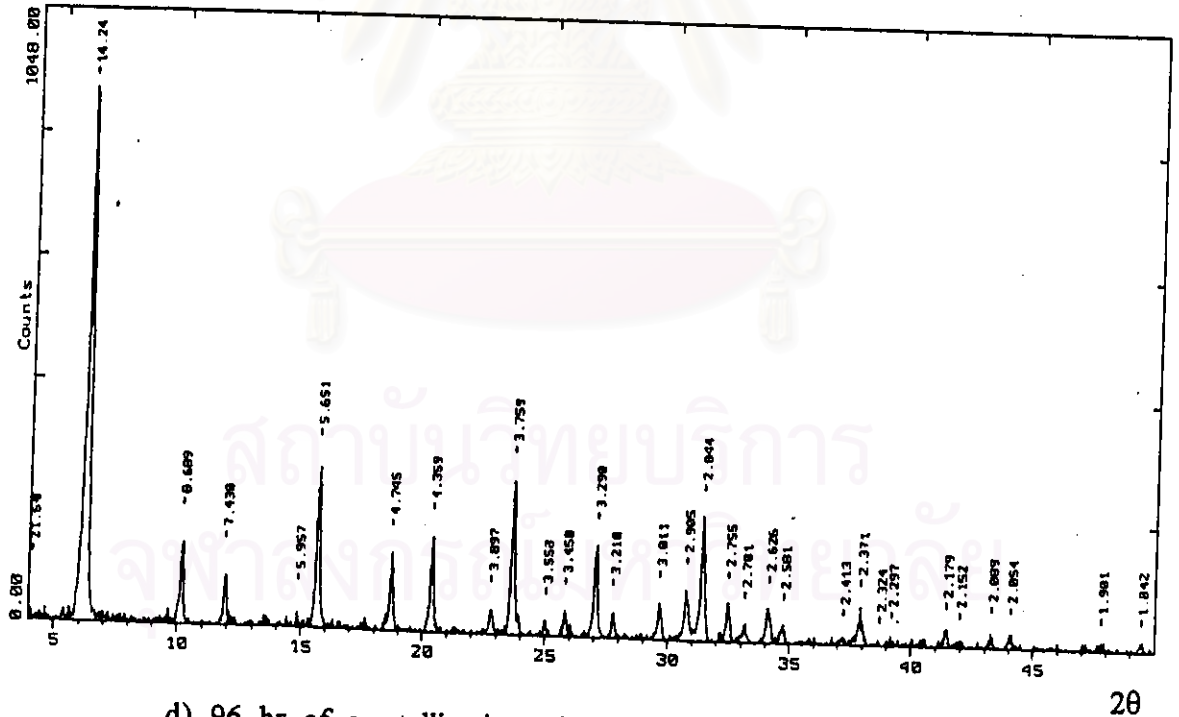

d) 96 hr of crystallization time

Figure 5.7 The XRD patterns of prepared catalysts at pH 13 for various crystallization times (continued)

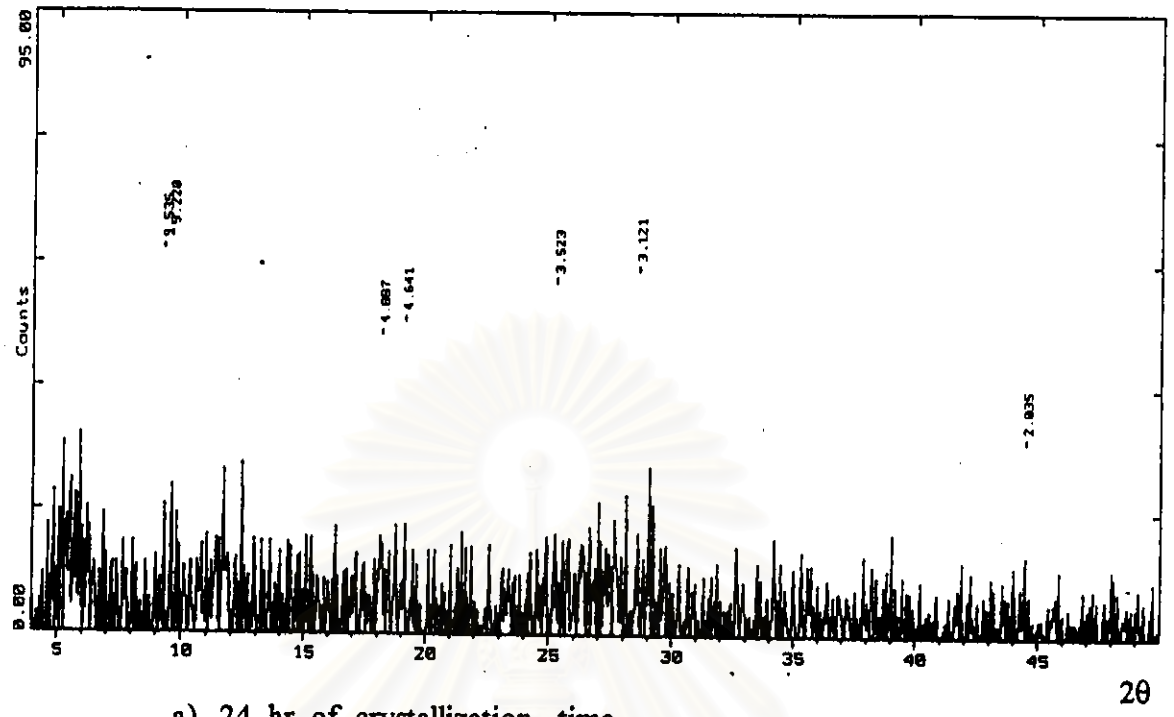

a) 24 hr of crystallization time

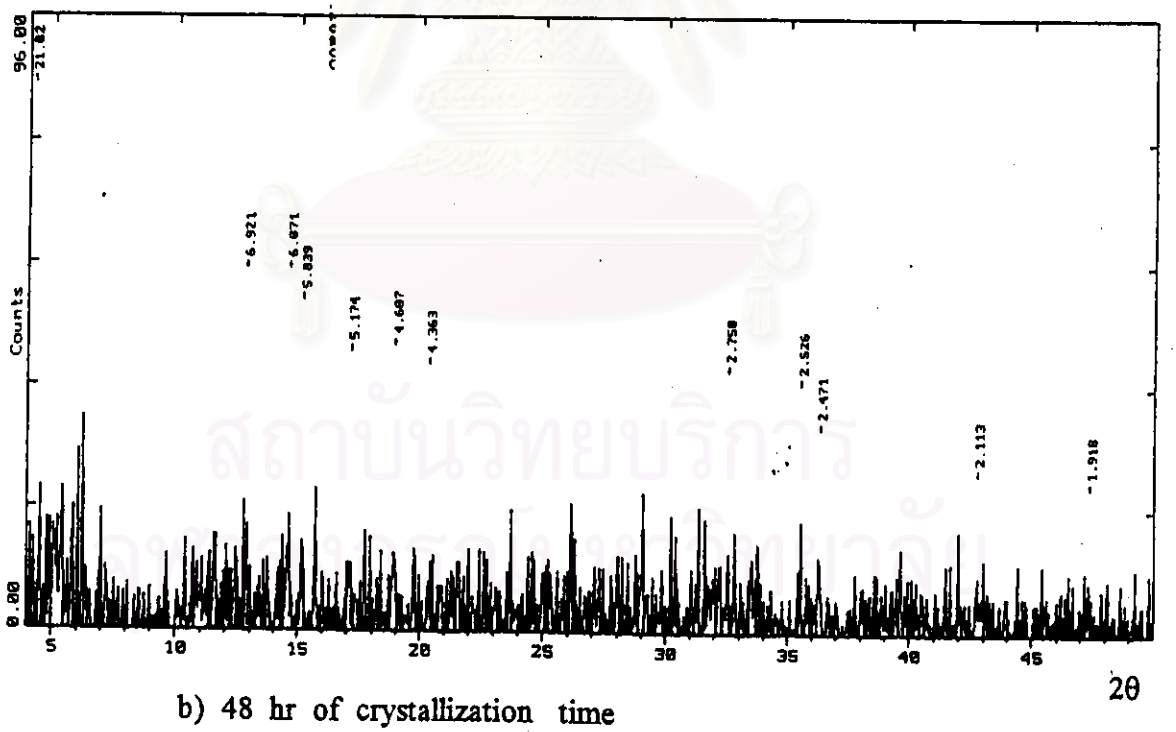

b) 48 hr of crystallization time

Figure 5.8 The XRD patterns of prepared catalysts at pH 12 for various crystallization times

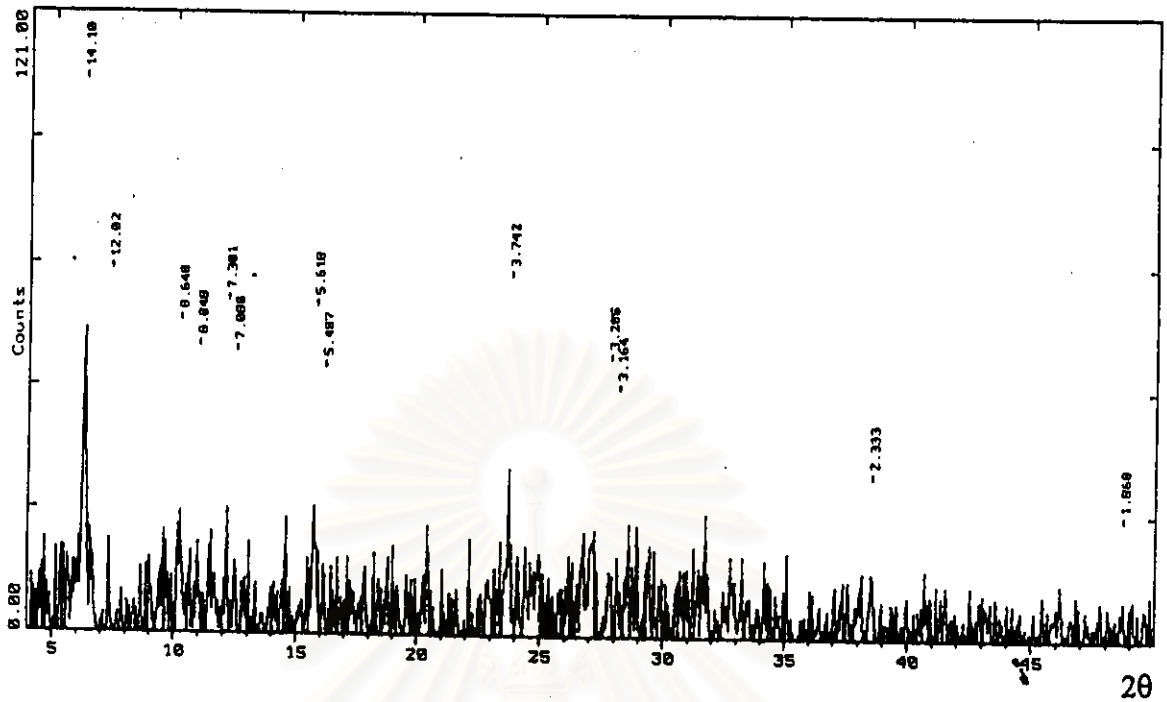

c) 72 hr of crystallization time

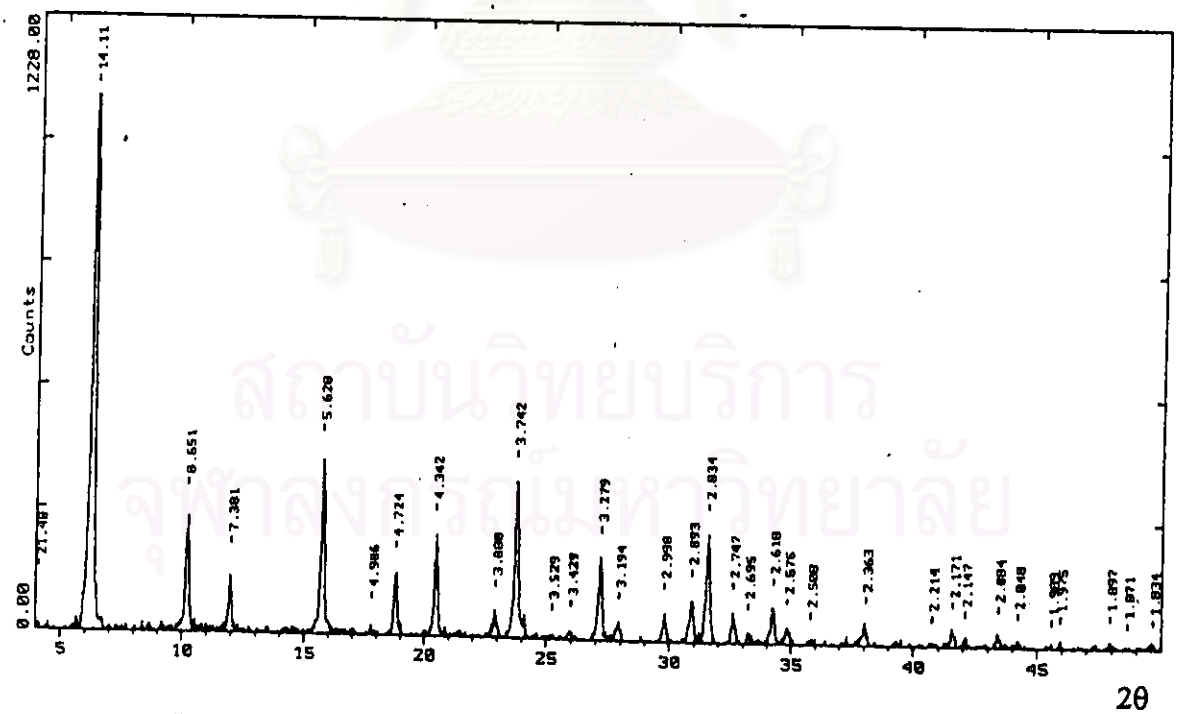

d) 96 hr of crystallization time

Figure 5.8 The XRD patterns of prepared catalysts at pH 12 for various crystallization times (continued)

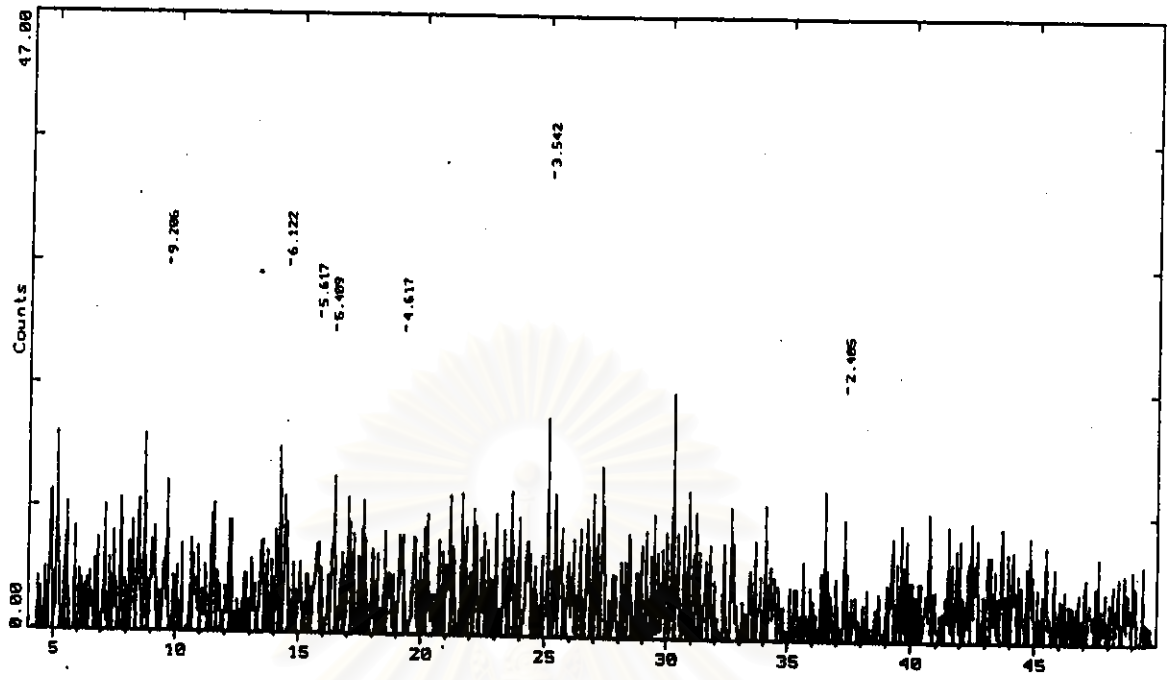

a) 24 hr of crystallization time

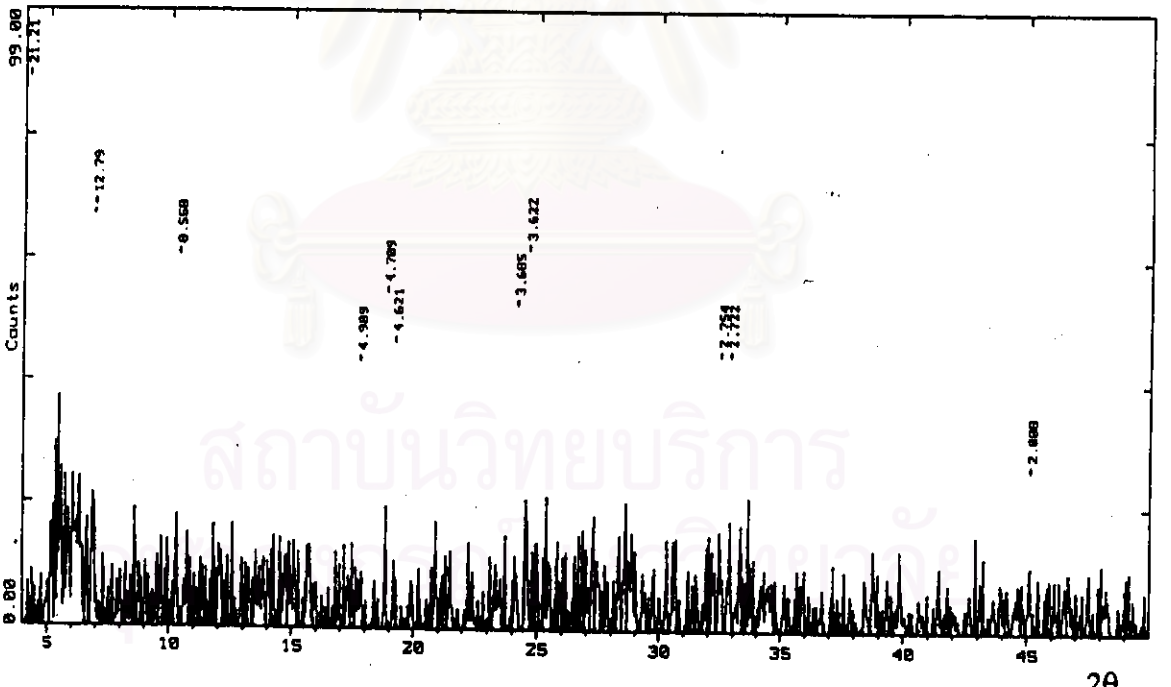

b) 48 hr of crystallization time

Figure 5.9 The XRD patterns of prepared catalysts at pH 11 for various crystallization times

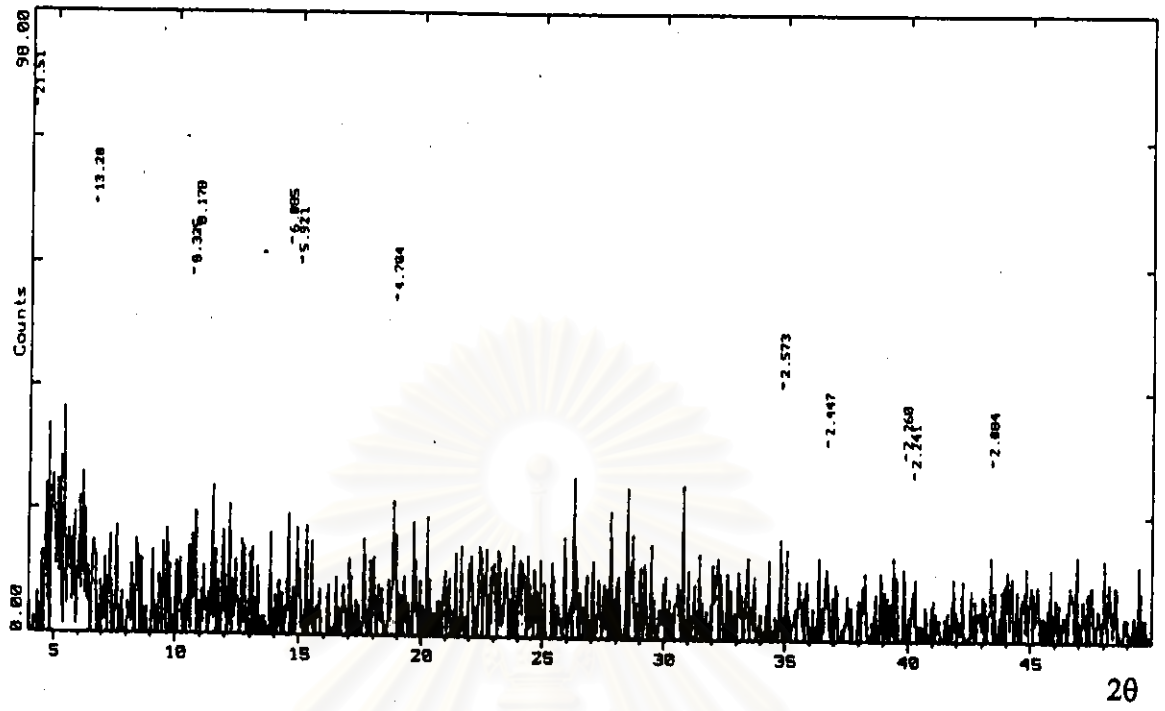

c) 72 hr of crystallization time

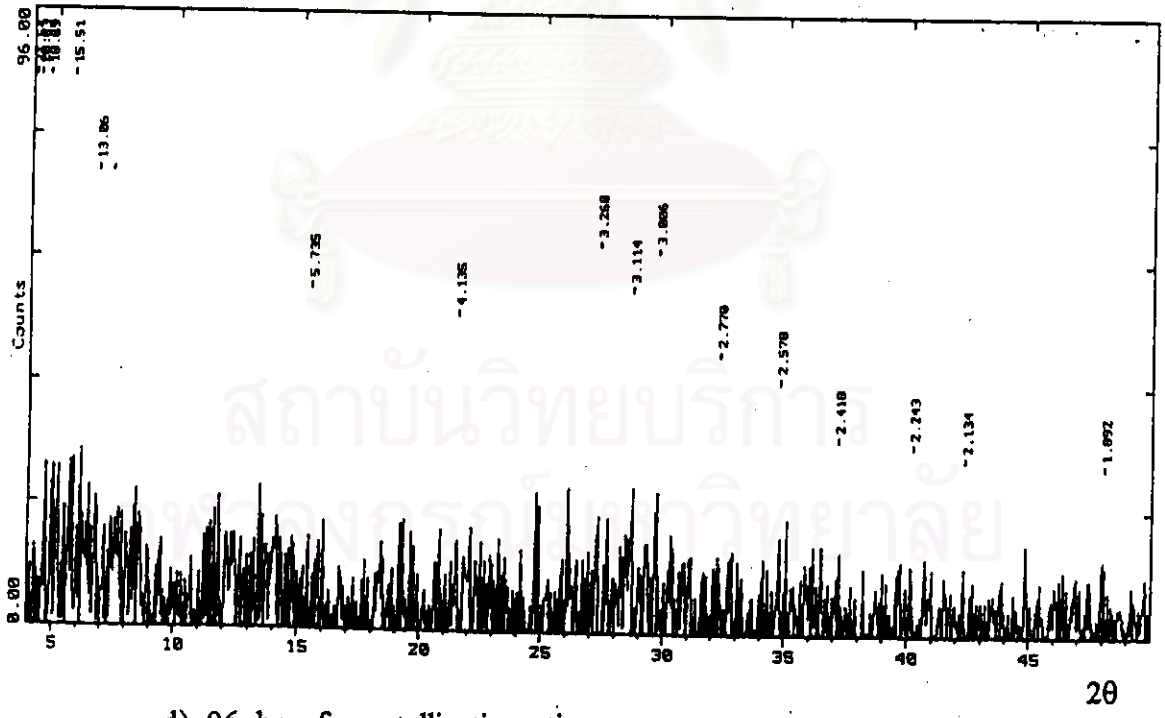

d) 96 hr of crystallization time

Figure 5.9 The XRD patterns of prepared catalysts at pH 11 for various crystallization times (continued)

growth of zeolite. However, with too high pH value, the poor crystallization of desirable NaY-type zeolite and the predominantly formed impurity phase were appeared. This may be explained that too high concentration of OH^- brought about the dissolution of Si and Al species and transform the former phase to another phase.

5.1.3 Effect of crystallization temperature of NaY-type zeolite synthesis

As shown in Figure 5.10 and Figures 5.11 - 5.13, the degree of crystallization and the XRD patterns of catalysts with H_2O/SiO_2 ratios of 46.25 and gel mixture pH of 13.7 prepared by using different crystallization temperatures are illustrated.

The excellent monophasic and highest crystallization degree of the desirable NaY-type zeolite was observed at crystallization temperature of 95 °C for 48 h. The further crystallization longer than 48 h caused the lower of the degree of crystallization with some impurity phases formed. The crystallization degree of the catalyst crystallized temperature of 85 °C was substantially maintained during 48 - 96 h.; however, the crystallization degree was less than that of the catalyst crystallized at 95 °C for 48 h. When the temperature was raised to 105 °C not only poor crystallization of NaY - type zeolite but also the predominantly formed impurity phase were observed from XRD pattern. After 96 h of the crystallization time, no characteristic peak of NaY-type zeolite but only impurity phase were obtained. It should be noted that NaY-type zeolite may crystallize within short period at high crystallization temperature, 105 °C. However, the XRD patterns during less than 24 h were not observed. These were recommended for further study.

It has been generally accepted that the crystallization temperature strongly influence the activation energy (E_a) required for the zeolite crystallization; E_a relates to condensation reaction between the crystal surface

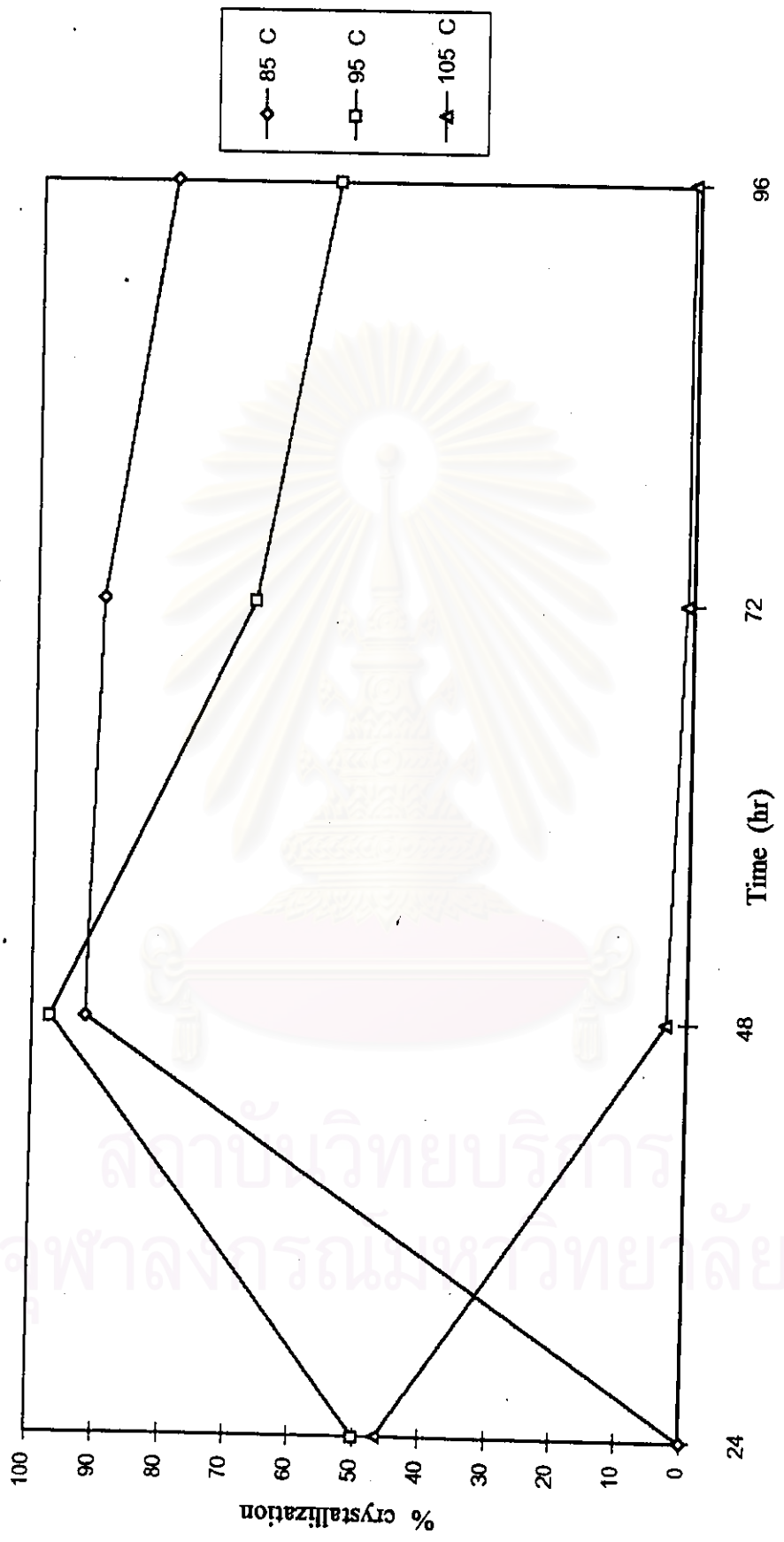

Figure 5.10 The degree of crystallization of prepared catalysts at different crystallization temperatures for various crystallization times

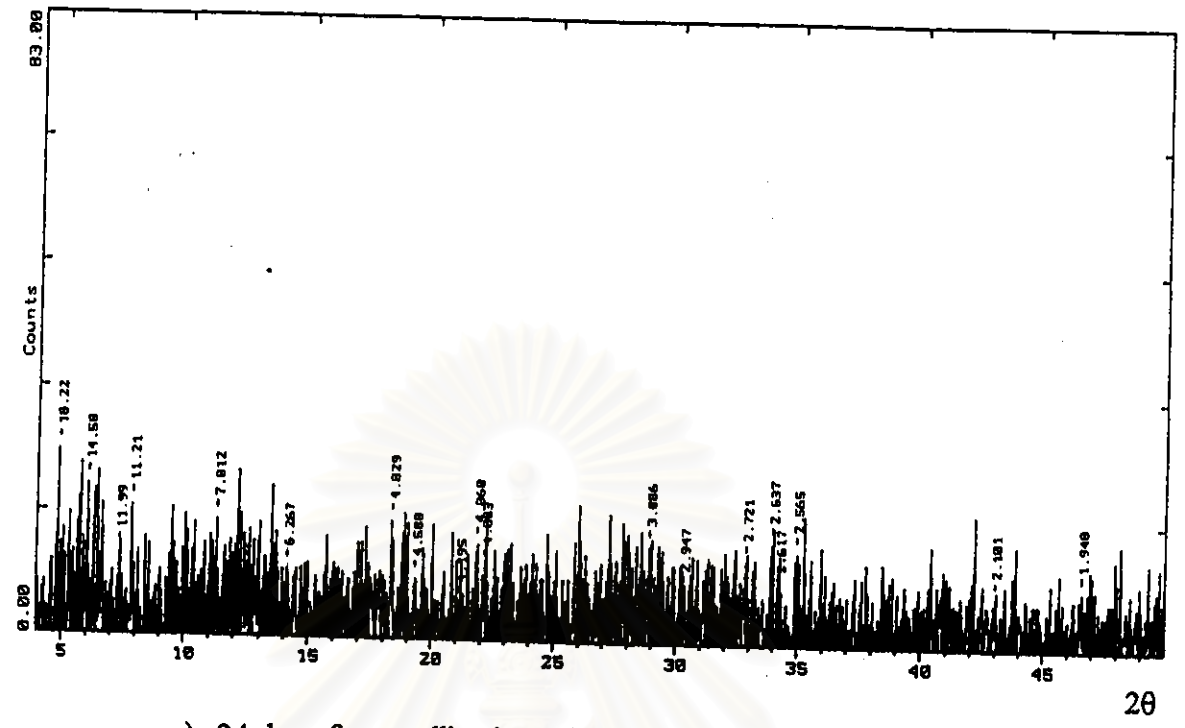

a) 24 hr of crystallization time

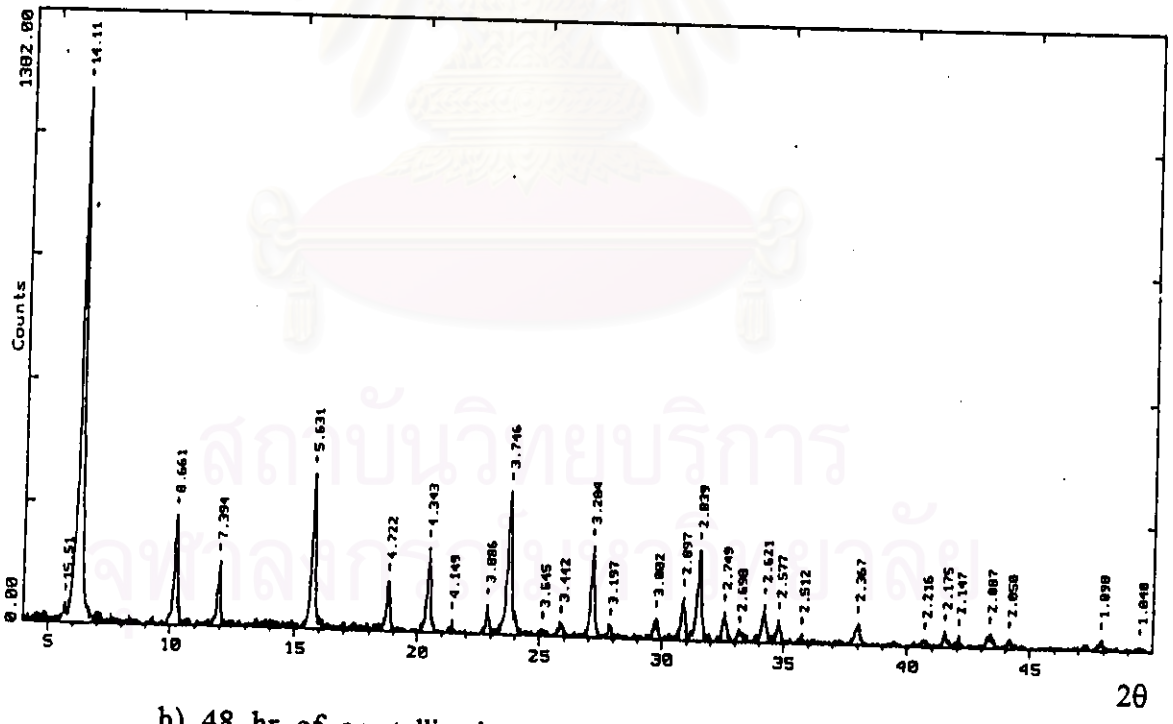

b) 48 hr of crystallization time

Figure 5.11 The XRD patterns of prepared catalysts at crystallization temperature of 85°C for various crystallization times

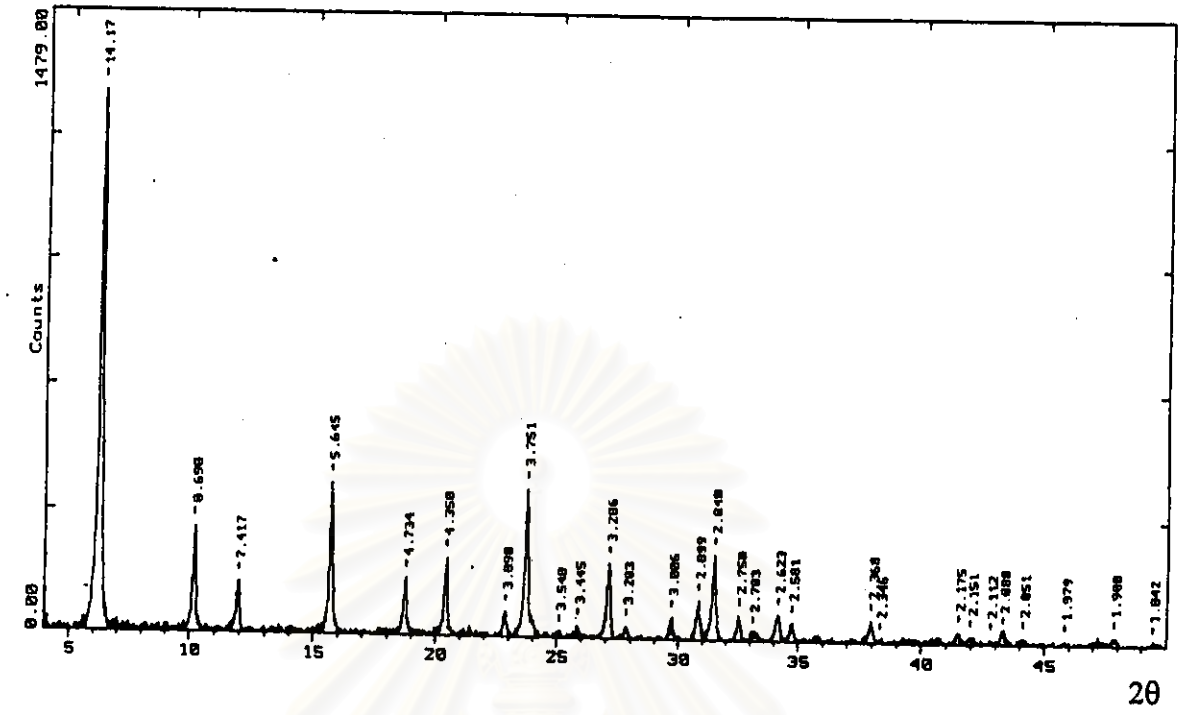

c) 72 hr of crystallization time

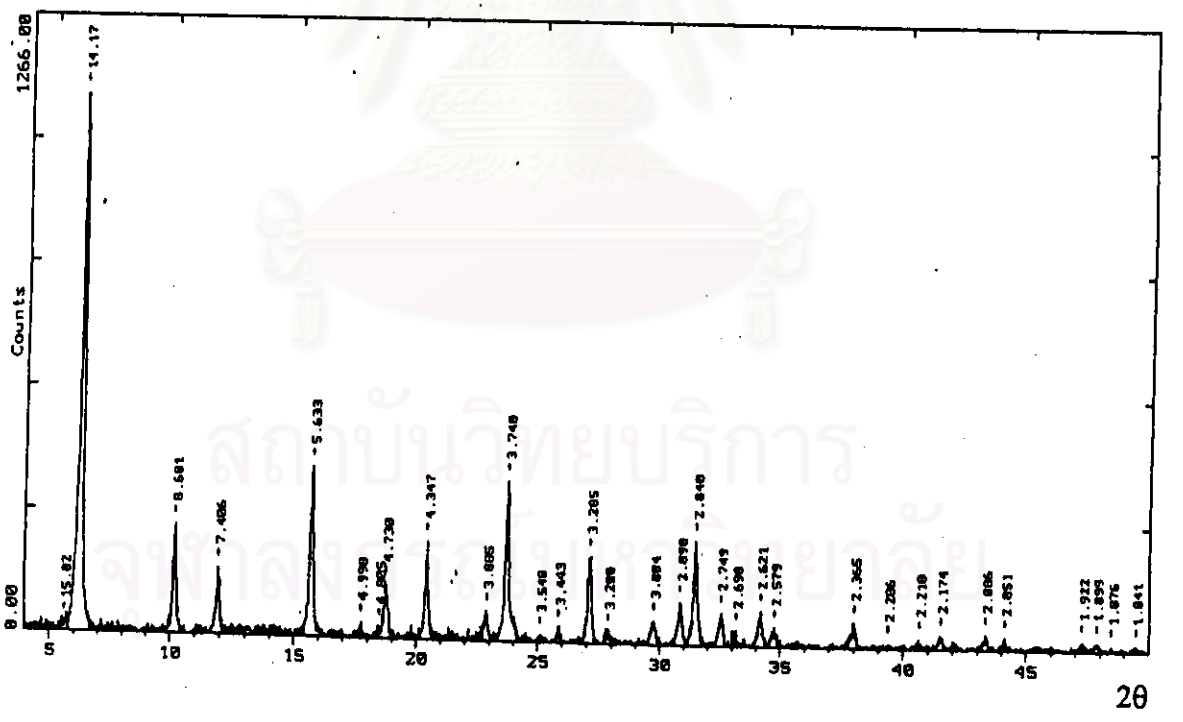

d) 96 hr of crystallization time

Figure 5.11 The XRD patterns of prepared catalysts at crystallization temperature of 85°C for various crystallization times (continued)

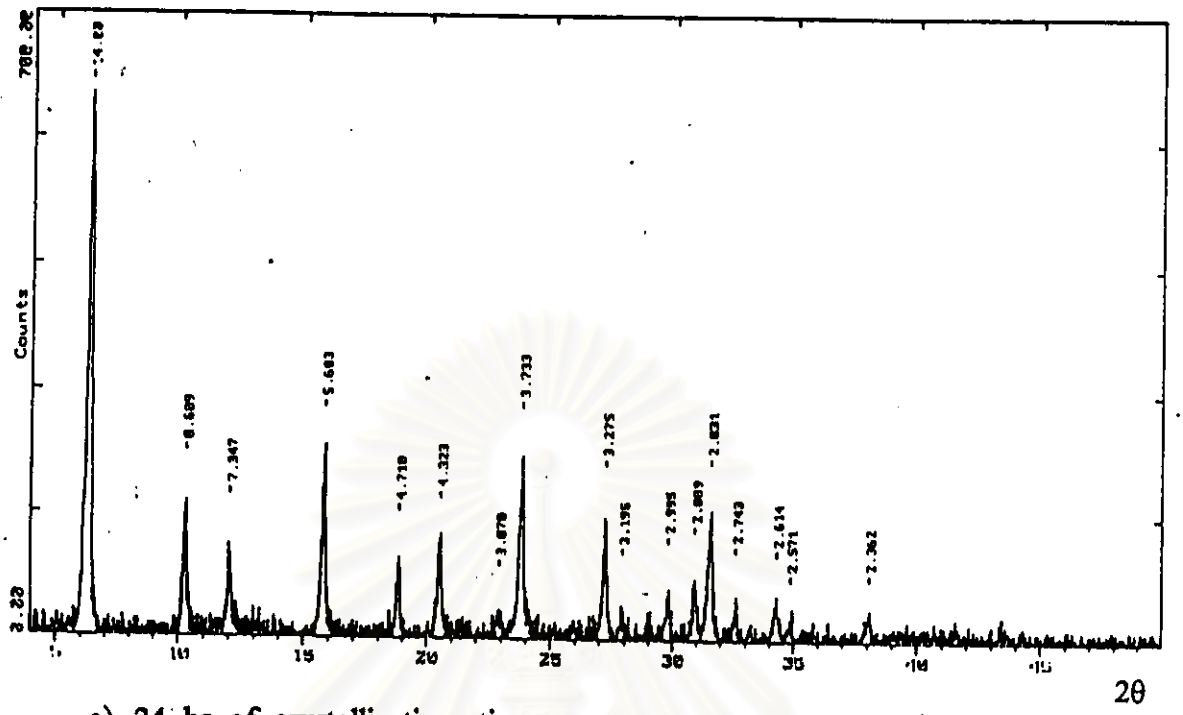

a) 24 hr of crystallization time

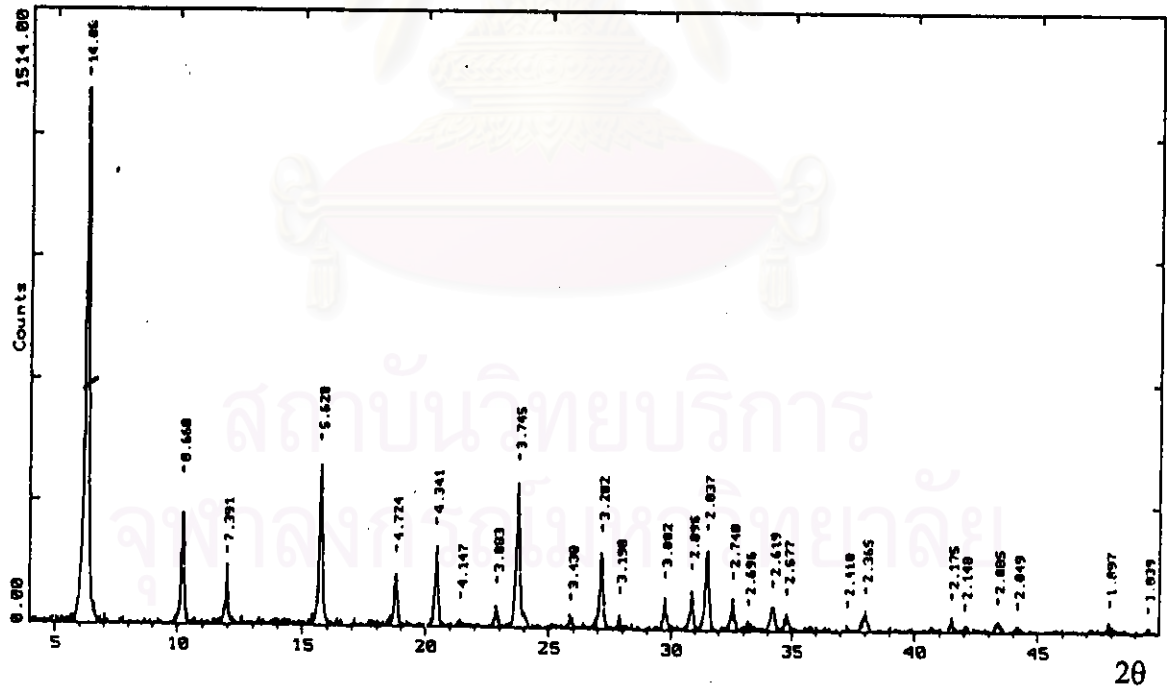

b) 48 hr of crystallization time

Figure 5.12 The XRD patterns of prepared catalysts at crystallization temperature of 95°C for various crystallization times

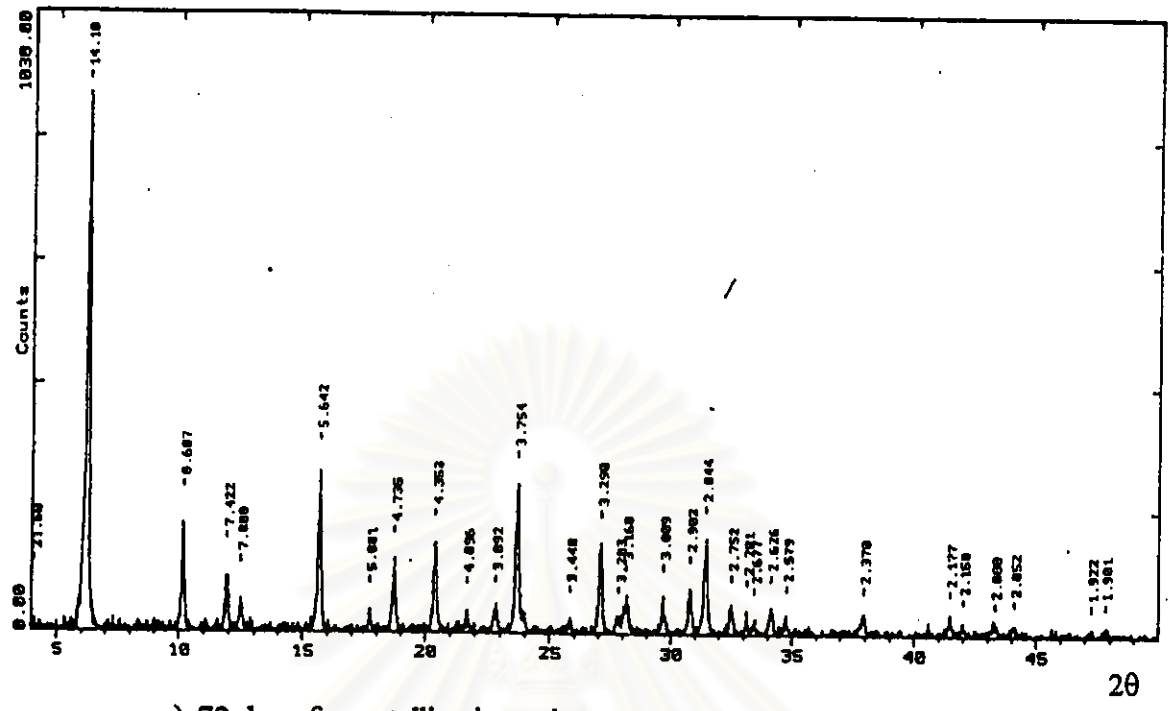

c) 72 hr of crystallization time

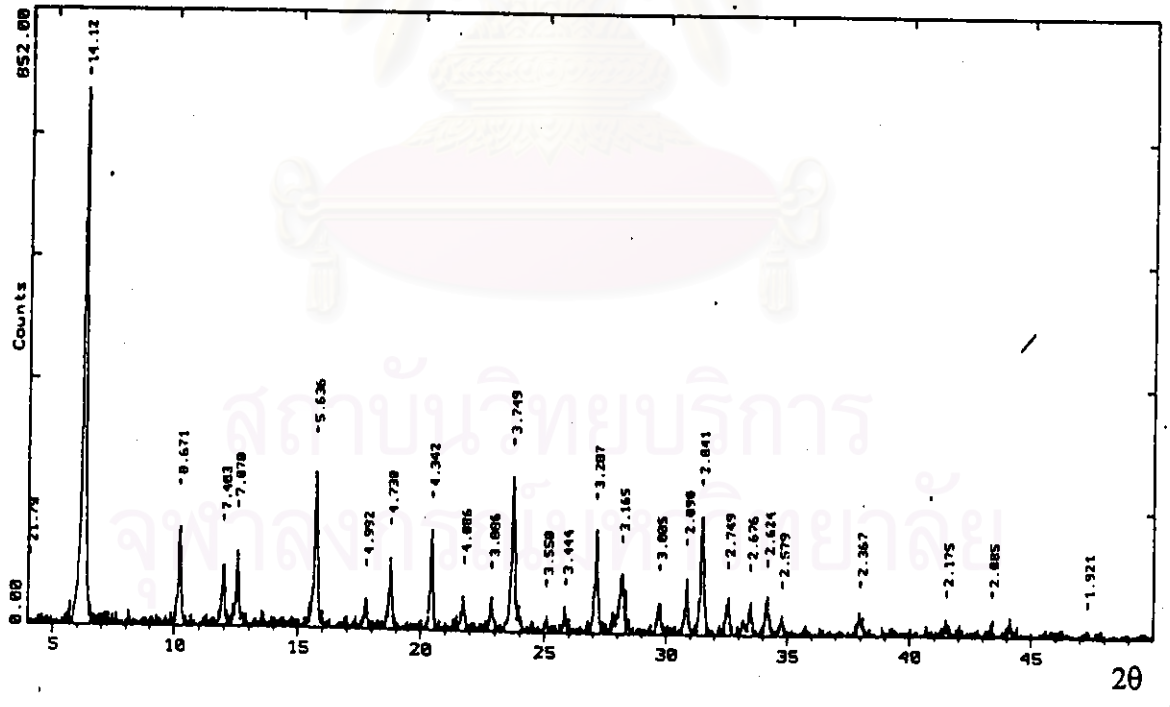

d) 96 hr of crystallization time

Figure 5.12 The XRD patterns of prepared catalysts at crystallization temperature of 95°C for various crystallization times (continued)

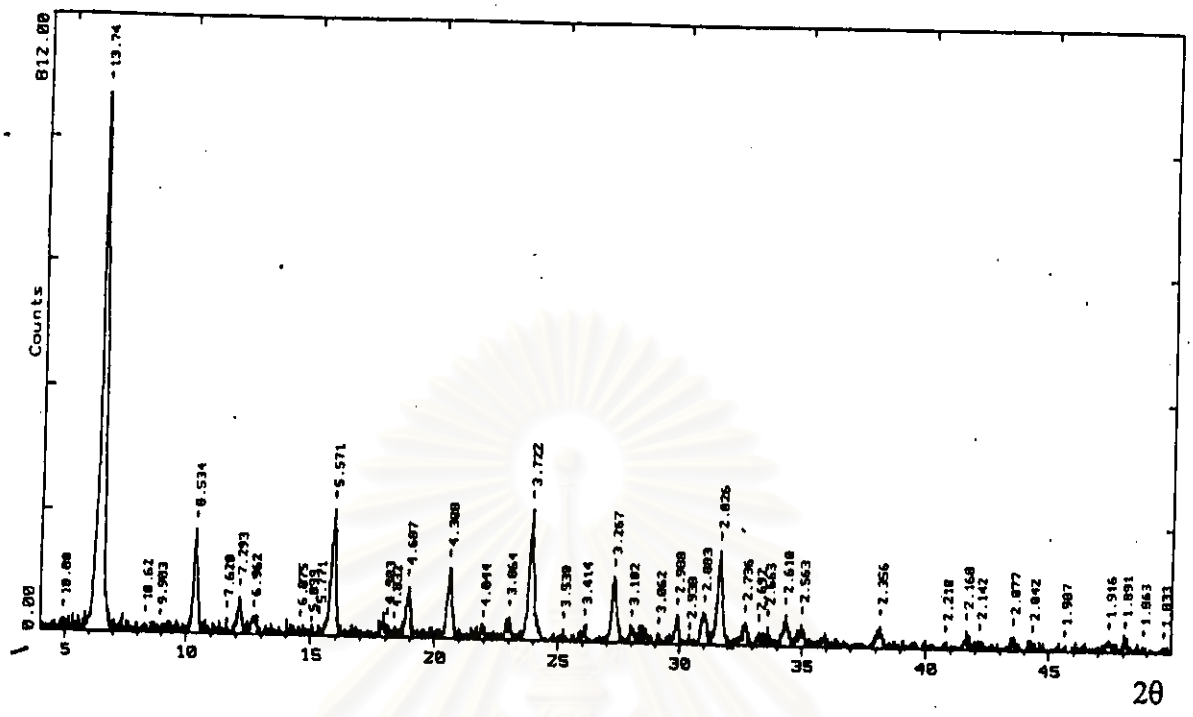

a) 24 hr of crystallization time

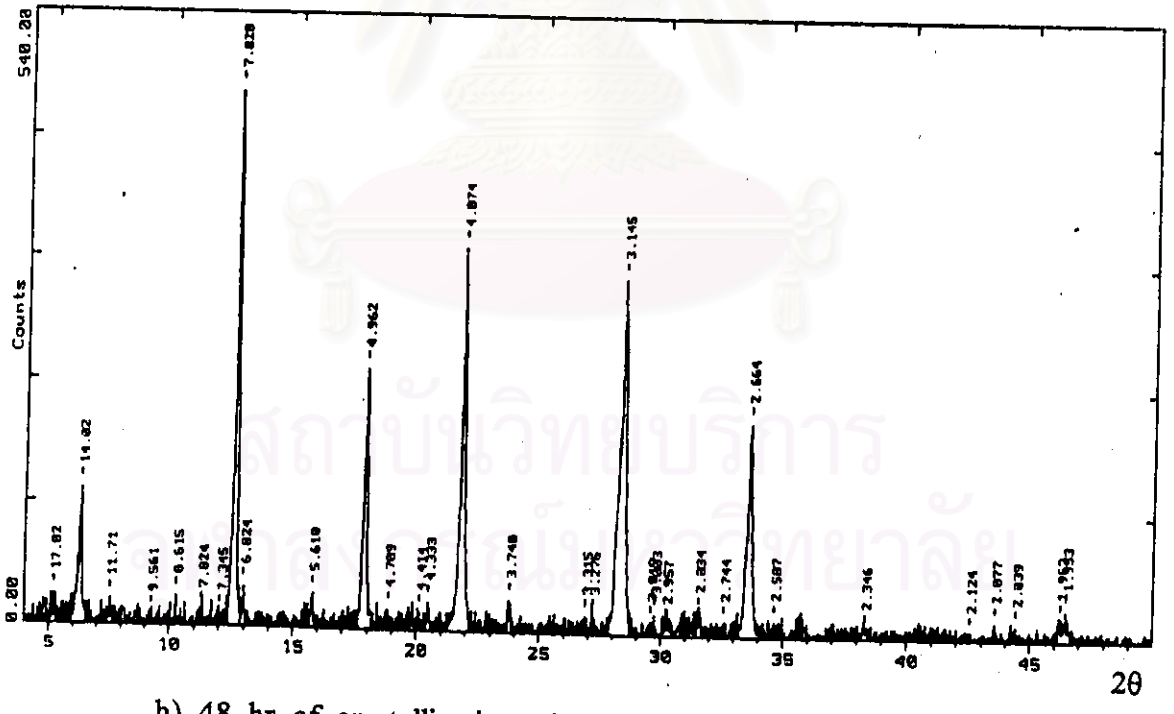

b) 48 hr of crystallization time

Figure 5.13 The XRD patterns of prepared catalysts at crystallization temperature of 105°C for various crystallization times

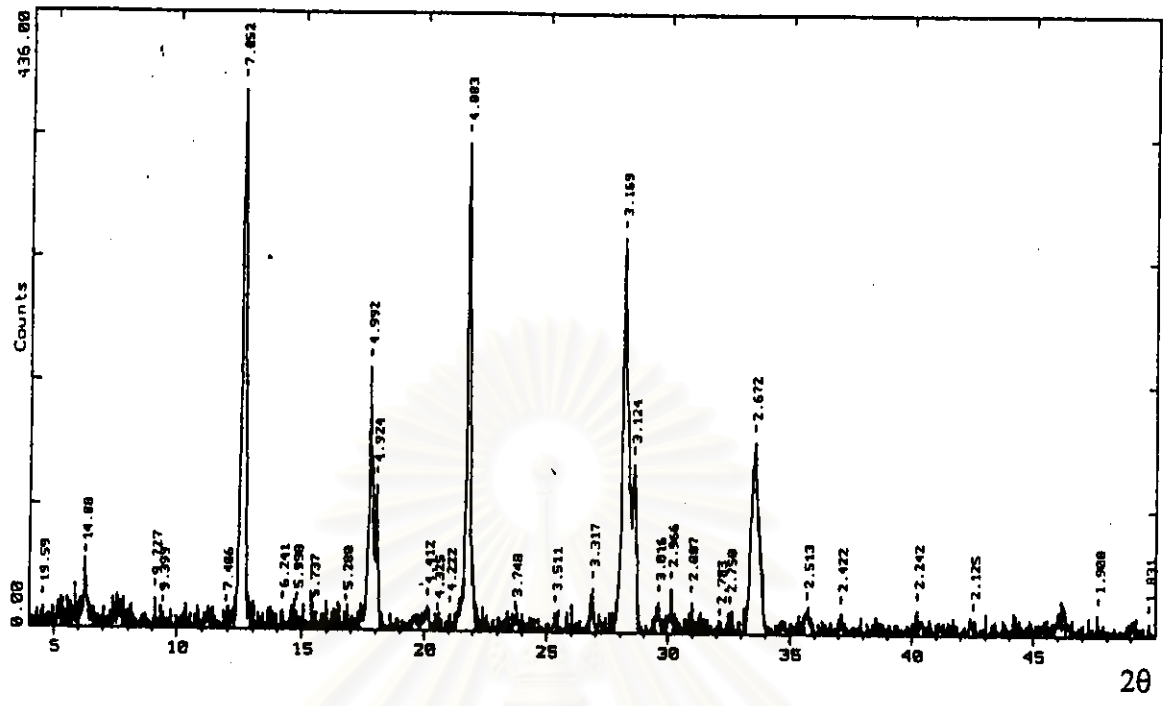

c) 72 hr of crystallization time

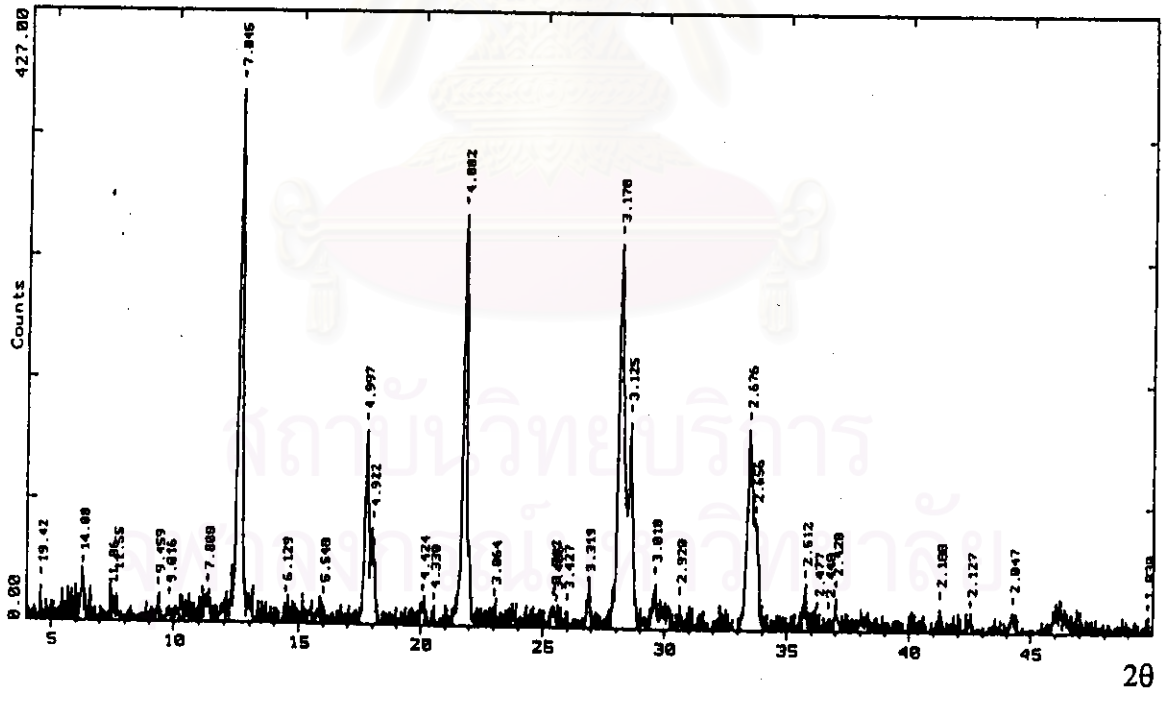

d). 96 hr of crystallization time

Figure 5.13 The XRD patterns of prepared catalysts at crystallization temperature of 105°C for various crystallization times (continued)

and crystal building unit (1). Hence, the appropriate crystallization temperature is crucial for perfectly desired product.

5.1.4 Comparison of XRD patterns of prepared catalyst with those of commercial catalyst

As shown in Figure 5.14, the XRD pattern of the optimum formula of NaY-type zeolite catalyst, i.e., H_2O/SiO_2 mole ratio of 43.5; pH 13.7; crystallization temperature of 95°C and 48 hr of crystallization time prepared in the laboratory, was almost similar to that of commercially available NaY-type zeolite " JRC-Z-Y". This indicates the successful synthesis of NaY-type zeolite catalyst with the structurally related to the natural mineral faujasite-type zeolite.

5.2 Specific Surface Area

The BET surface areas of the catalysts are shown in Table 5.1. The BET surface areas of optimum synthesized NaY-type zeolite catalyst and of commercial JRC-Z-Y zeolite were nearly in the same range. This is consistent with the above-mentioned result that the XRD pattern of optimum synthesized NaY-type zeolite catalyst is similar to that of JRC-Z-Y zeolite catalyst. When the specific BET surface areas of NH_4Y, HY zeolite catalysts have been considered, the specific BET surface area of NH_4Y was nearly similar to the specific BET surface area of NaY-type zeolite. However, the specific BET surface area of HY was less than that of NaY -type zeolite catalyst. This may be due to some collapse of the framework structure or some blockage of pore channels by ion-exchanging. These expectations are confirmed by the comparison of XRD patterns of these catalysts, as shown in Figure 5.15. The less BET surface area of catalyst correspond to the lower intensity of XRD pattern which reflects the lower crystallinity of crystal.

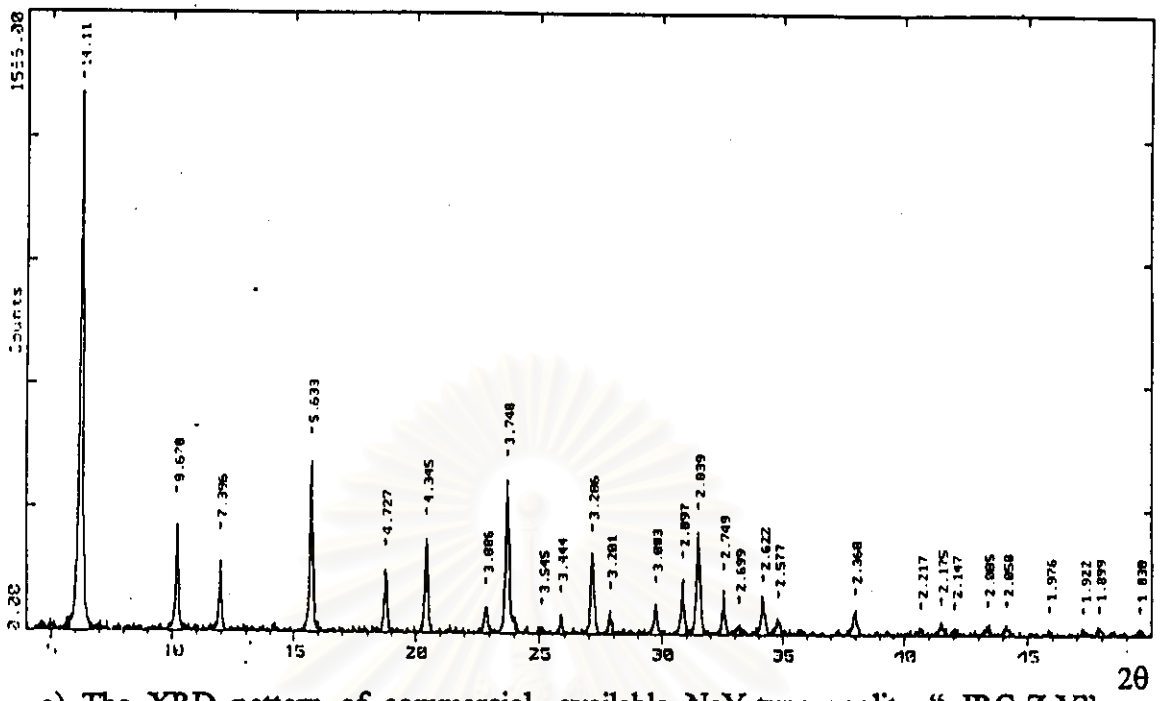

a) The XRD pattern of commercial available NaY-type zeolite " JRC-Z-Y"

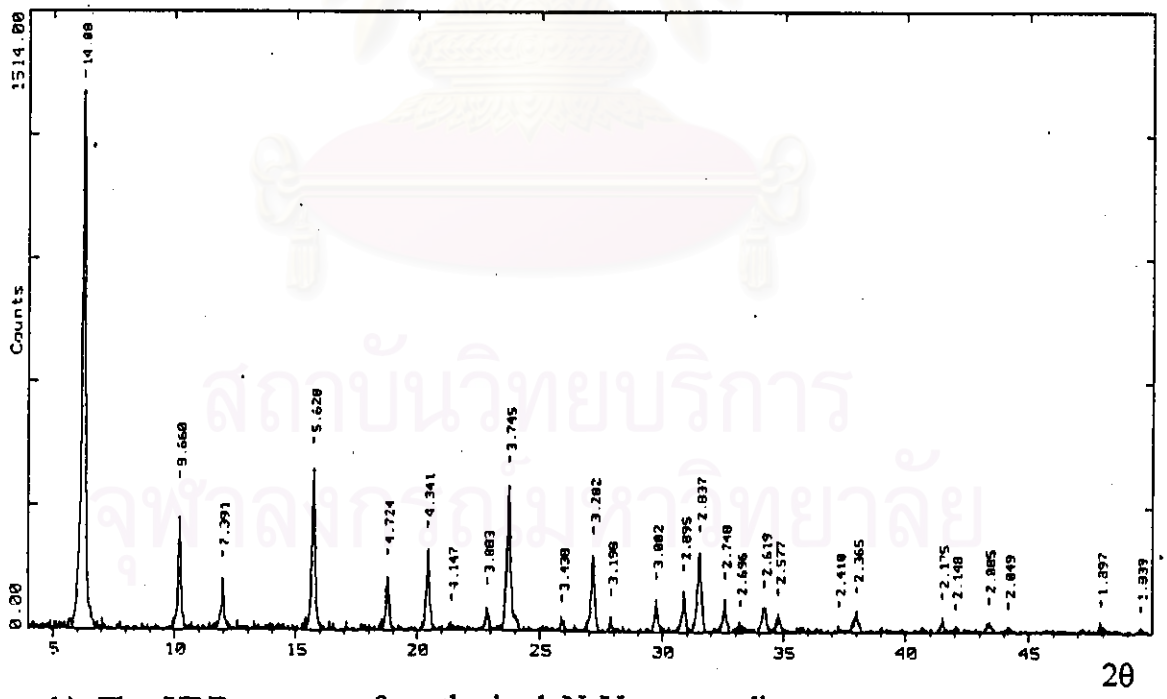

b) The XRD pattern of synthesized NaY-type zeolite

Figure 5.14 The comparison of XRD pattern of synthesized NaY-type zeolite with those of commercial available NaY-type zeolite " JRC-Z-Y"

Table 5.1 BET surface areas of the catalysts

Catalyst	BET surface areas (m^2/g of catalyst)
JRC-Z-Y	758
NaY	725
NH_4Y	705
HY	637

5.3 Morphology

Morphologies of the catalysts were observed with scanning electron microscope (SEM). SEM photographs of the catalysts are shown in Figure 5.16. All the catalysts were composed of crystals in approximately uniform size. This crystal habit is typical for the faujasite structure.

5.4 Acidity

The TPD profiles of desorbed ammonia from NaY, HY, NH_4Y and H-JRC-Z-Y (proton type of commercial JRC-Z-Y zeolite) zeolite catalysts are shown in Figure 5.17. The similarity of NH_3-TPD profiles of HY and HJRC-Z-Y zeolite catalysts was observed. These profiles did not clearly show the high temperature peaks, approximately 350 °C, mostly the low temperature were obviously observed around 180°C. However, as for HY and H-JRC-Z-Y, the higher temperature peaks around 350 °C were rather noticeable. As the low temperature peaks and high temperature peaks were assigned to weak and strong acid sites, respectively, it can be understood that HY and H-JRC-Z-Y contained more strong acid sites than the others.

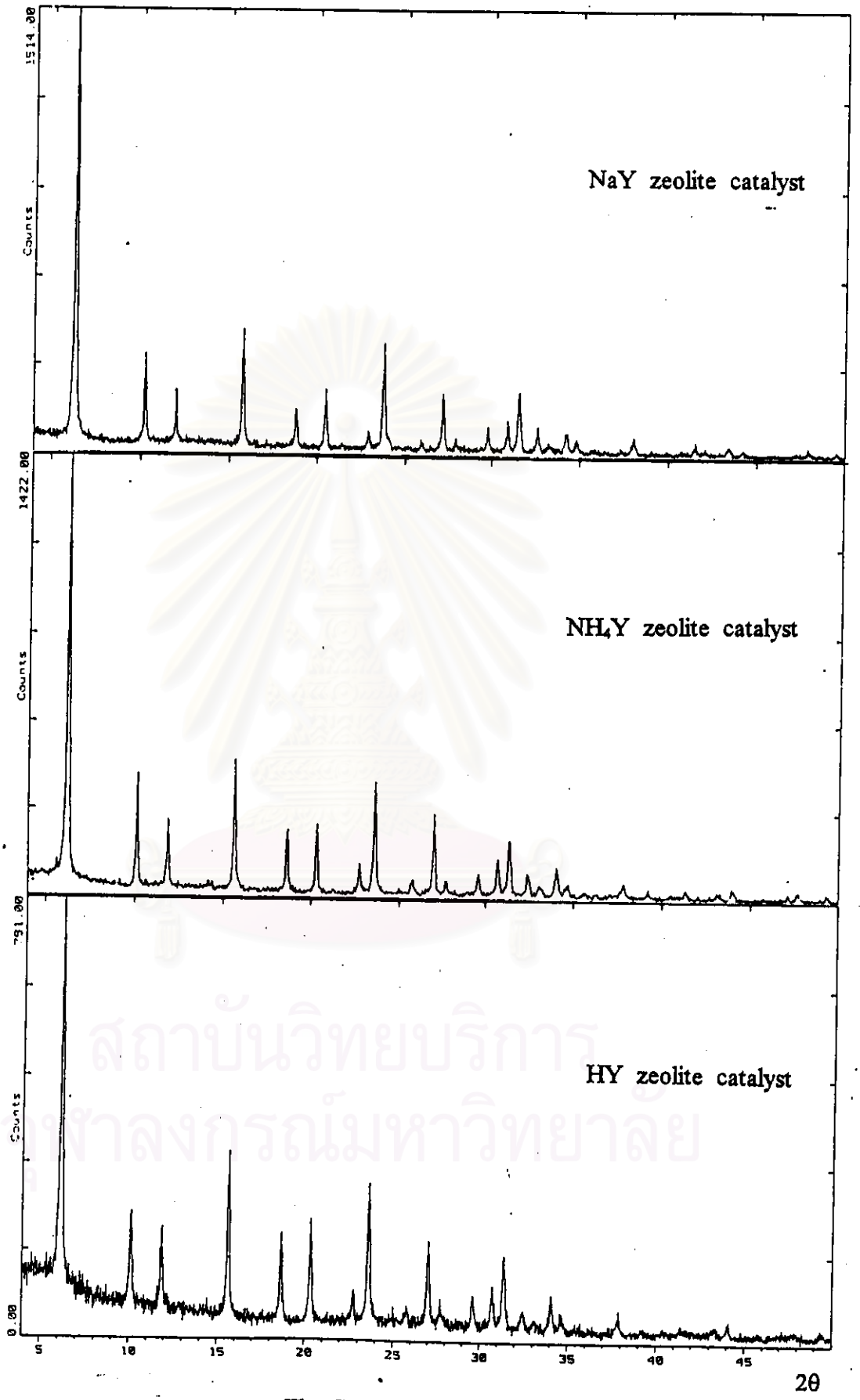

Figure 5.15 The XRD patterns of the catalysts

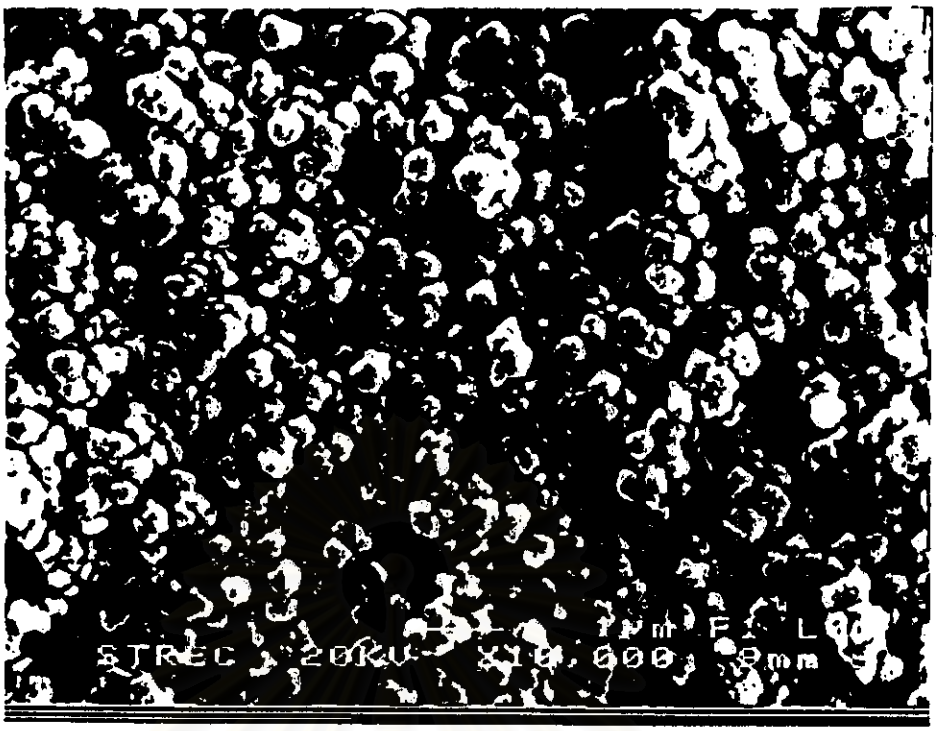

a) NaY zeolite catalyst

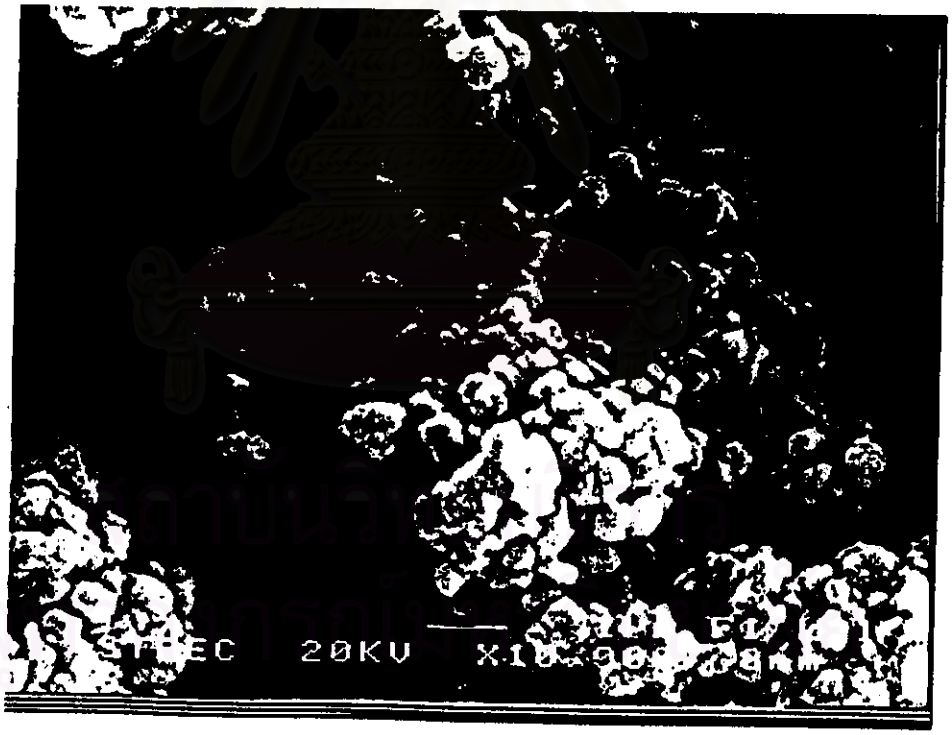

b) NH_4Y zeolite catalyst

Figure 5.16 SEM photographs of the catalysts

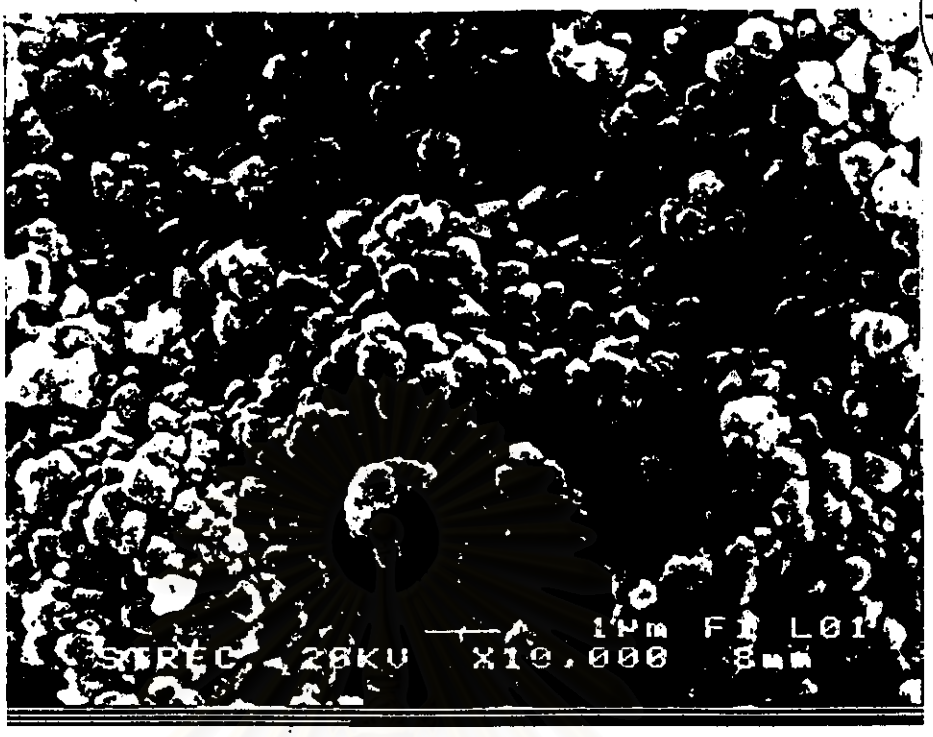

c) HY zeolite catalyst

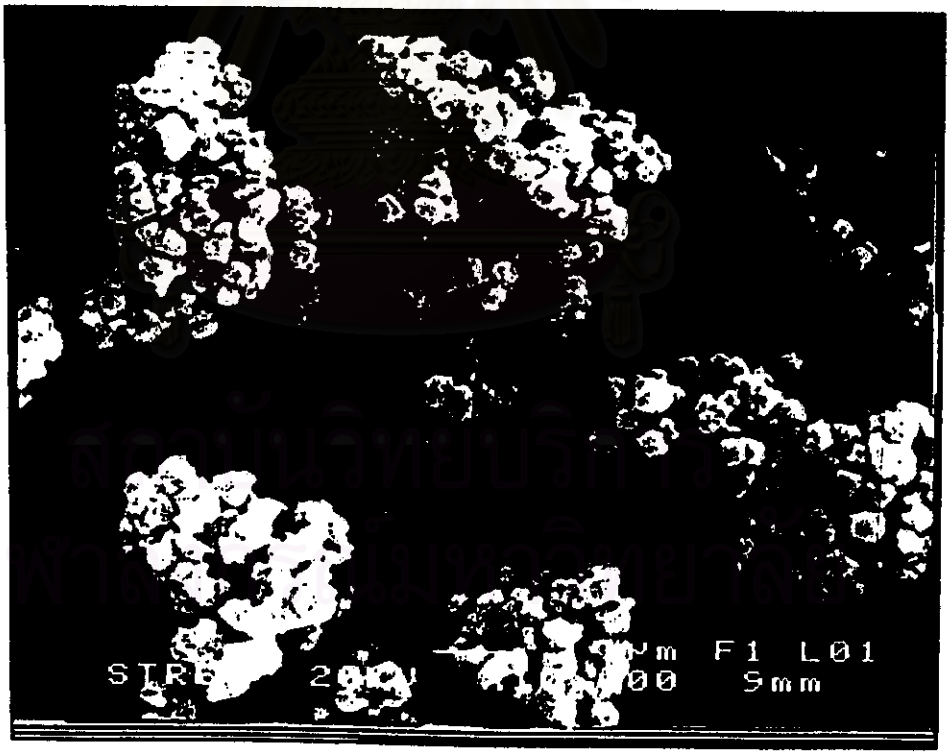

d) commercial JRC-Z-Y zeolite catalyst

Figure 5.16 SEM photographs of the catalysts (continued)

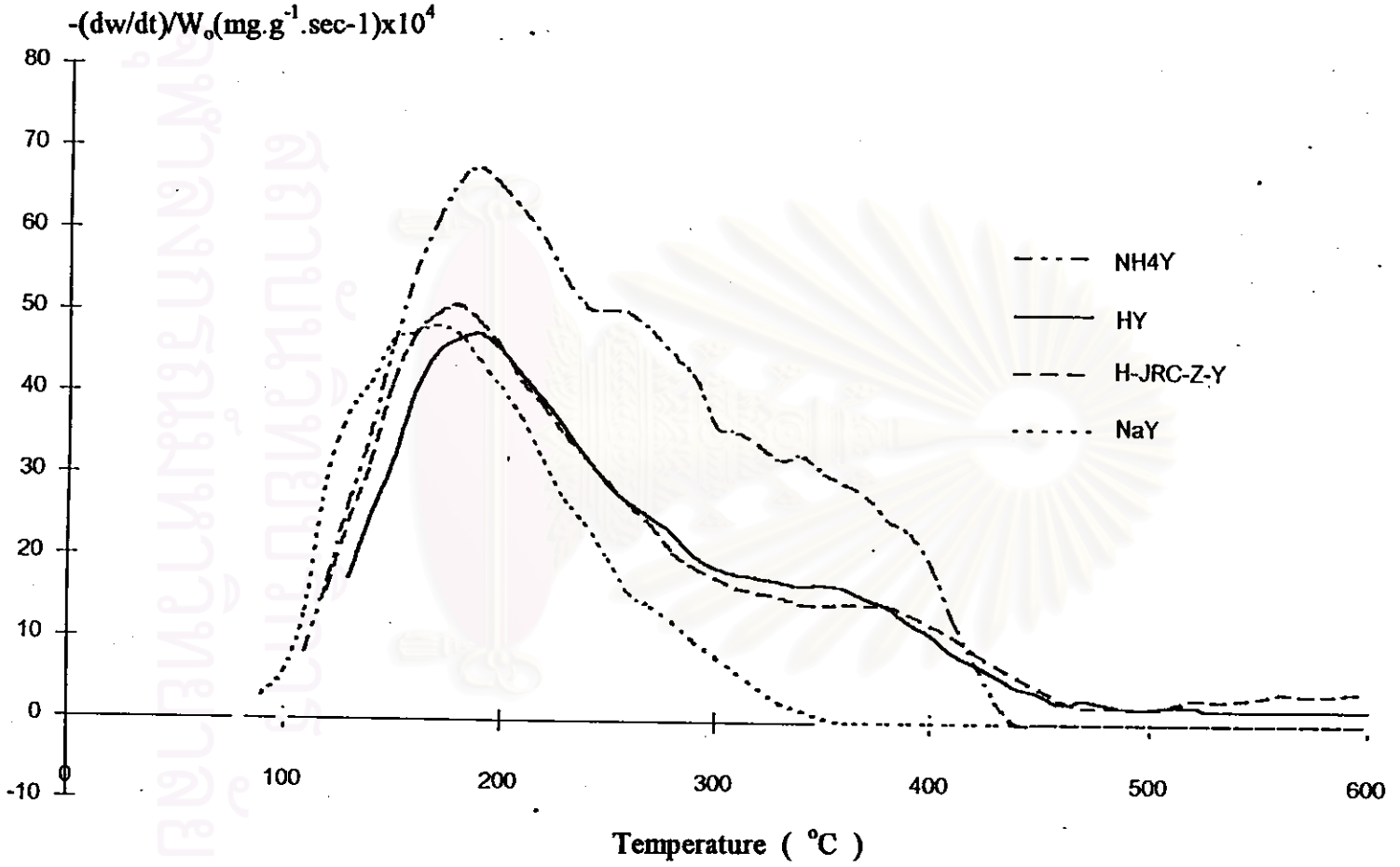

Figure 5.17 TPD profiles of desorbed NH_3 from the catalysts

5.5 Catalytic Cracking Reaction of n-Octane Hydrocarbon

5.5.1 Effect of GHSV on n-octane cracking

The conversion of n-octane and product distribution obtained were at 500 °C , The results obtained from varying space velocities, 1000 to 5000 h^{-1} ,30 min on stream are shown in Figures 5.18 a to 5.18 c. The n-octane conversion decreased with the increasing GHSV due to less contact time. As for the product distribution shown in Figure 5.18 a , it has been found that ethene and propene amount significantly decreased with the higher GHSV. On the other hand , the higher amount of iso-butane, butene, and iso-pentane were obtained at the increasing GHSV. Although various mechanisms of n-octane cracking have been suggested by many researches, the generally accepted one is as follows (15) :

Step 1 : Mild thermal cracking initiation reaction

$$nC_8H_{18} \rightarrow CH_4 + R\text{-}CH{=}CH_2$$

Step 2 : Proton shift

$$R\text{-}CH{=}CH_2 + [\,H\text{-}Zeolite] \rightarrow R\text{-}\overset{+}{C}H\text{-}CH_3 + [\,Zeolite^-\,]$$

Step 3 : Beta scission

$$R\text{-}\overset{+}{C}H\text{-}CH_3 \rightarrow CH_3CH_2{=}CH_2 + \overset{+}{C}H_2CH_2\,CH_2\,CH_3$$

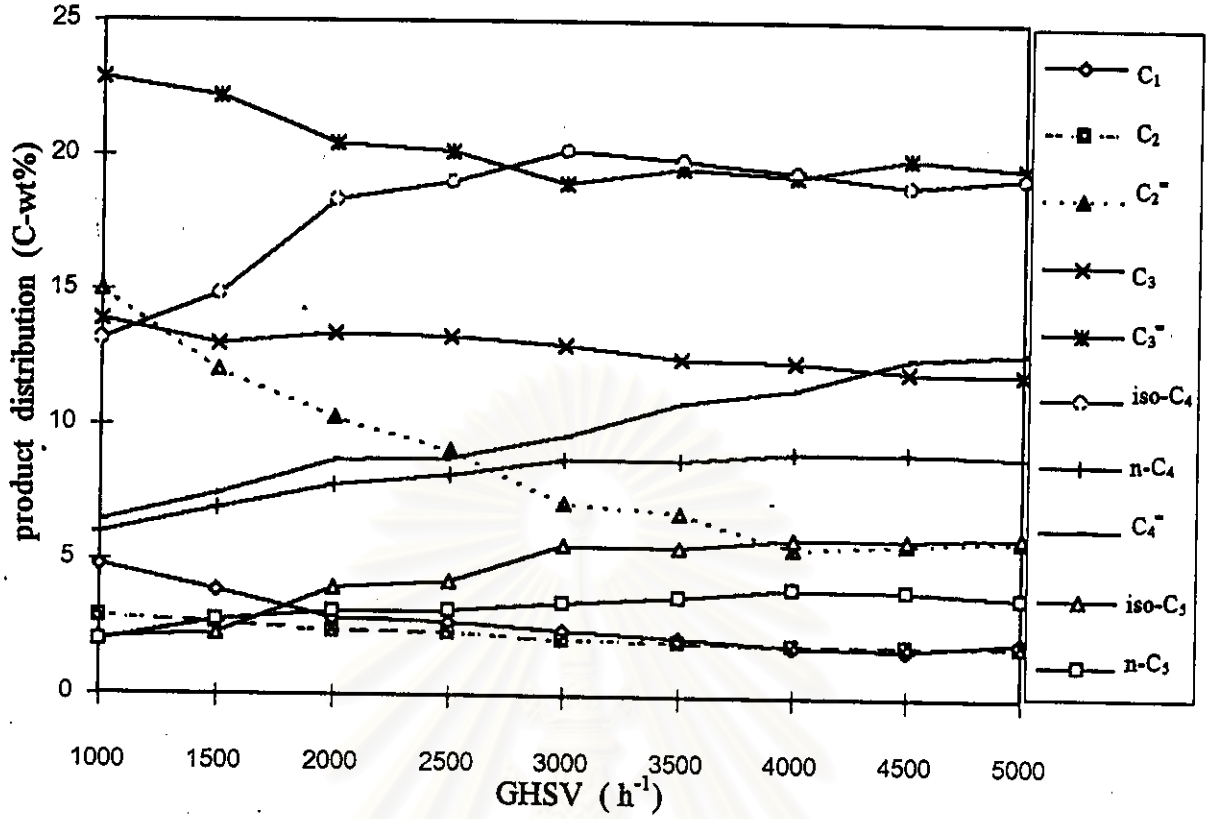

a) the C_1 - C_5 product distribution

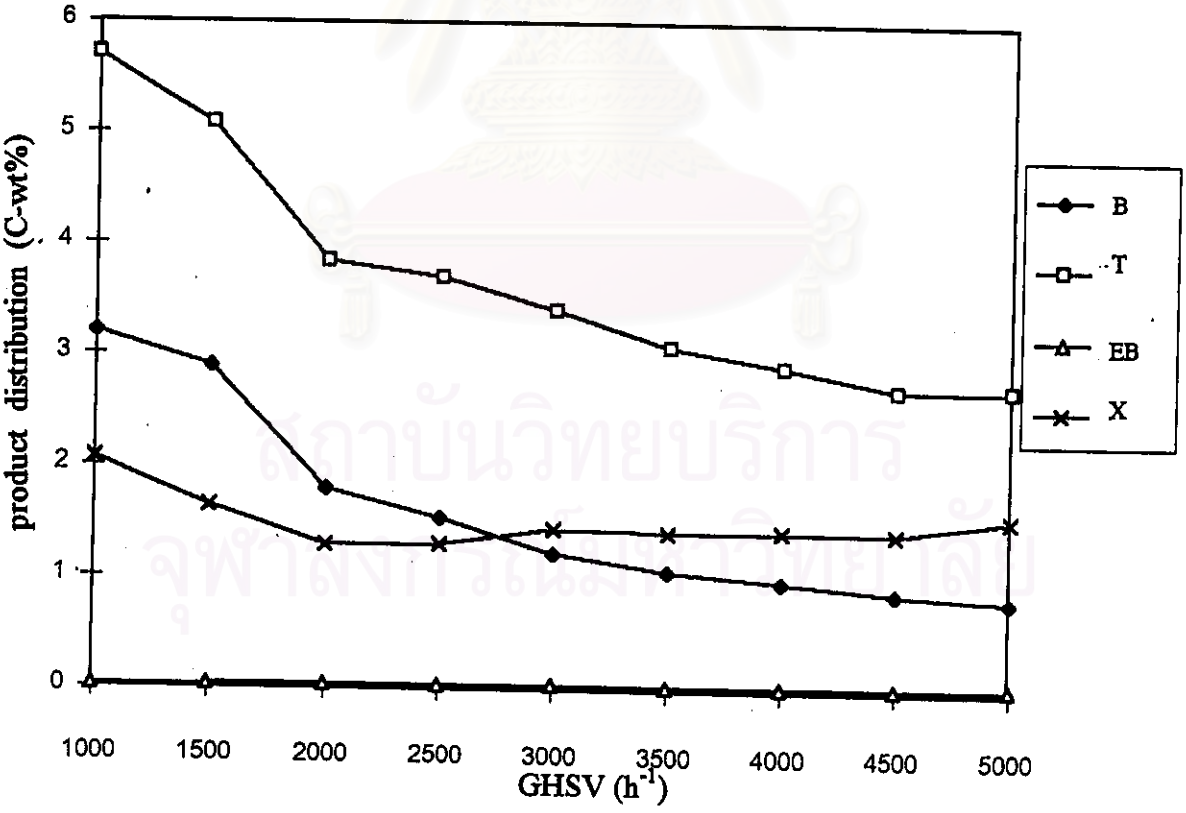

b) the aromatic product distribution

Figure 5.18 Catalytic cracking of n-octane on HY zeolite catalyst at various space velocities

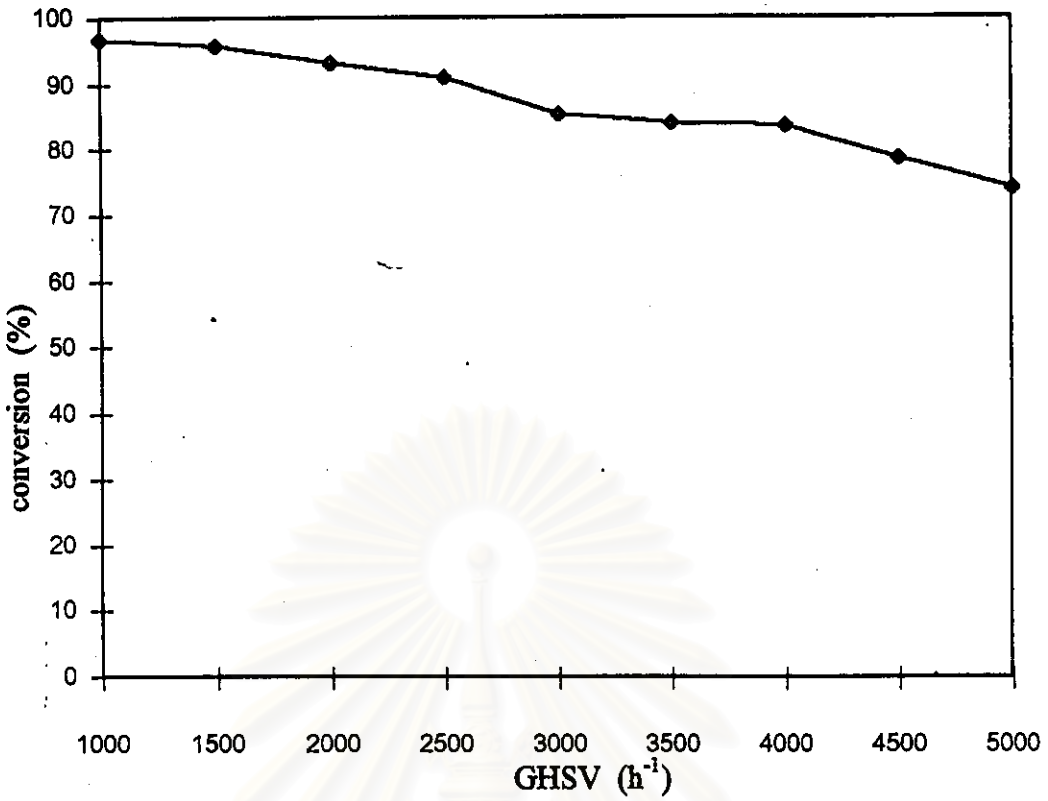

c) n-octane conversion

Figure 5.18 Catalytic cracking of n-octane on HY zeolite catalyst at various space velocities (continued)

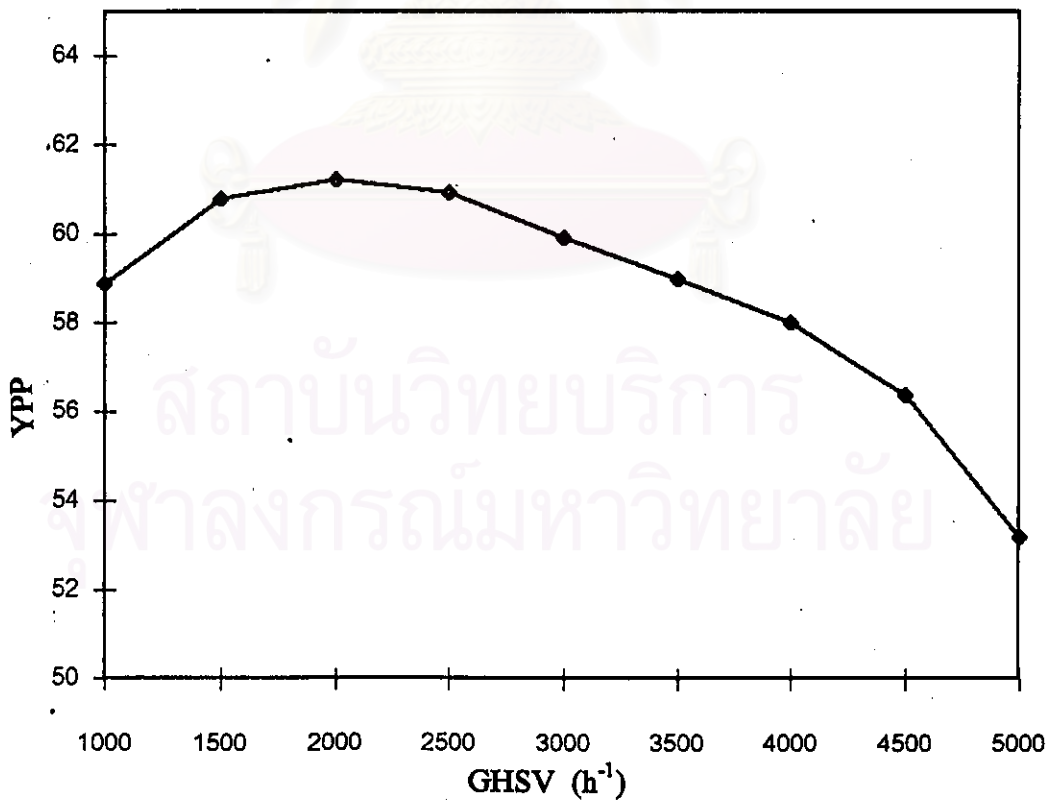

Figure 5.19 The GHSV effect on YPP yield of n-octane cracking on HY zeolite catalyst .

Step 4 : Rearrangement toward more stable structure.

The order of carbonium ion stability is tertiary > secondary > primary

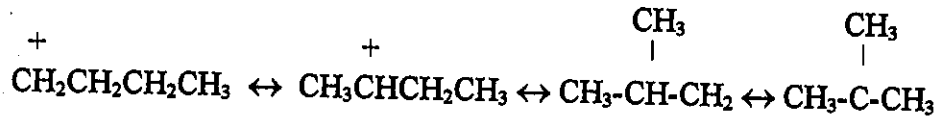

Step 5 : Hydrogen ion transfer

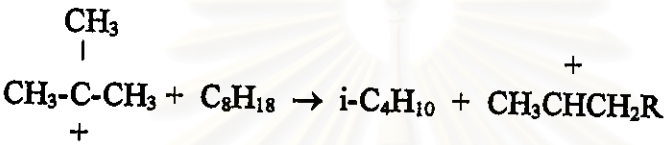

The carbonium ion was formed initially by mild thermal cracking of n-octane hydrocarbon to methane and 1-heptene molecules. The latter molecule was added with a proton from the catalyst to form a large carbonium ion which decomposes according to the beta rule (carbon-carbon bond scission takes place at the carbon in the position beta to the carbonium ion) to form a smaller carbonium ion and propylene. The smaller carbomiun ion rearrange toward more stable structure, tertiary carbonium ion. Then, the tertiary carbonium ion propagates the chain reaction by accepting a hydrogen ion transferred from another n-octane molecule to form isobutane molecule and new large carbonium ion. Thus another large carbonium ion is formed and the chain is ready to repeat itself.

When the above-mentioned mechanism has been considered , it can be understood that much more propene amount was formed at the given temperature during the longer contact time (or low GHSV) via β-scission of the repeated cycles of catalytic cracking. It has been expected that such products as isobutane, butene, and isopentane may proceed further cracking

reaction during the long contact time to light paraffin products. Though the catalytic cracking was believed to be the main reaction occurred, the thermal cracking at sufficiently high temperature should not be ruled out. It has been accepted that ethene can be easily formed by thermal cracking especially at high temperature around 500-600 °C and enough long contact time (17). The effect of thermal cracking will be discussed later.

As shown in Figure 5.18 b, the selectivity for aromatic was substantially decreased with the increasing GHSV. This should be ascribed to the short contact time at high GHSV, and therefore less aromatics were formed via aromatization of higher olefins. It may be concluded that the optimum GHSV for the maximum yield per pass (YPP) was 2000 h^{-1} as shown in Figure 5.19. The YPP of desired product group included $C_3^=$, iso-C_4 , n-C_4, $C_4^=$ iso-C_5 , benzene, tolulene, ethylbenzene , xylene.

5.5.2 Effect of reaction temperature on n-octane cracking

The n-octane conversion and product distribution obtained at 2000 h^{-1}, 30 min on stream are shown in Figures 5.20 a to 5.20 c. The reaction temperatures were varied ranging from 300 to 600 °C. The conversion of n-ocatne increased with the higher reaction temperature as shown in Figure 5.20 c. It has been obviously shown in Figure 5.20 a that the amounts of isobutane and isopentane markedly decreased with the higher reaction temperature . This should be attributed to the further cracking at high reaction temperature. The higher amounts of ethene and propene at reaction temperature above 450 °C were expected to be formed through thermal cracking in addition to catalytic cracking.

To investigate the effect of thermal cracking, the blank test was carried out at different temperatures during 450 to 600°C by using the same reaction conditions as mentioned above. The result shown in Table 5.2 reveals that

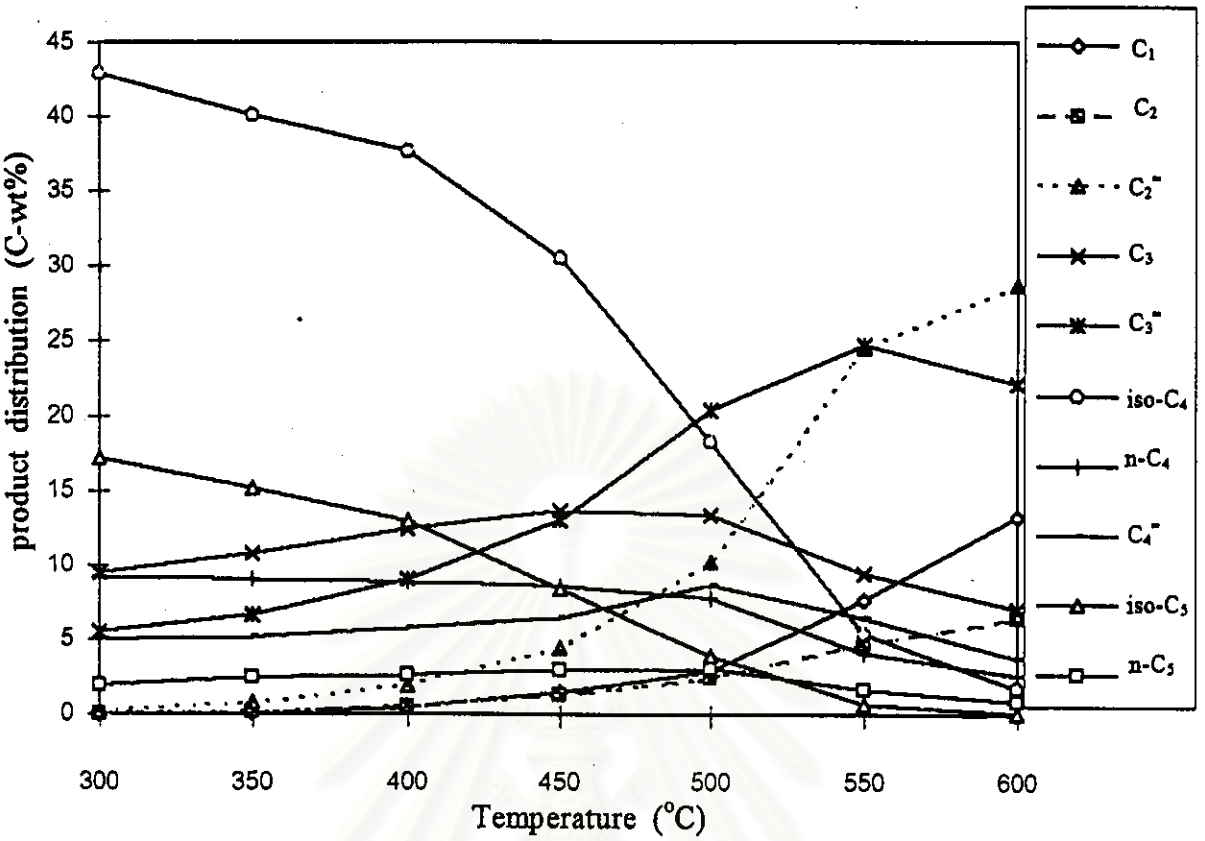

a) the C_1 - C_5 product distribution

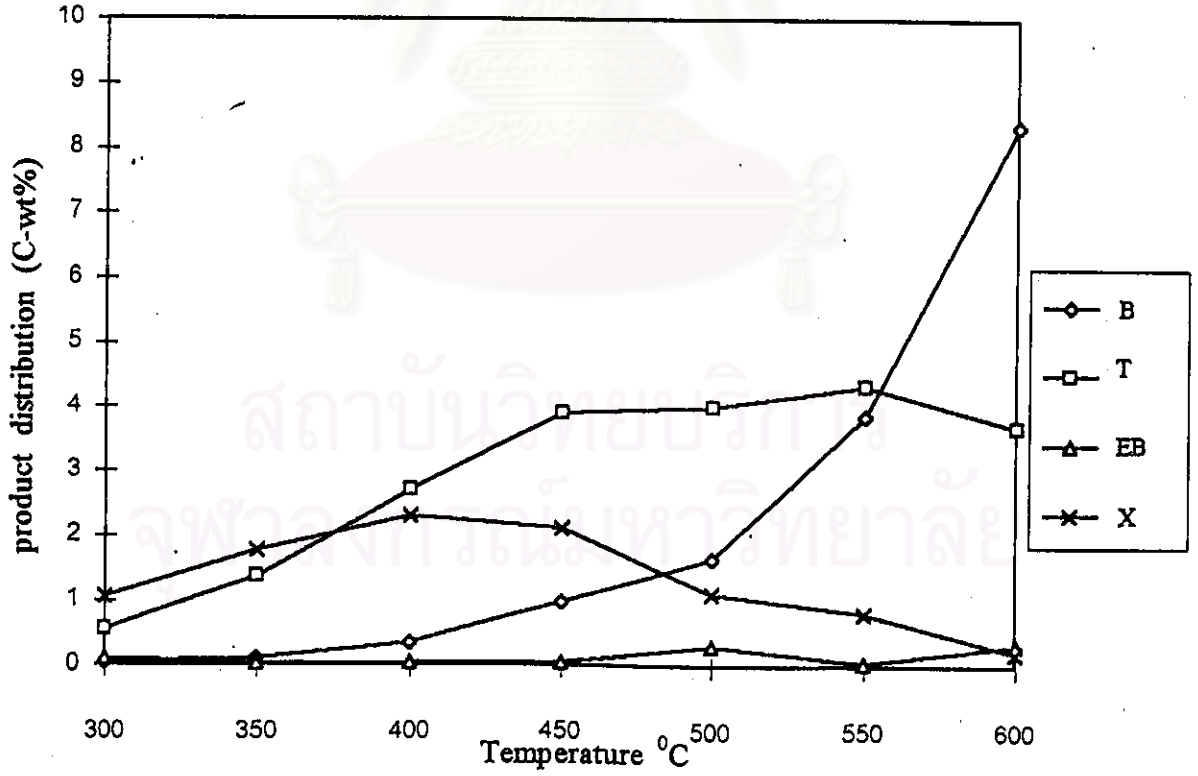

b) the aromatic product distribution

Figure 5.20 Catalytic cracking of n-octane on HY zeolite catalyst at various reaction temperatures

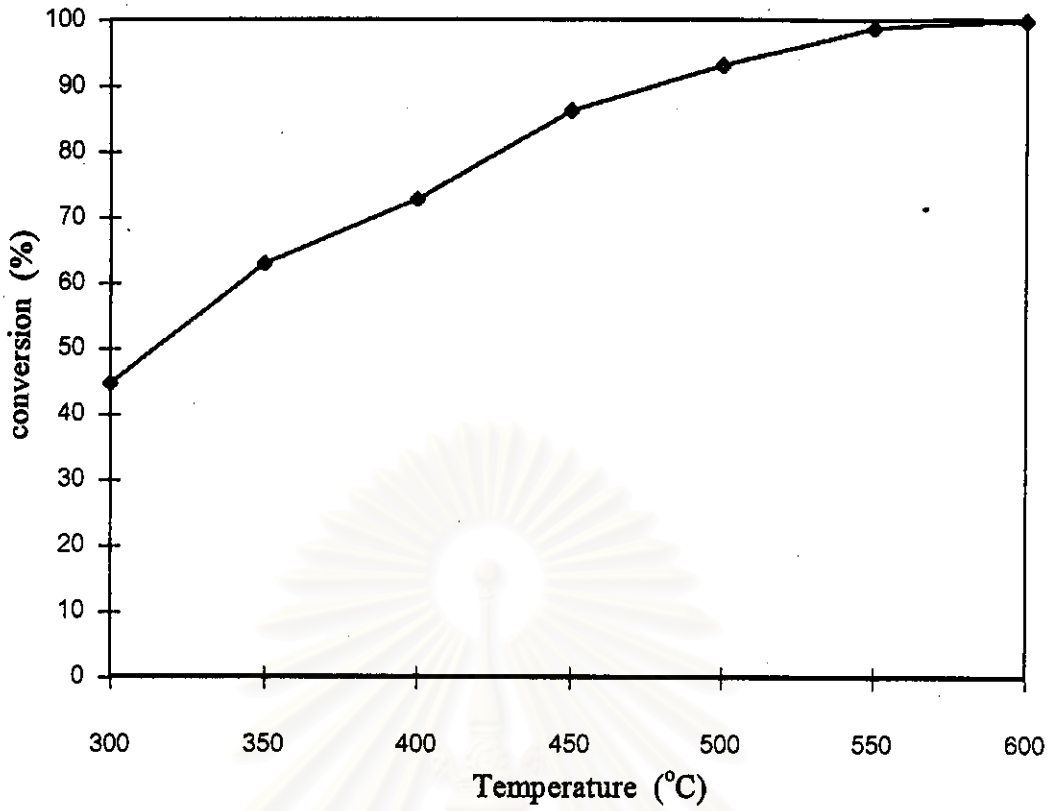

c) the n-octane conversion

Figure 5.20 Catalytic cracking of n-octane on HY zeolite catalyst at various reaction temperature (continued)

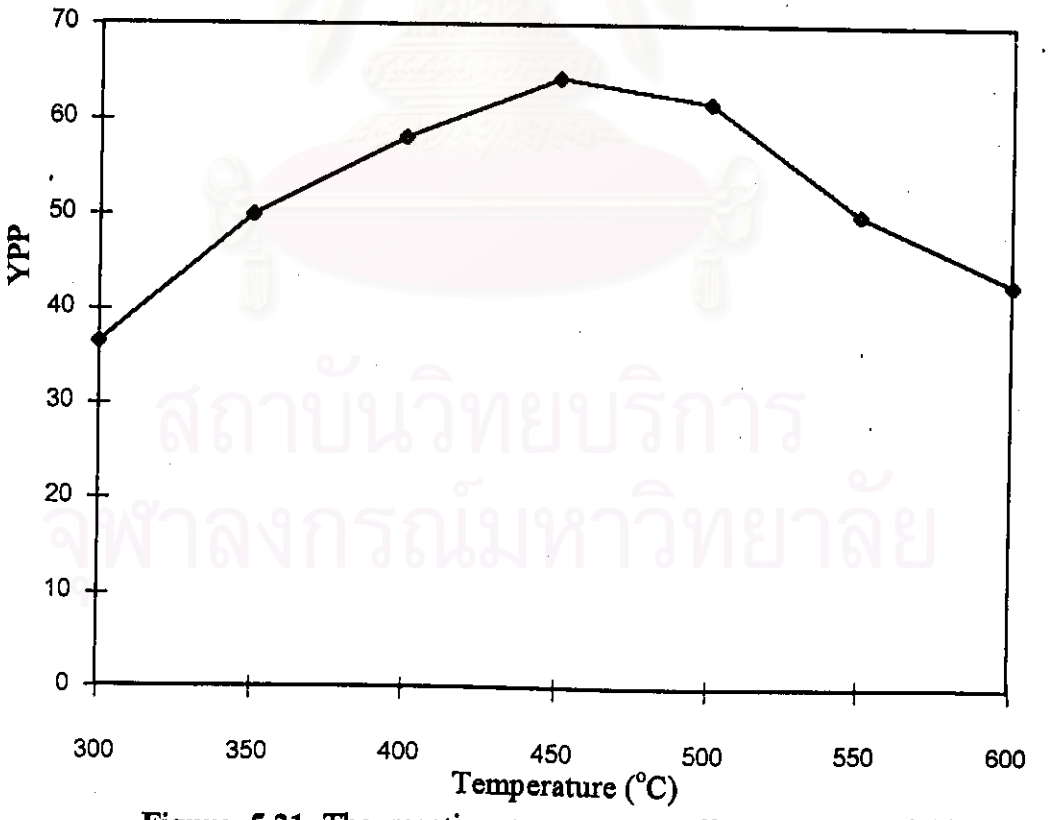

Figure 5.21 The reaction temperature effect on YPP yield on n-octane cracking on HY zeolite catalyst

ethene and propene can be substantially formed at high reaction temperature above 450 °C. As shown in Figure 5.21, the maximum YPP of the desired products was obtained at 450 °C. Therefore, the reaction temperature of 450 °C was selected as the optimum temperature for n-octane cracking.

Table 5.2 The thermal cracking effect on catalytic cracking of n-octane

Temperature (°C)	Conversion (%)	Product Distribution (wt%)						
		C_1	C_2	$C_2^=$	C_3	$C_3^=$	C_4	$C_4^=$
450	1.3	1.5	0.1	11.3	0	14.8	0	11.4
500	3.0	4.1	0.6	31.8	0.1	19.9	0	15.4
550	24.3	6.8	1.0	43.0	0.3	21.0	0	9.3
600	51.7	6.8	1.5	44.8	0.4	20.2	0.1	12.1

5.5.3 Effect of time on stream on n-octane cracking.

Figures 5.22 a to 5.22 c show the product distribution and n-octane conversion obtained on HY catalyst at 450 °C , 2000 h^{-1} at different times. on stream during 10 to 60 min. The conversion of n-octane slightly decreased during the observed time period. As shown in Figure 5.23, the maximum YPP of the desired products was obtained at 30 min on stream.

5.5.4 Comparison of the catalytic performances of different types of Y-Zeolite

To investigate the catalytic performances of n-octane cracking on different types of Y-zeolite, four kinds of catalyst were used in this study. Three of them were self-prepared, i.e. NaY, NH_4Y and HY, and another one, H-JRC-Z-Y, was supplied by Tosoh Corporation. As shown in Figure 5.28,

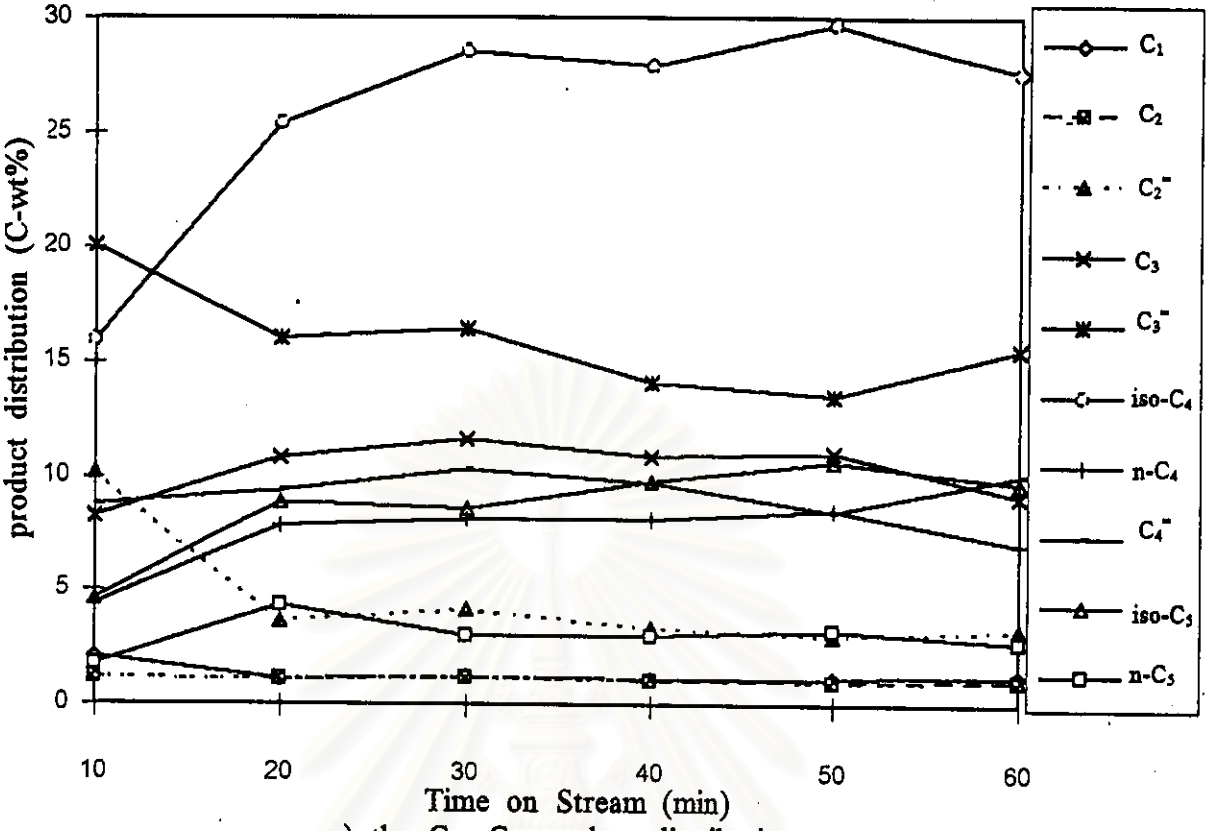

a) the C_1 - C_5 product distribution

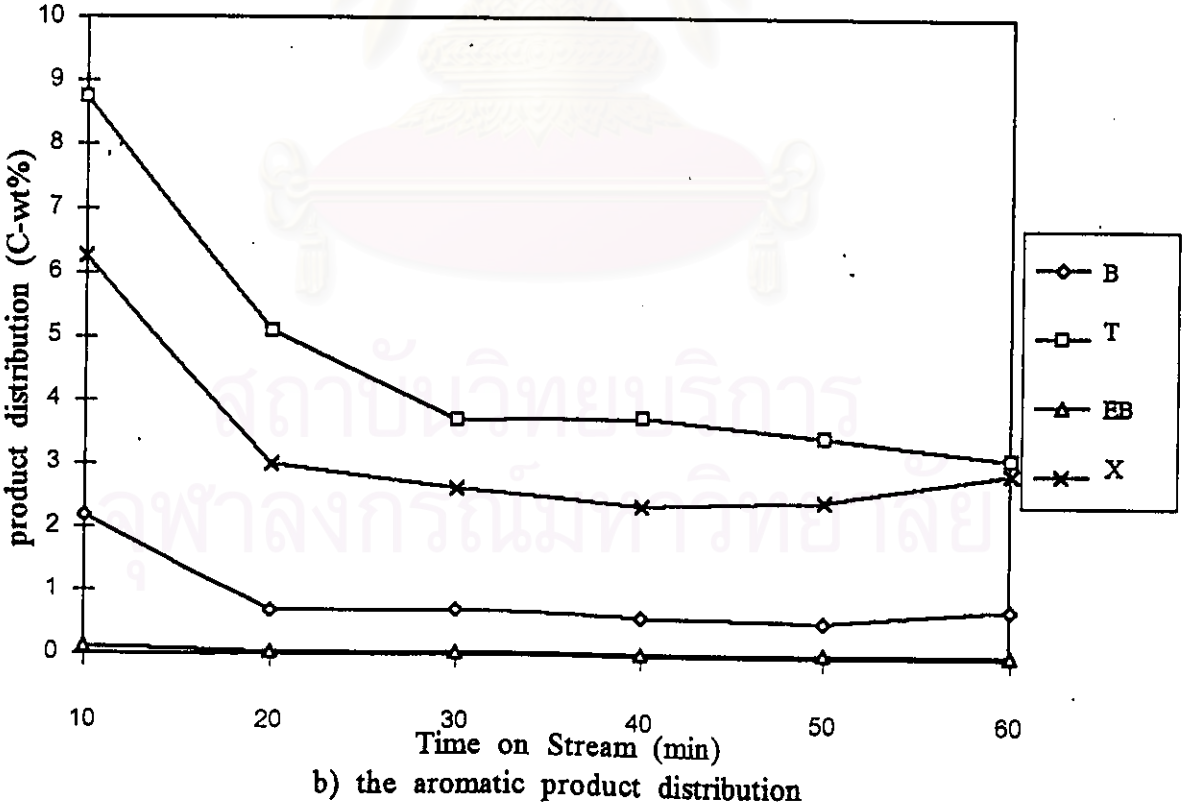

b) the aromatic product distribution

Figure 5.22 Catalytic cracking of n-octane on HY zeolite catalyst at various time on streams

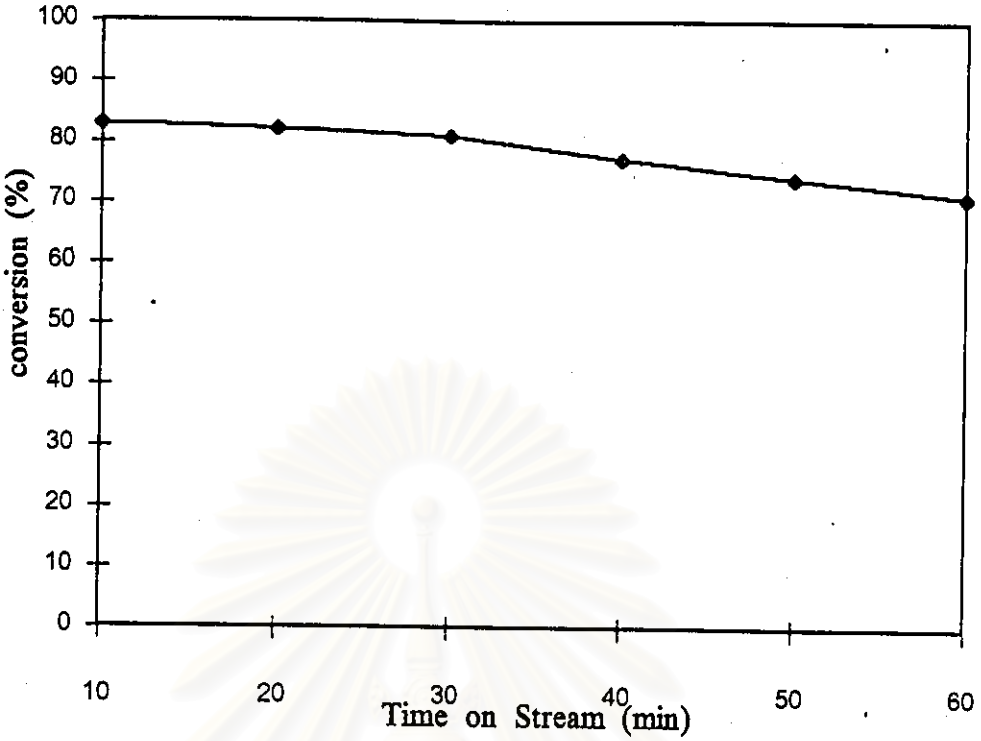

c) the n-octane conversion

Figure 5.22 Catalytic cracking of n-octane on HY zeolite catalyst at various time on streams (continued)

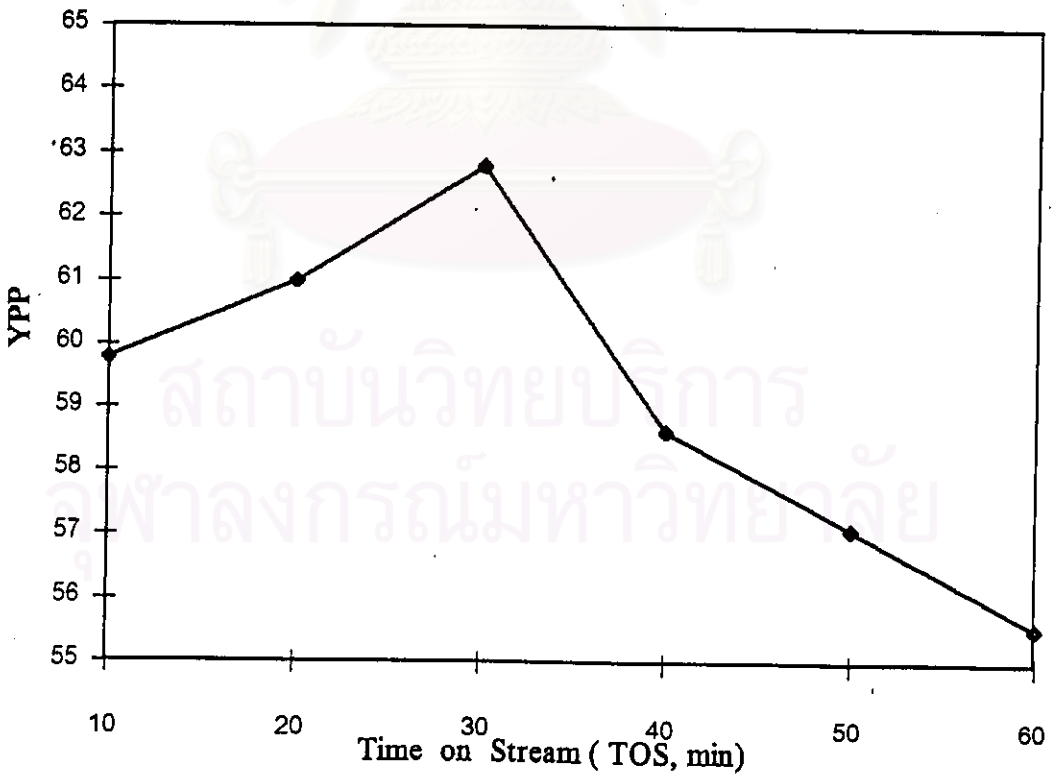

Figure 5.23 The time on stream effect on YPP yield of n-octane cracking on HY zeolite catalyst

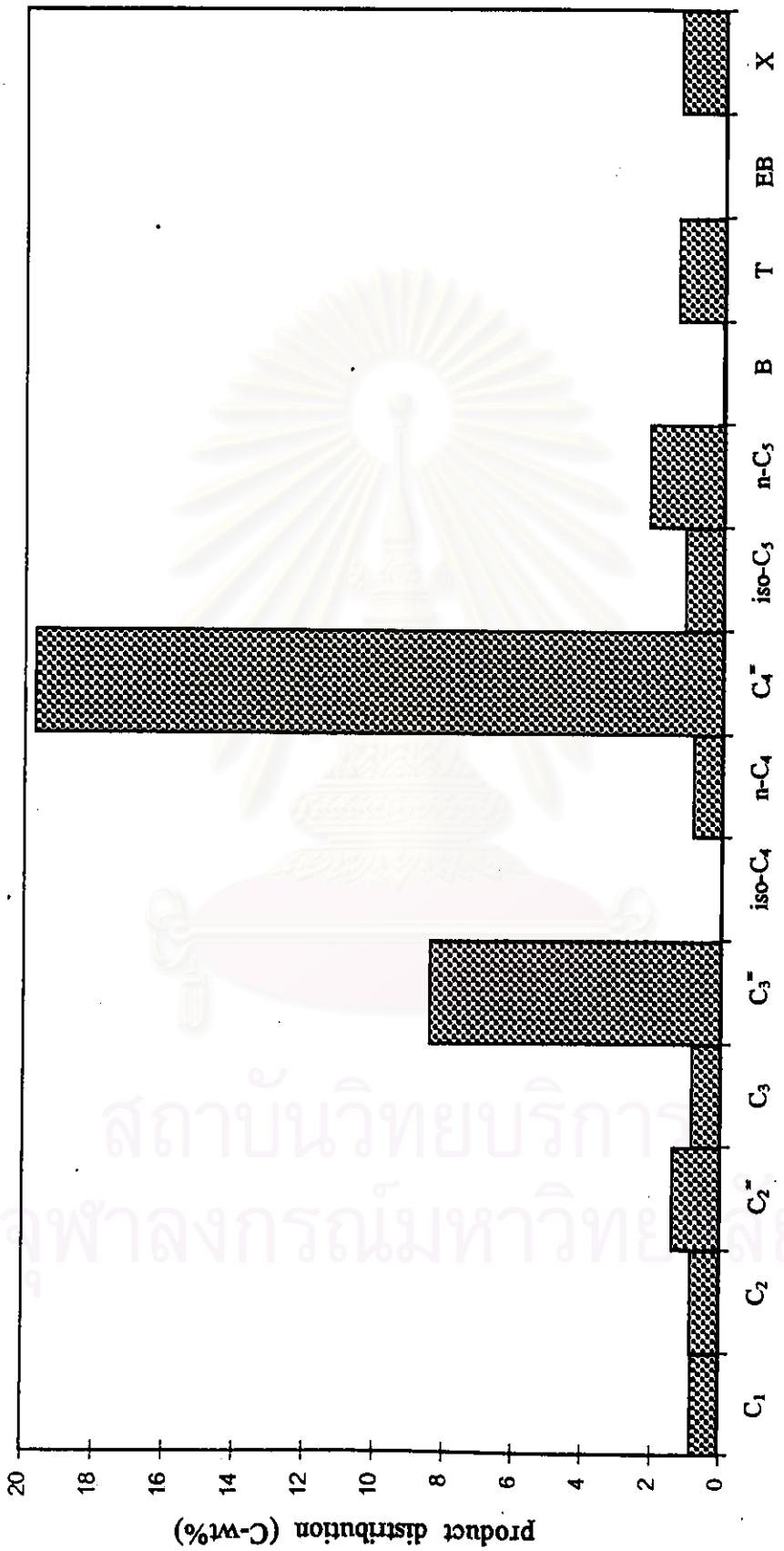

Figure 5.24 The product distribution of n-octane cracking on NaY catalyst

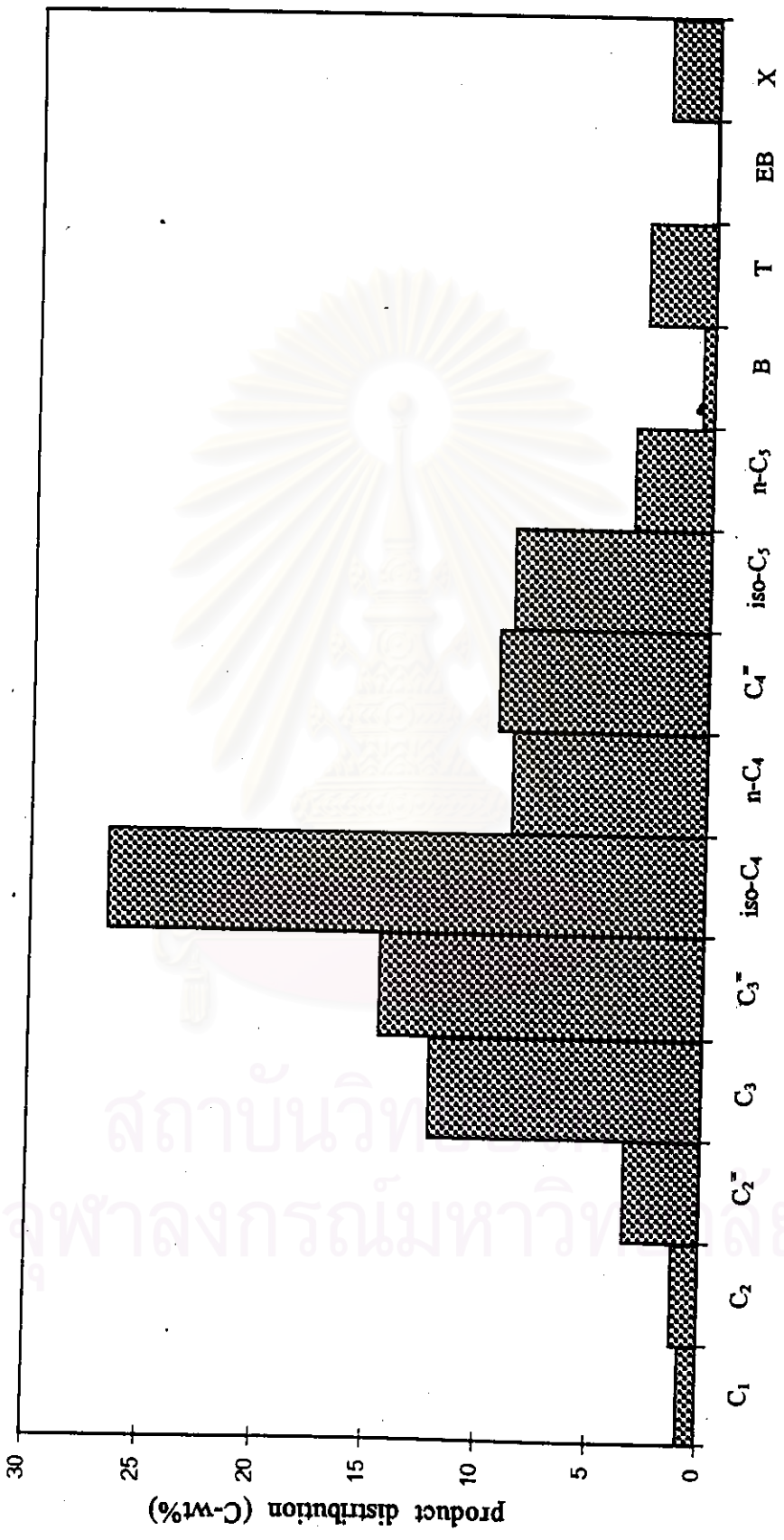

Figure 5.25 The product distribution of n-octane cracking on NH_4Y catalyst

Figure 5.26 The product distribution of n-octane cracking on HY catalyst

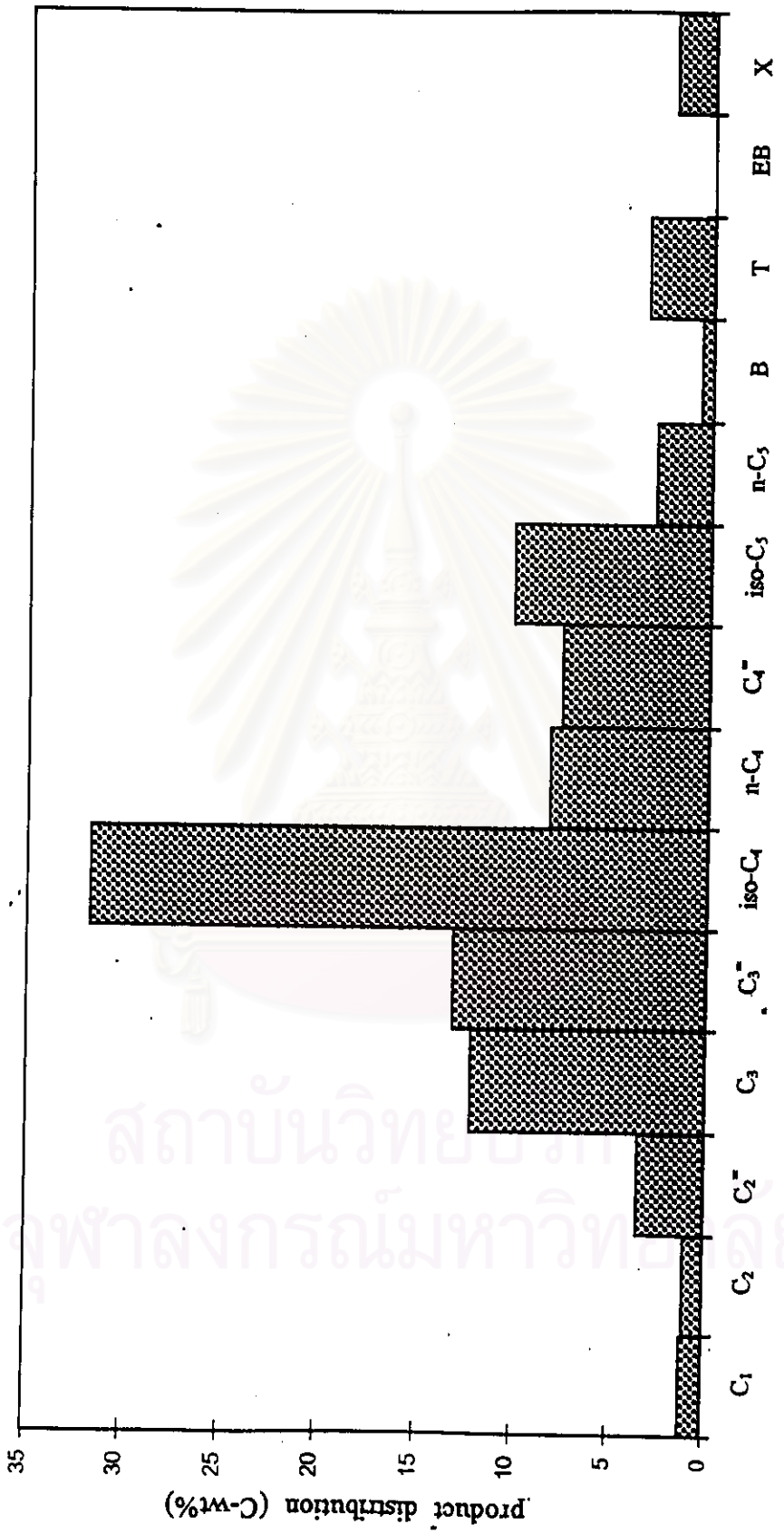

Figure 5.27 The product distribution of n-octane cracking on H-JRC-Z-Y catalyst

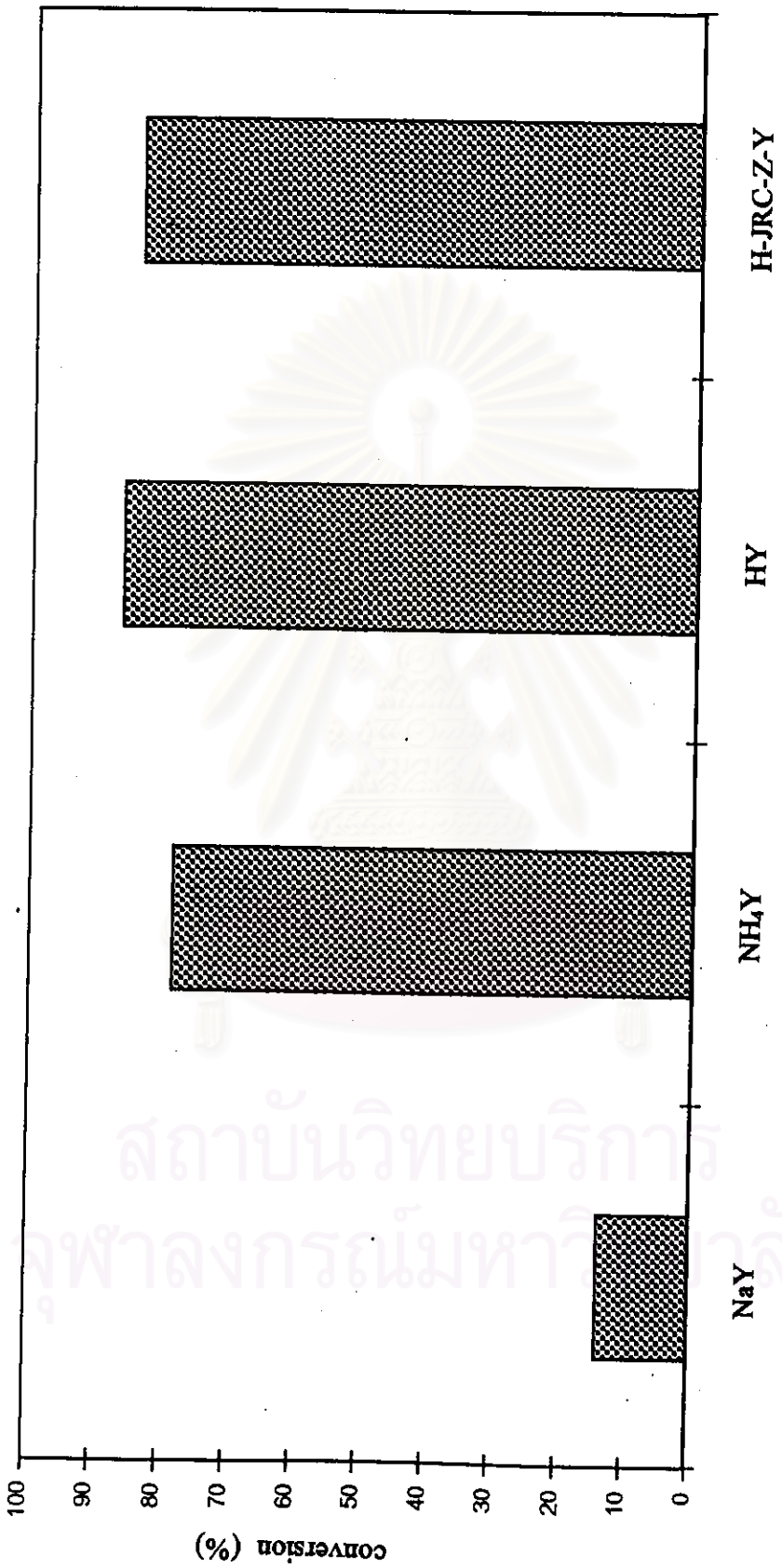

Figure 5.28 The conversion of n-octane cracking on the various types of catalyst

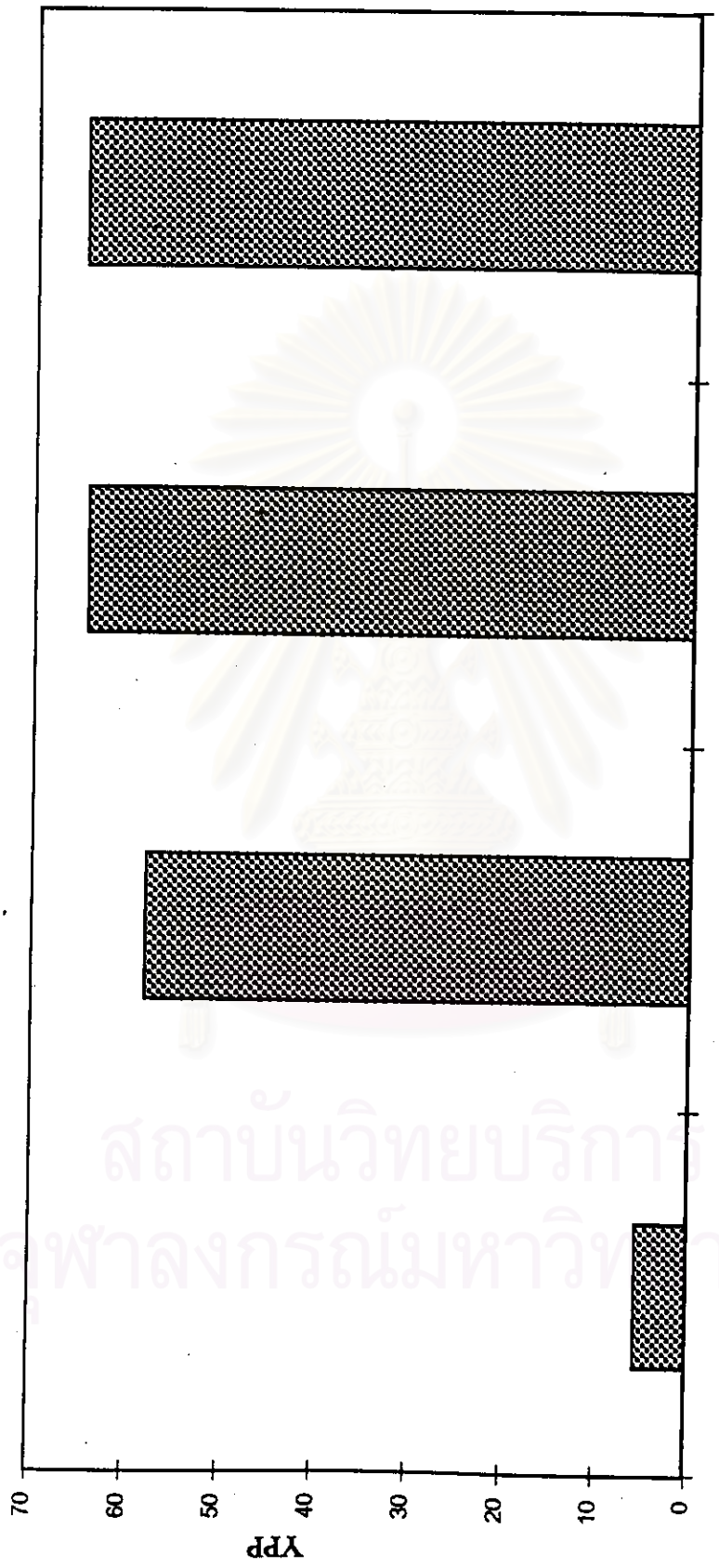

Figure 5.29 The YPP yield of n-octane cracking on the various types of catalyst

NaY catalyst showed very low conversion of n-octane. HY catalyst exhibited higher conversion and substantially similar to that obtained on H-JRC-Z-Y. It has been suggested that the higher amount of strong acid site possessed by H-type catalysts should be responsible for the high catalytic activity. NaY catalyst showed very poor selectivities for high octane number products and much n-octane remained unconverted. The maximum YPP of the desired products was obtained on HY and H-JRC-Z-Y in approximately the same level as shown in Figure 5.29.

5.5.5 Prolonged operation of n-octane cracking on HY catalyst

The product distribution and conversion of n-octane at 450 °C, 2000 h^{-1} during the long period from 1 to 10 h is shown in Figure 5.30. The n-octane conversion decreased with the longer time on stream, and after 8 h on stream the conversion was less than 50%. The coke formed on HY catalyst should cause less catalyst activity during the long reaction time. It should be noted that isobutane amount significantly decreased during the prolonged operation. This means that iso-butane should be the product substantially formed through catalytic cracking, and thermal cracking had little influence on isobutane formation.

5.5.6 Regeneration of HY catalyst

The fresh HY catalyst was used to carry out n-octane cracking at 450 °C, 2000 h^{-1} for 30 min on stream. The used catalysts were regenerated by heating in an air flow at 550 °C for 1 h and 1.5 h. They were designated as "regen.1" and "regen.2" as shown in Figure 5.31. Each regenerated catalyst was tested on n-octane cracking with the same reaction conditions.

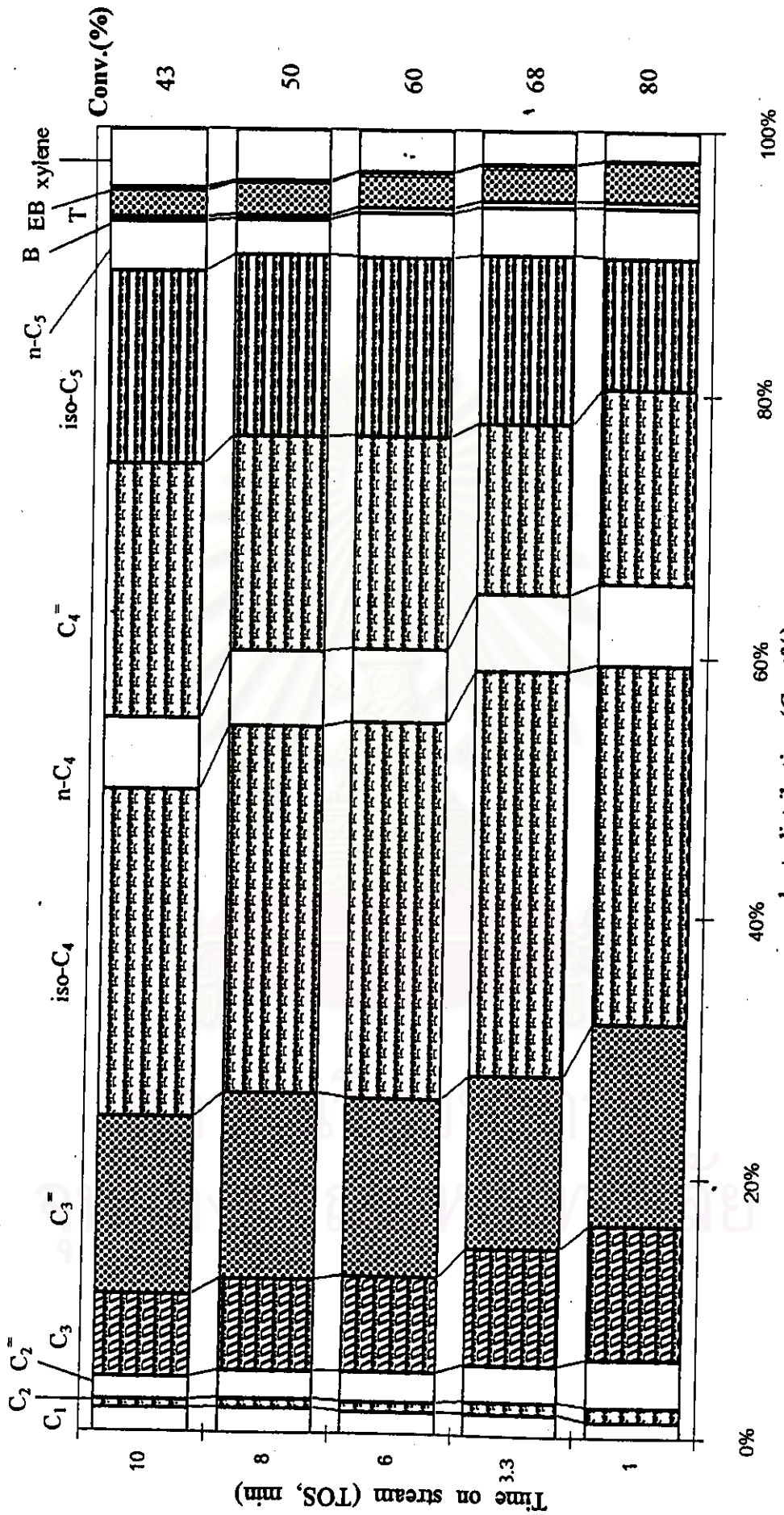

Figure 5.30 Prolong operation of n-octane cracking on HY zeolite catalyst

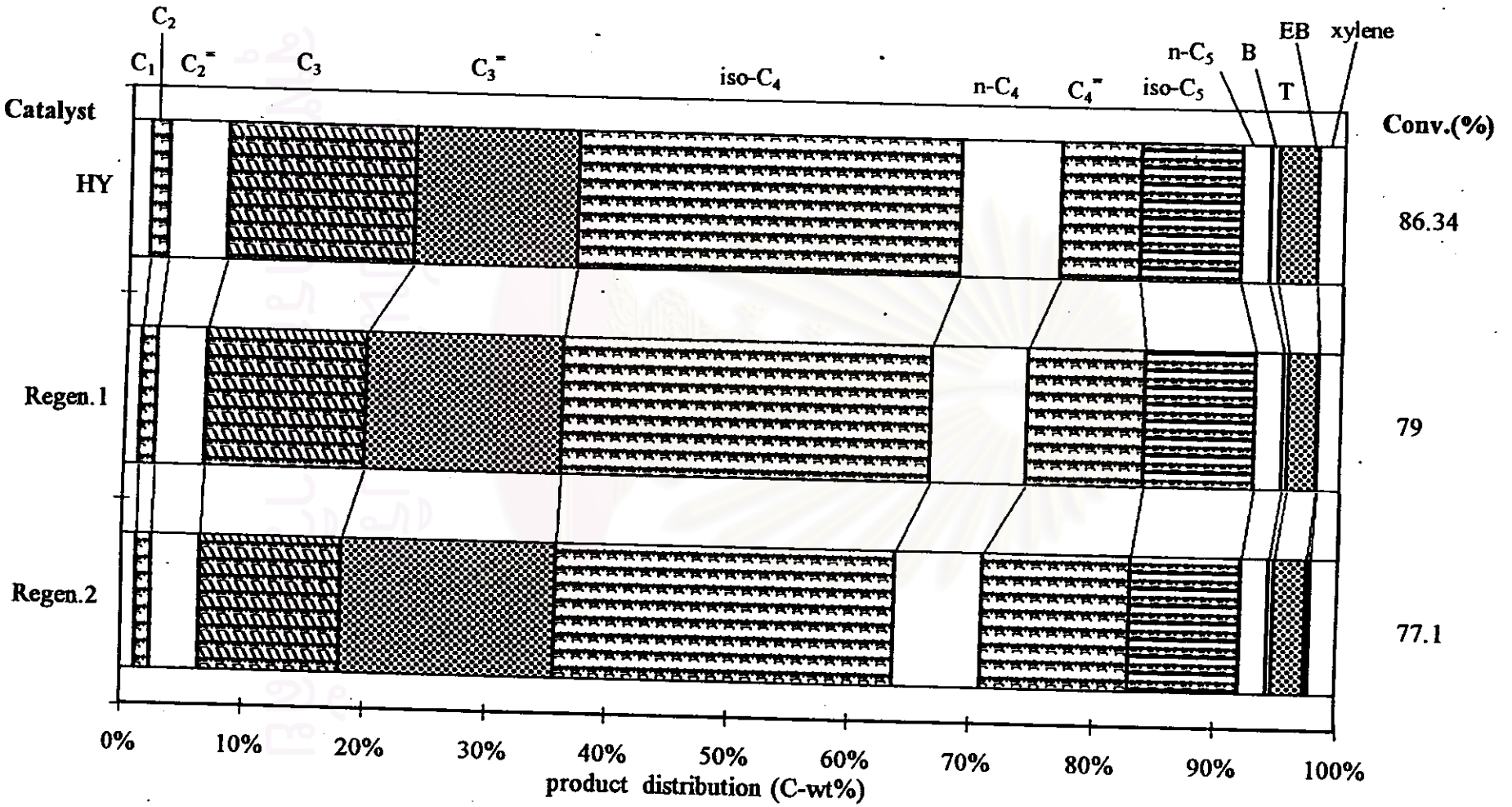

Figure 5.31 The regeneration of used HY zeolite catalyst

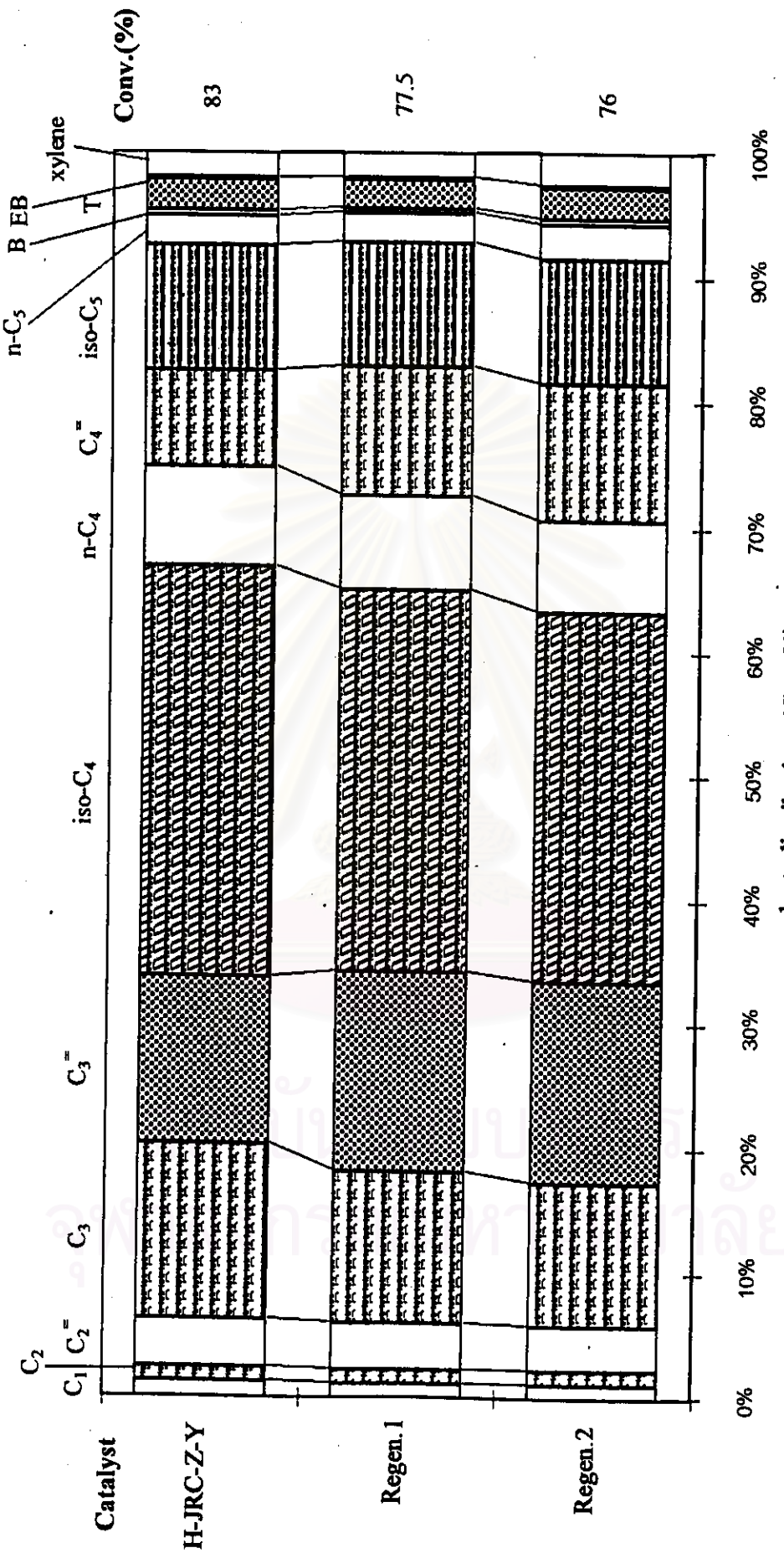

Figure 5.32 The regeneration of used H-JRC-Z-Y zeolite catalyst

It has been found that HY catalyst was not completely regenerated under the regeneration conditions used. For comparison the same test was done on H-JRC-Z-Y, as shown in Figure 5.32, and the same result was obtained. From Figure 5.33, it has been found that the decreased intensity of the XRD patterns was obtained on regenerated HY catalysts. This revealed the partly structural collapse at such high regeneration temperature, 550 °C. This may cause slightly less catalytic activity of the regenerated catalysts.

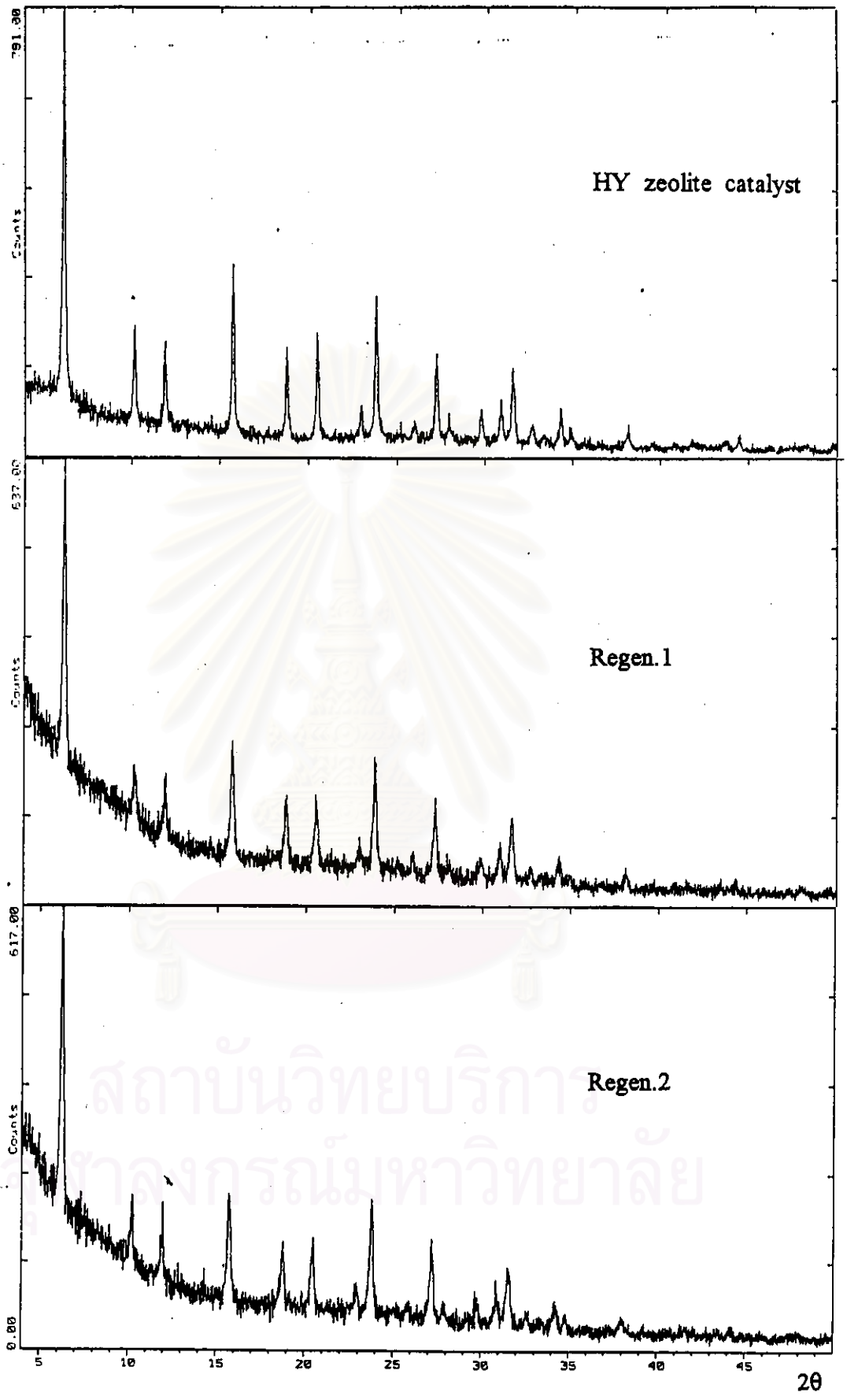

Figure 5.33 The XRD patterns of regenerated HY catalysts